Tip Clearance and Angle of Attack Effects upon the Unsteady Response of a Vibrating Flat Plate in Crossflow

by

Daniel Joseph Lewis

Thesis submitted to the Faculty of the

Virginia Polytechnic Institute and State University

in partial fulfillment of the requirements for the degree of

MASTER OF SCIENCE

in

Mechanical Engineering

APPROVED:

W. F. O'Brien, Co-Chairman

A. Bölcs Co-Chairman

J. Moore

R. J. Roby

February 1993
Blacksburg, Virginia

C.2

Tip Clearance and Angle of Attack Effects upon the Unsteady Response of a Vibrating Flat Plate in Crossflow

by

Daniel Joseph Lewis

Committee Co-Chairmen: Albin Bölcs and Walter F. O'Brien

Mechanical Engineering

Abstract

The influence of tip clearance and angle of attack upon the mid-span unsteady pressure response of a vibrating flat plate was investigated experimentally. Unsteady pressure measurements were taken for a variety of incidence angles, vibration frequencies and tip clearances over a Mach number range of 0.2 to 0.6.

It was found that changes in tip clearance had an effect on measured pressure fluctuations at higher angles of attack and larger Mach numbers. It was also observed that the amplitude of the unsteady pressure increased as the incidence angle was increased.

The plate was mechanically induced to oscillate in translation, simulating the first bending mode. Averaged Fast Fourier Transforms were used to determine pressure oscillation amplitudes and phase lags with respect to the plate motion.

Acknowledgments

I would like to express my profound gratitude to both Professors Walter F. O'Brien and Albin Bölcs for their invaluable assistance in making this project possible. Without their help this exchange could not have come about. Thanks are due to committee members and Professors John Moore and Richard J. Roby for their support.

I would like to thank everyone in the LTT in Lausanne, including Magnus, Heiko, Peter, Matthias and Vassilis. I would especially like to thank Mssrs. Rossini and Mottier for all their patience and assistance in assembling the test stand.

I would also like to thank everyone in the Turbo Lab down in the dungeon for their help and support.

None of this would have been possible without the support of my parents, Dan and Maureen, and my sisters, Kathy and Keri. Finally, I want to thank, the soon-to-be-newest member of my family, my fiancée, Annie Sévin.

Table of Contents

Table of Figures

Table of Tables

Nomenclature

τ	tip clearance/chord
tau	tip clearance/chord
c	chord length (mm)
Cp	pressure coefficient
α	angle of attack (°)
AOA	angle of attack (°)
uCp	unsteady pressure coefficient
k	reduced frequency
M	Mach number
u	free stream velocity (m/s)
phi	phase lag of pressure signal
a	amplitude of blade vibration (m)
Δp	amplitude of pressure oscillation (mbar)
$p_\infty - p_S$	dynamic pressure (mbar)

1. Introduction and Motivation

The main goal of this project was to investigate the effects of tip clearance on the flow over a vibrating flat plate at angle of attack in crossflow. There were two major motivations for investigating the effect of tip clearance on the unsteady pressures on an oscillating blade: to determine the effects of the tip gap flow on the unsteady loading of a blade, and to observe how the clearance needed to allow blades to vibrate in cascade work affects the measurements done at mid-span.

There has been much work recently on the measurement and prediction of flow in the tip gap region of turbomachinery. There has also been an increasing amount of work being done in the research of blade flutter. It has been debated whether there was any influence of the tip flow and tip leakage vortices on the unsteady forces on a blade that could force it into flutter.

During many unsteady aerodynamic tests, sections of blades rather than full scale blades are under consideration. For these tests it is necessary to have a gap at one end of the blade to allow the blade to freely vibrate without rubbing against the end walls. If the section under consideration is a mid-span section, this gap is not present in the full scale compressor or turbine. The present investigation was originally conceived to examine how this space and the size of the gap may affect the measurements that are usually made at the mid-span of the test section.

2. Literature Review

There does not exist much literature on the interactions between tip leakage flows and unsteady blade aerodynamics. Each area has usually been examined independently of the other. The study of tip leakage flows has concentrated on the flow structure within the tip gap, losses produced in the tip gap and how to reduce the losses. The studies of the unsteady aerodynamics have mainly focused on the effects of the unsteadiness and whether the blade is stable or unstable. One exception to this division of the two areas is a study by Watanabe and Kaji (1987). This paper will be discussed later.

2.1 Tip Clearance Flows

The majority of recent work on tip leakage flows has consisted of trying to form a picture of the flow structure inside the tip gap. The main parts of the flow in the gap consist of a separation bubble on the blade tip and the contraction of the flow as it tries to move through the tip gap. These are shown in Figure 1. It has been theorized and observed in various studies and methods that the flow across the tip gap is almost perpendicular to the chord line (Dishart and Moore, 1989; Sjolander and Amrud, 1986). This is thought to be due to the pressure gradient across the blade being stronger than the pressure gradient along the blade. As the flow comes over the tip corner a separation bubble is formed. This flow then reattaches and subsequently exits the tip gap. It is when this flow encounters the main flow in the blade passage that a vortex is formed. Sjolander and Amrud (1986) reported seeing multiple tip leakage vortices formed as the tip gap was increased. Yaras and Sjolander (1989) found that a tip leakage vortex formed at about 20% of chord length. They also reported that it appeared that the multiple tip vortices found earlier rolled up into one main tip leakage vortex further downstream. Bindon

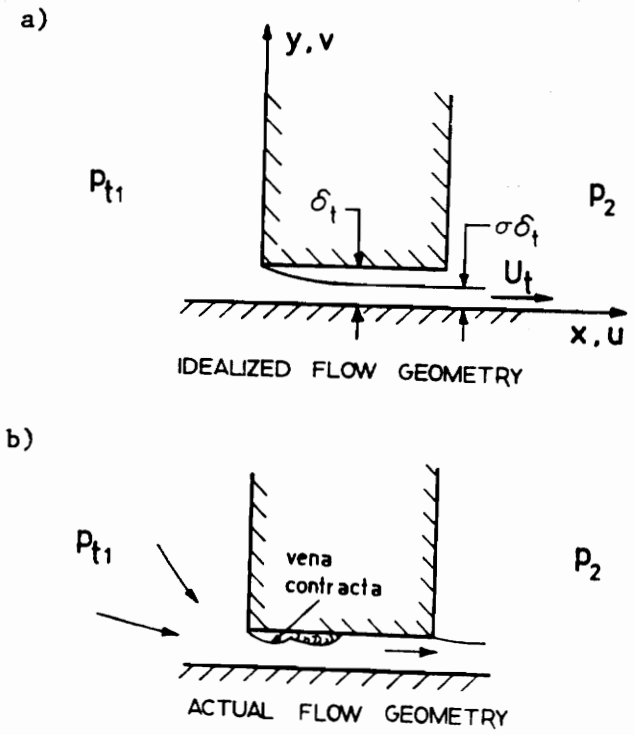

Figure 1: Model of Tip Clearance Flow (from Moore and Tilton, 1987)

(1988) found that most of the losses occurred over the last 20% of chord length. He suggested that this was because the leakage flow over the first part of the blade quickly reattached and resulted in little loss, while over the latter part of the blade stagnating flow in the separation bubble on the blade tip formed a vortex creating the large losses. He also observed that the stagnating flow in the separation bubble on the blade tip seemed to have velocity in the streamwise direction.

The tip leakage flows influence the blade pressure distributions. Their influence extends down the blade towards the hub. Moore and Tilton (1987) reported the vortex influence moved towards the hub along the first 50% of the blade chord, it had reached 12% of the blade height at this point, from there the distortions did not travel further towards the hub. They reported that the pressure surface was unloaded within a distance of two tip gap heights of the blade tip. Other works have reported that the velocity was distorted within a layer ten times the tip clearance (Senoo, 1987). For an average tip clearance of about 1% chord this yields roughly the same range of influence as determined by Moore and Tilton. Sjolander and Amrud (1986) reported that the blade loading was greatly disturbed within a range of six to eight tip clearances of the tip itself.

Various parameters of both the blade geometry and the flow conditions can influence the tip leakage flow. The tip corner radius is one of these influencing conditions. Sharp corners tend to lead to quick separation of the tip clearance flow (Moore *et. al.*, 1988), whereas rounded corners could be anticipated to reduce the amount of separation that occurs (Bindon, 1988). This might not be the best solution. Heyes *et. al.* (1991) compared the results of flat tipped blades and blades with squealers on either the suction or pressure side. They concluded that in order to improve results, lower losses, designers should concentrate on lowering the mass flow through the tip gap, the discharge

coefficient, rather than concentrating on the loss being produced across the tip. Other studies have investigated the inlet flow conditions and their effects on the tip leakage flow. Yamamoto (1988) came to the conclusion that a change in the incidence angle does not greatly affect the leakage flow and that the tip clearance effects did not move upstream to influence the inlet flows.

Various models have been developed in attempts to describe the flow in the tip gaps. Most of these models have been for subsonic flow and aim to predict the mass flow rates and flow directions in the tip, and the losses due to the tip clearance flow. The first simple model was developed by Rains in 1954. This model covered incompressible flow and accounted for the separation bubble on the tip and the reattachment of the flow afterwards. Various additions have since been made to this model to account for various phenomena. Moore and Tilton (1987) found discrepancies in Rains' model for its limiting cases of endwall flow and flow on the pressure side near the tip gap. They corrected these discrepancies with solutions from Rayleigh. This new model included mixing of the flow. It proved to have fairly good agreement with their experimental results for the static pressures in the gap. Moore *et. al.* (1988) used a two-dimensional laminar incompressible flow model with a Navier-Stokes program to calculate pressure coefficients and contraction coefficients. Recently, Moore and Moore (1990) have computed leakage flow with a three-dimensional viscid incompressible code. Yaras *et. al.* (1988) developed a simple model for predicting flow directions and velocities within the tip gap. This model has been expanded by Yaras and associates in other papers (Yaras and Sjolander, 1989; Yaras and Sjolander, 1990; Yaras and Sjolander, 1991; Yaras *et. al.*, 1991). A vortex model developed by Yaras and Sjolander (1990) was based on the diffusion of a line vortex. The effects of relative wall movement were also included (Yaras and Sjolander, 1991; Yaras *et. al.*, 1991). The model was based on the assumptions that the pressure

difference across the blade controlled the flow and that there was no change in chordwise momentum. For these models an empirical discharge coefficient is needed. Comparisons with measurements have indicated good agreement for flow rates and flow angles.

2.2 Unsteady Flows

A good detailed introduction to the general area of unsteady flows is provided by Fung(1969). Two other papers, by Fransson (1991) and Platzer (1990), provide more up to date information on this area. They both provide definitions of the various types of unsteady phenomena, including flutter, buffeting, stall flutter, and buzz, and give a history of problems encountered with flutter. In addition, Fransson provides a list of 95 references in this field. Figure 2 shows some of the different types of flutter and where they may occur on a compressor map.

One of the important criteria for unsteady phenomena is the reduced frequency, shown below, also known as the Storr Number or Strouhal Number. In this paper the term reduced frequency, k, will be used and the reference distance, d, will be one-half chord. The inverse of the reduced frequency, the reduced velocity, is also sometimes used. The reduced frequency gives an indication of how important the unsteadiness of the flow might be. For reduced frequencies around one the unsteadiness is said to be the controlling factor. At lower reduced frequencies the flow is said to be quasi-steady; the flow can be modeled as a series of steady state solutions one following another.

$$k = \frac{\omega d}{U} \qquad (1)$$

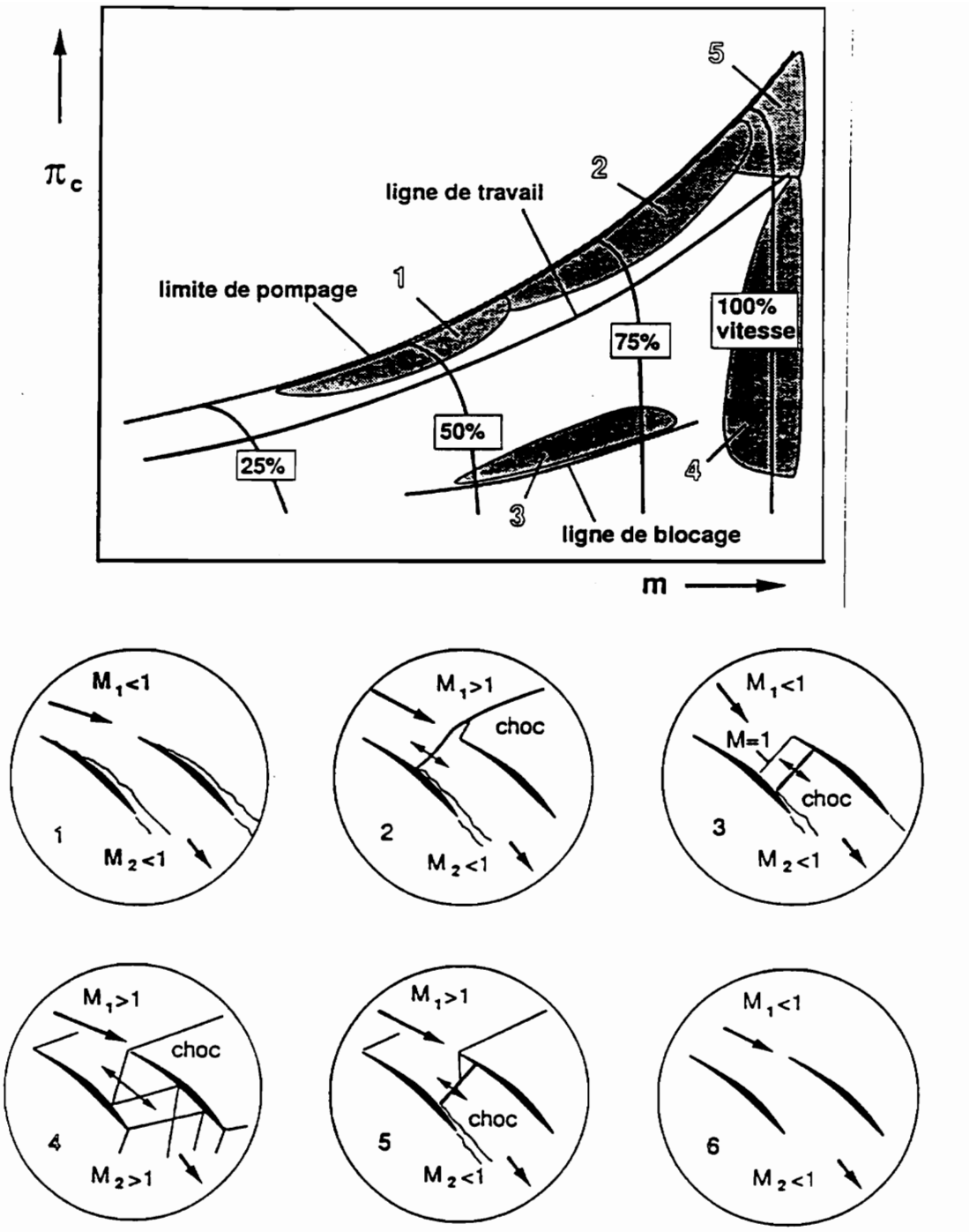

Figure 2: Transonic Compressor Characteristic with Principal Types of Flutter (from Bölcs, 1992)

Another parameter used in discussing unsteady flows is the unsteady pressure coefficient, defined below. It is similar to the steady pressure coefficient, yet also contains the vibration amplitude, a, and the blade chord, c. The other parameters needed include the amplitude of pressure oscillation, Δp, as well as the dynamic pressure, $(p_\infty - p_S)$.

$$uCp = \frac{\Delta p \cdot a}{(p_\infty - p_s) \cdot c} \qquad (2)$$

2.3 Unsteady flows with tip clearance

There seems to be little available literature on the interactions between oscillating blades and tip clearance flows. Most literature on unsteady flows examines the stability or instability of various interblade phase angles and flow conditions and does not examine the possible three-dimensional effects. However, a paper by Watanabe and Kaji (1987) does examine the interaction of tip clearance with oscillating blades. Various tip clearances were examined along with the unsteady pressures that resulted. Their experimental results showed that the aerodynamic forces were increased in the area near the blade tip. They found that with no load the damping forces were decreased with a tip clearance. However, when there was a load the tip clearance effects were diminished. They did not closely examine the flow within the gap but they did make some measurements downstream of the flow and were able to see the tip leakage vortex. A theoretical model was also developed based on a vortex lattice method. In comparing their theoretical model with their experimental results they found good qualitative agreement for larger tip gaps, while there was poor agreement at the smaller tip clearances. They concluded that this discrepancy was because of viscous forces having a larger effect at smaller tip clearances. The study by Watanabe and Kaji only covered subsonic flows and their model was based on

incompressible, inviscid potential flow theory. Yet, it does provide a starting point for studying the relation between unsteady flow and tip clearance flow.

3. Experimental Setup

This chapter will introduce the setup of the test apparatus, including the vibration system and data acquisition systems. The methods used for calibration will also be described.

3.1 Vibration system and cascade

Wind tunnel and test section

The wind tunnel used to conduct these tests was a variable area ratio converging diverging tunnel. In these tests the area was held constant, not diverging. The test section had a width of 100 mm. Two circular ports exist where plates can be placed to hold test profiles or to place test equipment. On one side of the test section a Plexiglas plate was placed to allow viewing of the tests and access for optical measuring techniques. The other side of the test section consisted of a steel plate that held the blade and its supports. This side was mirrored to allow reflective holography to be used if needed. There were places for two additional flat plates to closer approximate a cascade. However, these were not used in the tests conducted.

Blade Test Article

The blade was a flat brass plate with half-circle leading and trailing edges and a constant thickness as seen in Figures 3, 4 and 5. The dimensions are detailed in Table I. This profile was chosen because it is a simple profile whose flow characteristics are relatively well known. The same profile was also being used at the laboratory for initial investigations into transonic tip leakage flows.

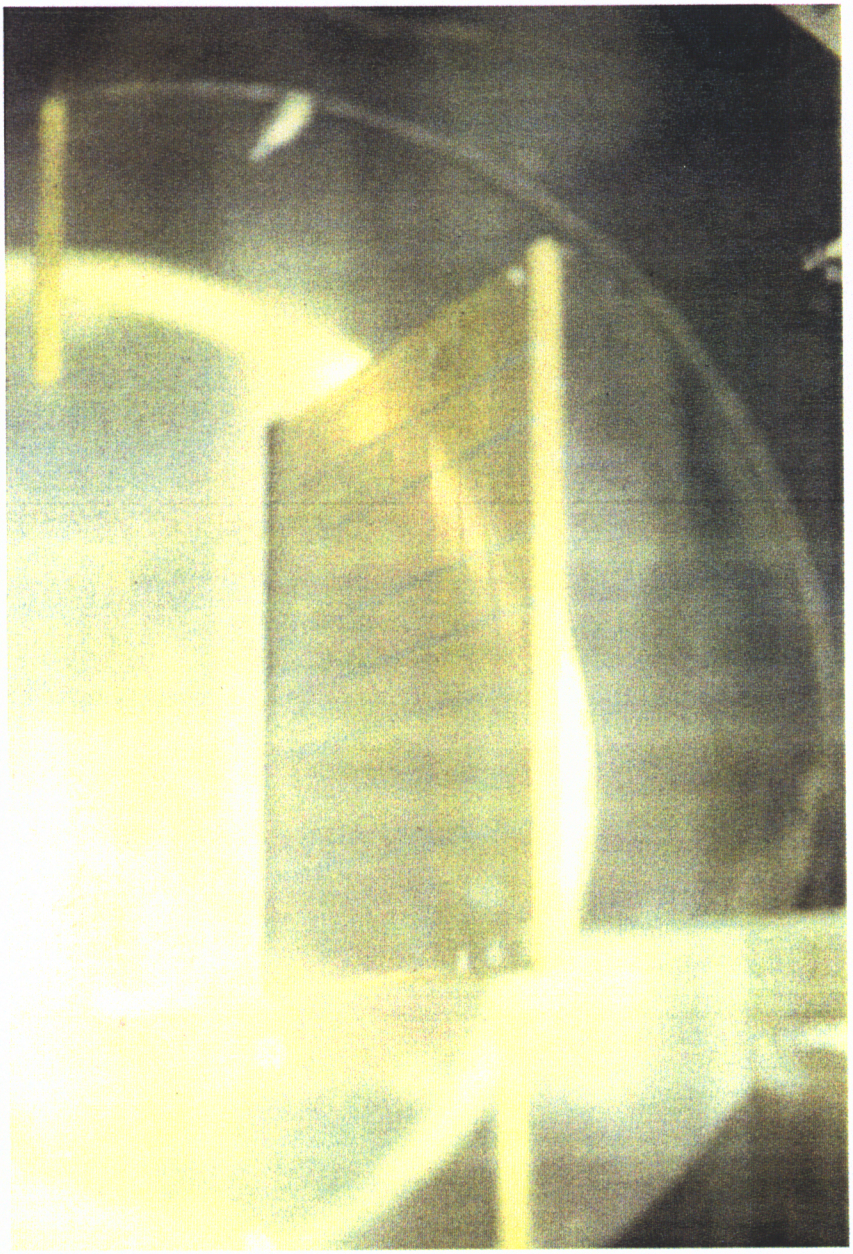

Figure 3: Flat Plate in Test Section

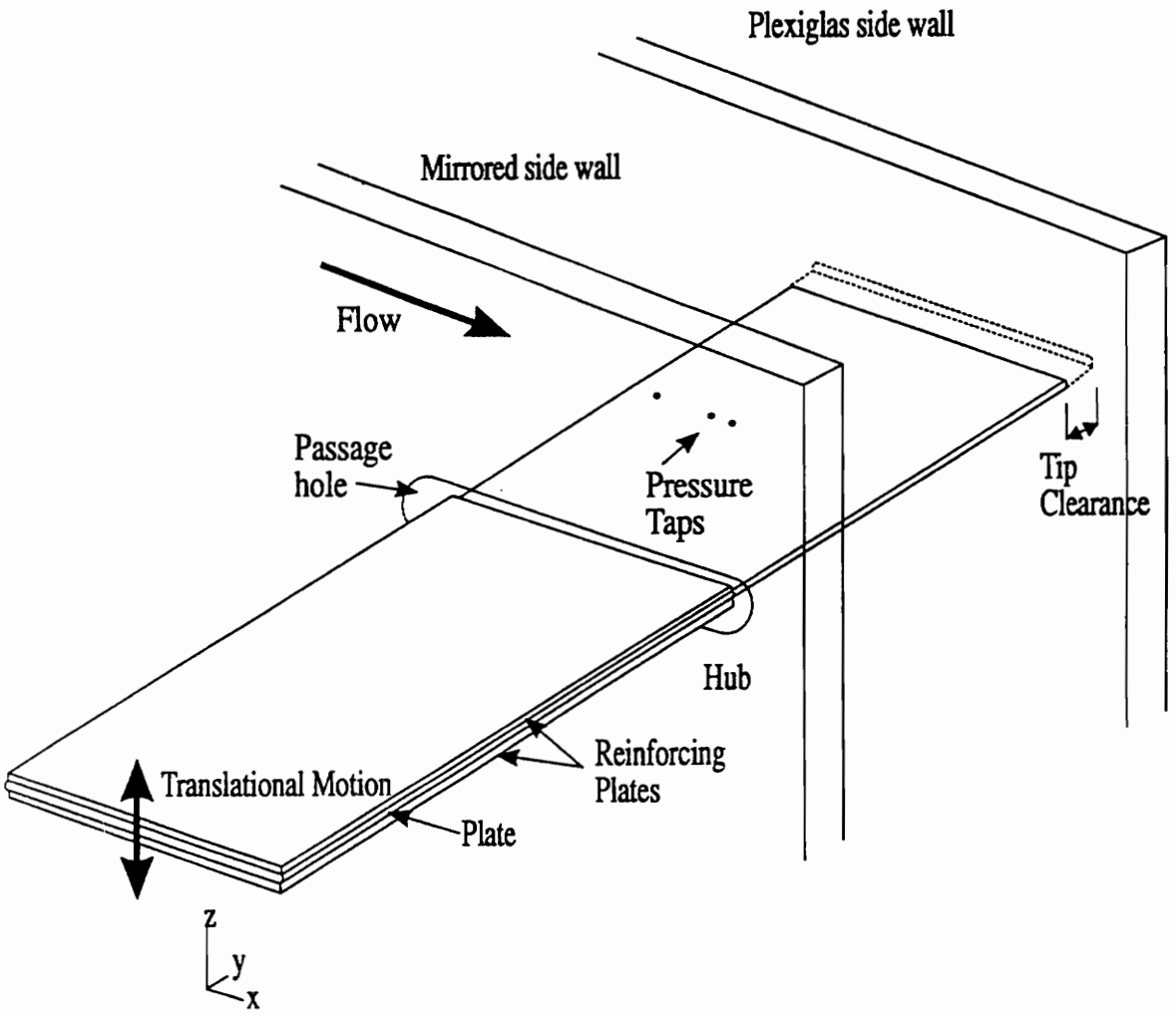

Figure 4: Pictorial Representation of Experimental Setup

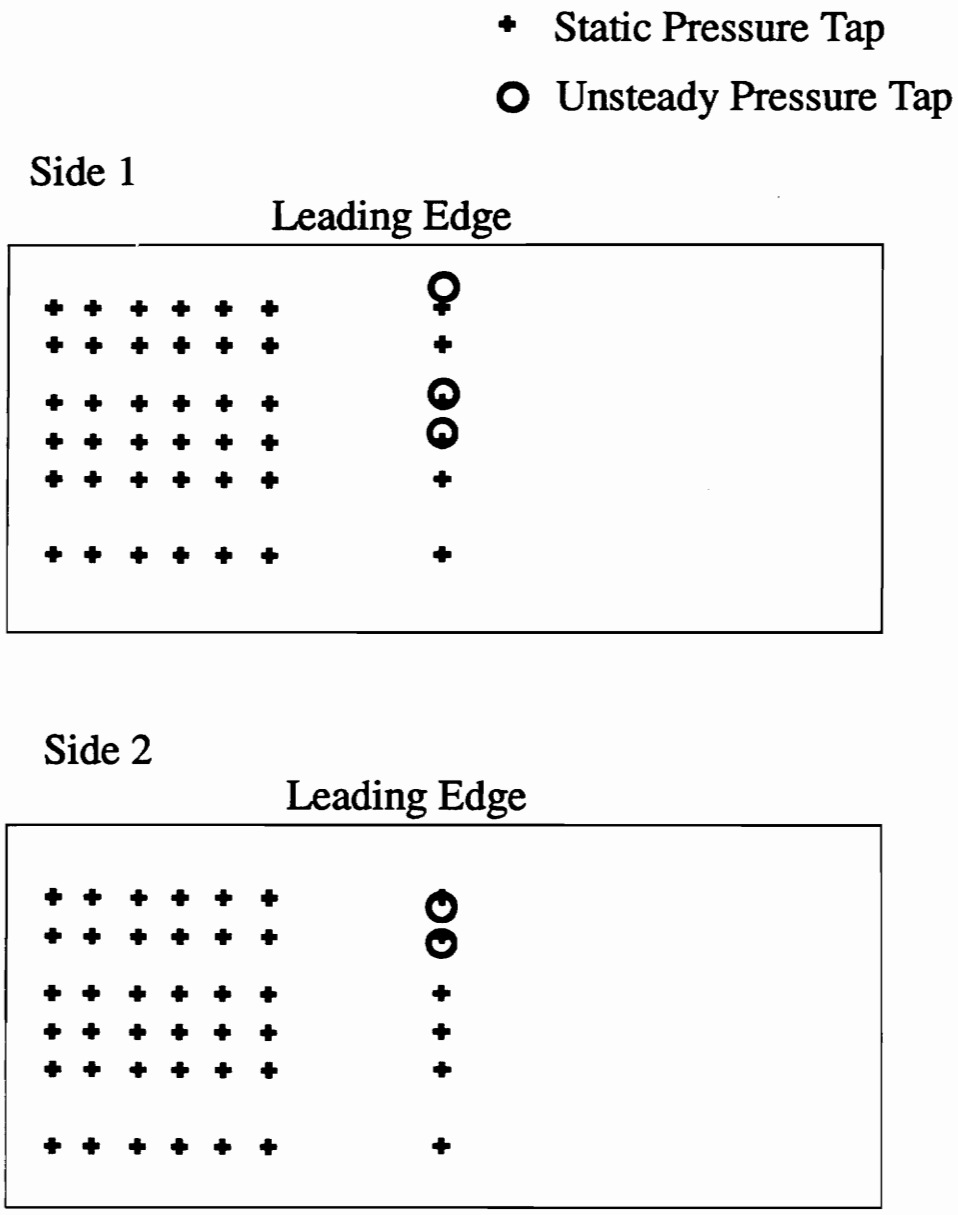

Figure 5: Schematic of Steady and Unsteady Pressure Tap Locations

To stiffen the blade two supporting pieces were screwed on to the blade, one on either side, on the area outside the test section, as seen in Figure 4. This increased the blade thickness to 10 mm initially and then to 12 mm.

The blade was instrumented with both steady and unsteady pressure measurement devices, shown in Figure 5. There were twelve stainless steel tubes imbedded in the surface, six on each side. These tubes were then pierced at various locations where it was desired to measure the pressure. Each tube had 7 holes in it. Table II gives the locations of the tubes and Table III indicates the positions of the pressure taps. All but the one hole where the pressure were to be measured was covered with cellophane tape. This setup allowed a wide range of static pressure locations with a minimal amount of equipment.

Table I: Blade Dimensions

chord	100 mm
thickness	4 mm
leading edge radius	2 mm
trailing edge radius	2 mm

Table II: Chordwise Locations of Static Pressure Taps

Side 1 (Distance from Leading Edge, x)	Side 2 (Distance from Leading Edge, x)
15 mm	20 mm
25 mm	30 mm
40 mm	45 mm
50 mm	55 mm
60 mm	65 mm
80 mm	85 mm

Table III: Spanwise Locations of Static Pressure Taps

Distance from Tip of Plate , y
5 mm
10 mm
15 mm
20 mm
25 mm
30 mm
50 mm

There were five Endevco unsteady pressure transducers imbedded in the blade as seen in Figure 6. These were placed in a line 50 mm from the tip of the blade. This would be the mid-span of the blade if it were to fully occupy the test section with no tip gap. The transducers were placed at mid-span since this is where most unsteady measurements are done and because the effect of tip clearance on these measurements was the major motivating factor for these tests. All five unsteady pressure transducers were located in the first 50% of chord, two on one side and three on the other. Since the blade was symmetric, the blade could be moved to negative angles of attack and thus the transducers that were on the pressure side would now be on the suction side. The opposite would be true for the transducers that had been on the suction side. In addition, the blade could be

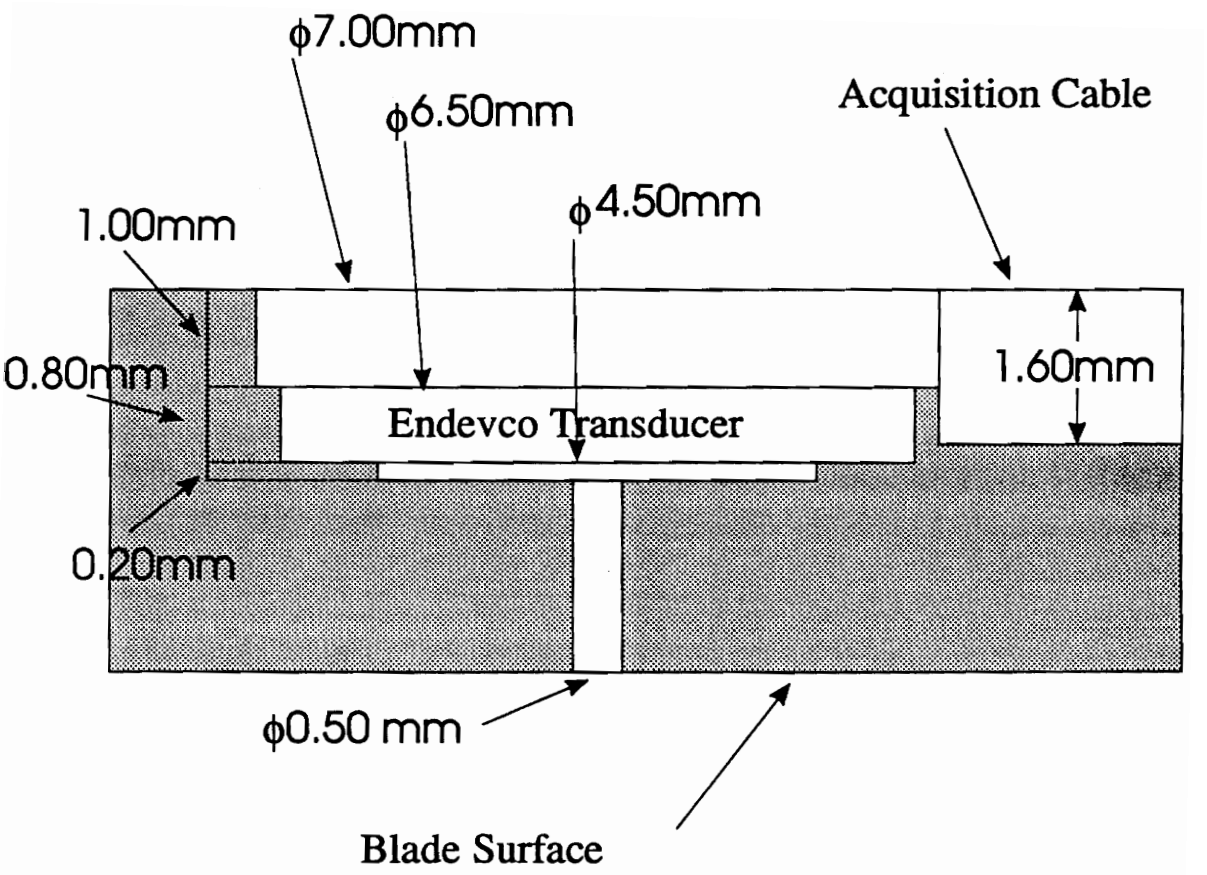

Figure 6: Unsteady Pressure Transducer Fixation

flipped around with the leading edge becoming the trailing edge to measure the last 50% of chord. Thus, with only five pressure transducers, measurements could be made at ten locations on both the pressure and suction sides of the plate. As a precaution, one of the transducers was placed close to mid-chord so that results could be compared when the blade was flipped around.

Vibration system

The blade was excited into vibration mechanically. There were two parts to the vibration mechanism. The first held the blade suspended in the hole for its passage into the test section; the second excited the blade into vibration. Figure 7 shows pictorial views of the system and Figure 8 shows a side photo of the vibration mechanism.

The blade was centered in the passage hole. The passage size decreased before entering the test section to reduce the amount of flow that could possibly enter the test section. At high angles of attack there was some flow into the test section through this passage. When centered there was a 1.5 mm gap all around the blade to allow it to vibrate freely. Two springs were used to connect the blade to the steel plate. They were connected to the blade by a clamping system. Clamps also held them on the surface of the steel plate. The whole system supporting the blade could be adjusted to allow the blade to be centered in the hole.

A slider crank mechanism was used to vibrate the blade. The crank consisted of a cylindrical axis with the crank attached eccentrically. The crank transformed the rotational motion of the cylindrical axis into a linear motion of the plate. The center of the crank was located 0.5 mm off the center of the cylindrical axis. This gave an amplitude of 0.5 mm for the vibration. However, due to flexing of the springs holding the blade, the amplitude of

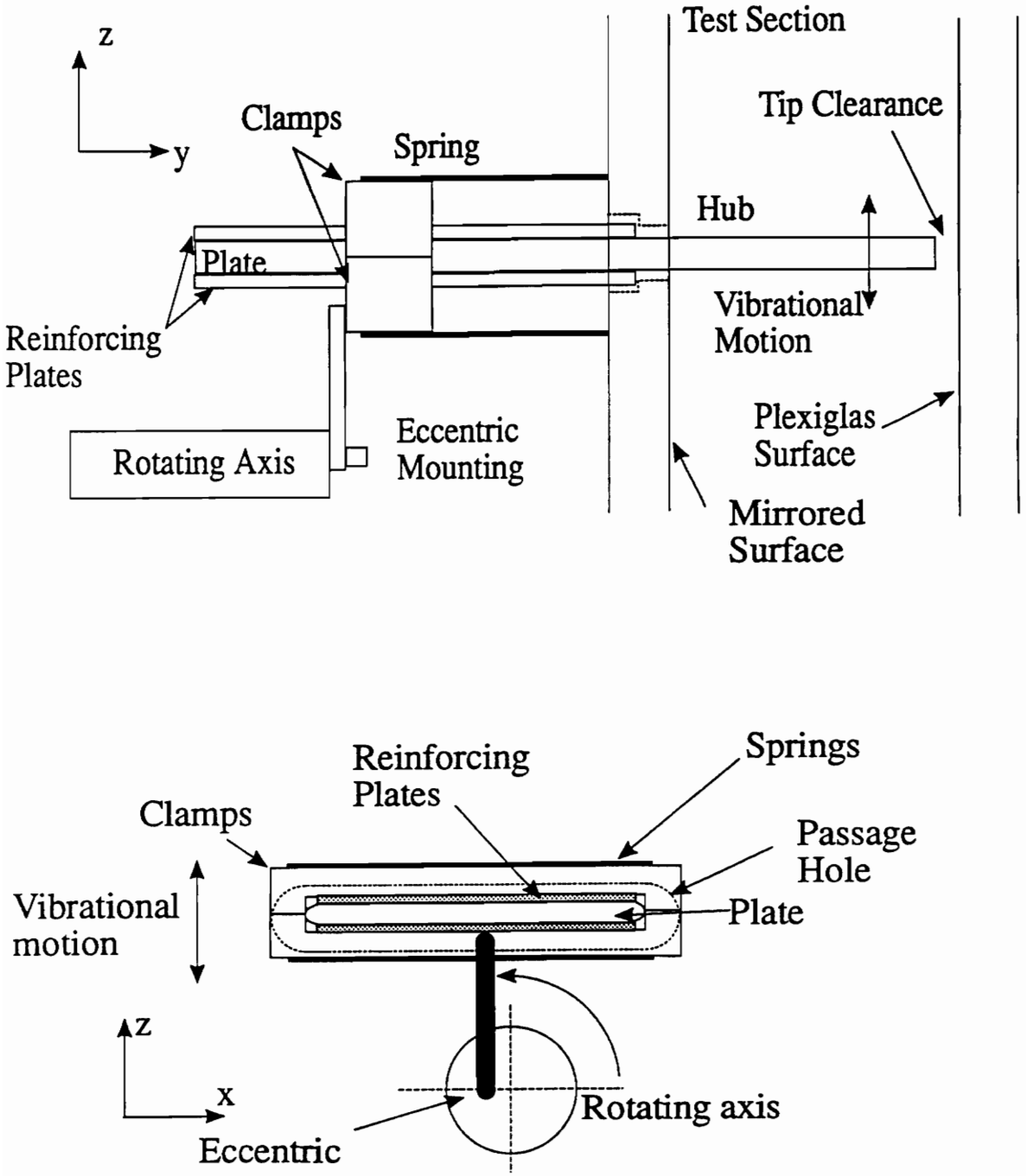

Figure 7: Pictorial of Vibration System

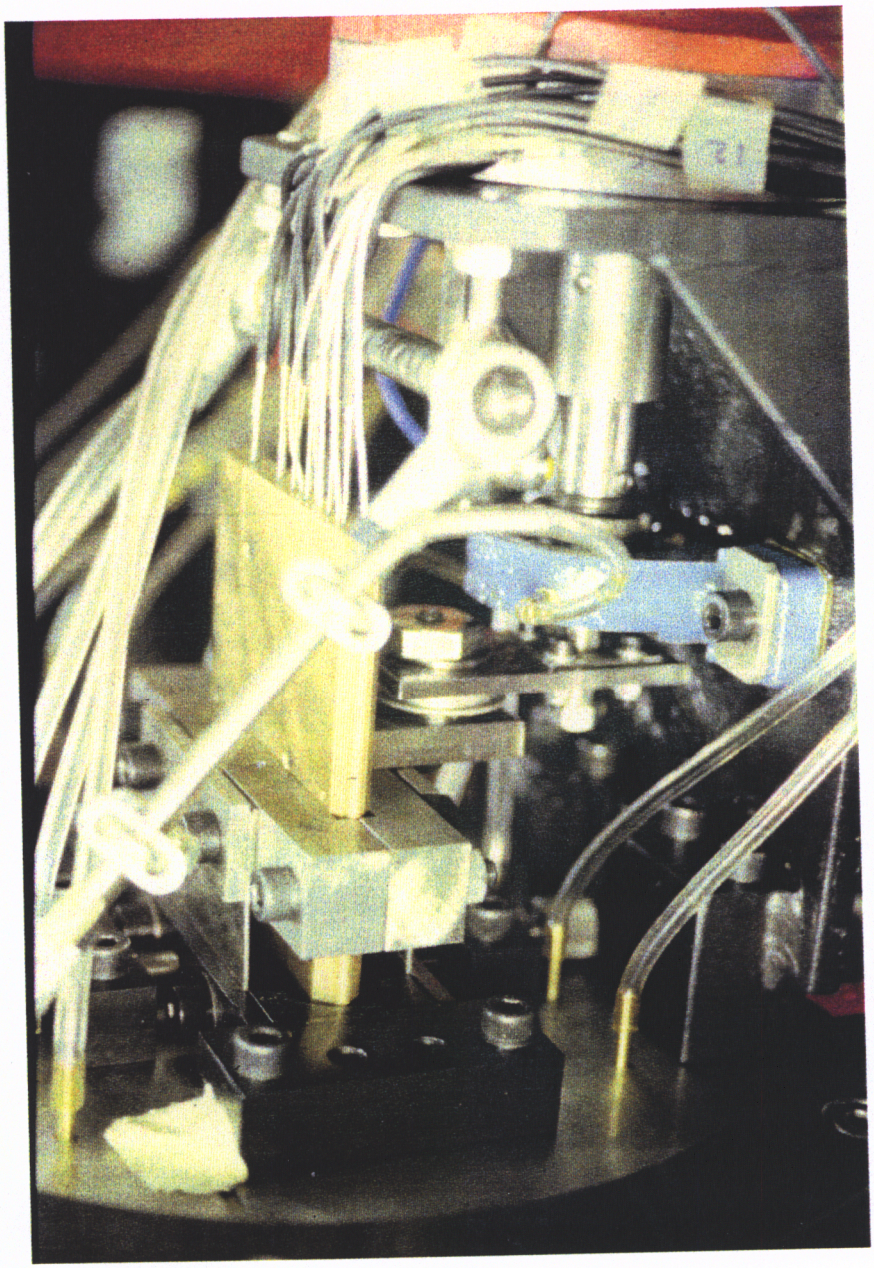

Figure 8: Vibration System

the blade vibration was measured to be only 0.3 mm. The axis was powered by a Volvo hydraulic motor. The maximum frequency obtained was 50 Hz.

Tests were done on the blade to determine its vibration characteristics. The amplitude of vibration was measured along the blade at various frequencies to verify if the blade was moving in pure translation or bending mode. These tests indicated that there was a resonance frequency of the blade between 125 Hz and 130 Hz, well away from where the tests would be conducted. The investigation of the amplitude showed that for lower frequencies, around 10 Hz, the amplitude of vibration at the tip was slightly less than at the base, on the order of 0.04 mm. The phase lag between the base of the blade and the tip of the blade was also measured and found to be on the order of 10°, which is insignificant compared to other errors present in the system. Thus, for the analysis the blade was assumed to be moving in pure translation with no phase lag along the blade height. It can be shown that the angle of incidence on the blade does not greatly vary over the period of oscillation of the blade. This is seen in Appendix II.

3.2 Data Acquisition

Steady Data Acquisition

Steady state pressures were measured at forty points in the test facility. The total pressure was measured in the settling chamber while the rest of the pressures measured were located in the test section. Twelve of these were located on the blade itself, as previously described, with the rest located on the side walls.

To measure the pressures four Scani-valve transducers were used. Thus, four pressures would be measured at a time. During the measurements the pressure would be

measured until the difference between two successive measurements was less than 2 mbar. At this point the pressure was considered to be stable and this value was recorded. Once all four of the pressures were recorded, the Scani-valves would advance to the next four pressure taps. Additionally, the total temperature was measured in the settling chamber.

Unsteady Data Acquisition

The unsteady data acquisition system acquired the signals from the five unsteady pressure transducers (Endevco Model 8515B-50) and performed some initial treatment of the signals. Table IV gives the locations of the unsteady pressure transducers. The signals from the pressure transducers passed through a high pass filter before being amplified and then going through a low pass filter. The high pass filter was used to reduce the DC signal before amplification. After the amplification the signals passed through a low pass anti-aliasing filter with a cut off frequency of 250 Hz. The signals then entered the sequential data acquisition board. The Burr Brown data acquisition board was initialized to acquire data at 500 Hz. Figure 9 shows a schematic of the acquisition systems. The data was acquired for three separate scans of 8192 points in each scan. During the scan the results were held in memory buffers and then transferred to the hard disk drive after each scan.

A Bruel-Kjaer accelerometer was placed on the blade outside of the test area to produce a reference signal for the determination of the phases of the pressures. The accelerometer signal passed through the same acquisition system as the pressure signals. It is also seen in Figure 9.

Table IV: Locations of Unsteady Pressure Transducers

Distance from Leading Edge, x	Distance from Tip of Blade, y
Side 1	Side 1
10 mm	50 mm
38 mm	50 mm
48 mm	50 mm
Side 2	Side 2
22 mm	50 mm
32 mm	50 mm

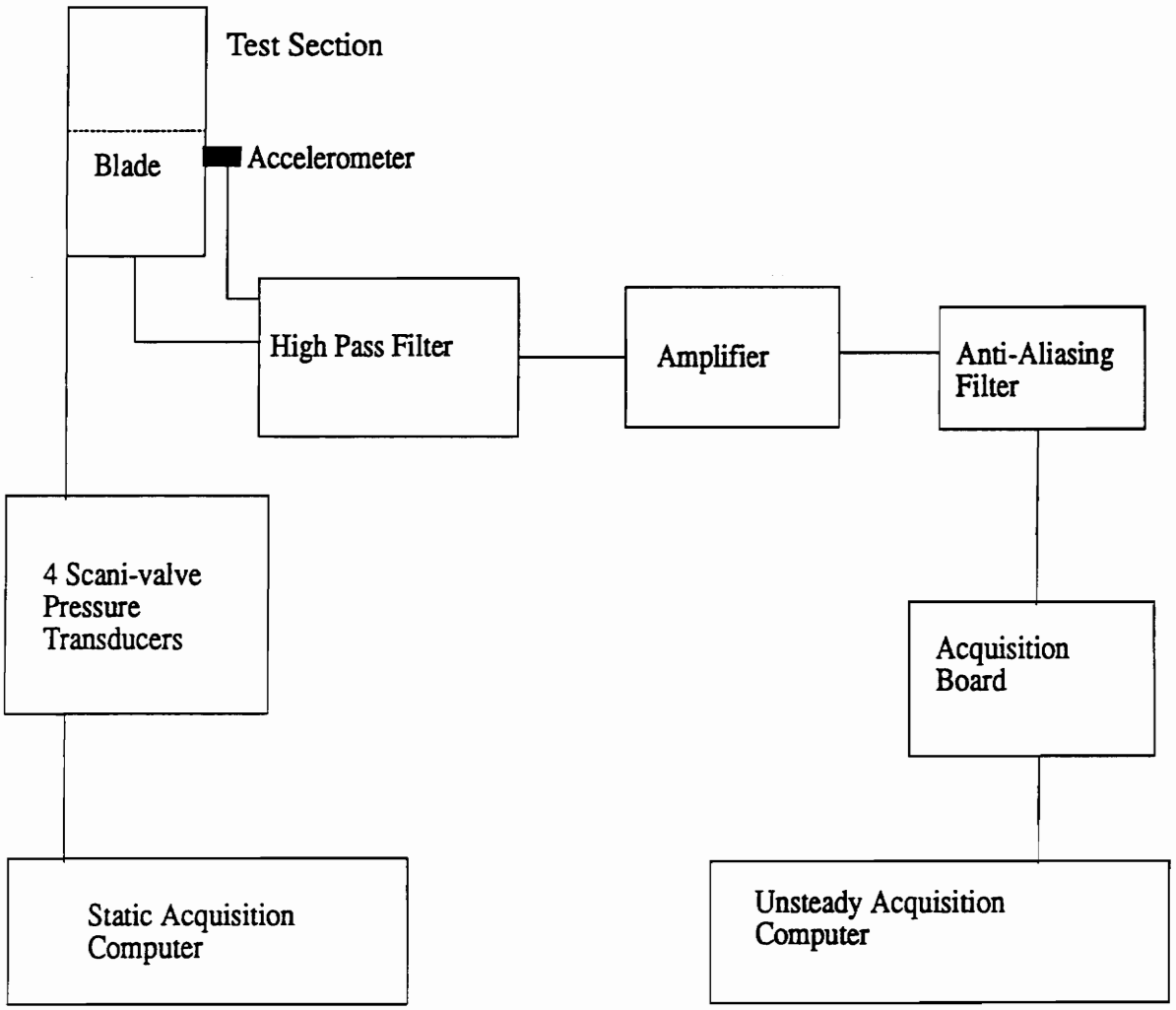

Figure 9: Data Acquisition System

3.3 Calibration

Steady State Calibration

The steady state calibration was performed before each series of tests. There existed a calibration program to calculate the new calibration coefficients needed for the Scani-valve pressure transducers based on the input pressure. The procedure consisted of reading the ambient pressure from a high precision manometer and then entering this value into the calibration program on the acquisition system. The program would then determine the new coefficients for the pressure transducers. These values were then entered into the acquisition system by hand. The output was verified to determine that the correct pressure was output by the system.

Unsteady Calibration

Dynamic calibration of the unsteady pressure measurement system was also performed before each series of tests. A steady state calibration was performed initially before any of the tests were conducted. The steady state calibration was not constantly performed since the static content from the pressure transducers was being eliminated in a high pass filter located immediately after the pressure transducers. The steady state calibration was done mainly to verify the calibration of the reference pressure transducer. The dynamic calibration was done on the entire system, including both the high pass and anti-aliasing filters, as well as the amplifier.

The static calibration consisted of applying compressed air to the reference pressure transducer and measuring the pressure with a Betz manometer. The pressure was varied through a pressure regulator and the output from the transducers was recorded. A

straight line was drawn between the points and compared to the previous calibrations to verify the transducer.

For the dynamic calibration it was necessary to have a reference transducer. Initially, three transducers were calibrated and compared for steady pressures using the procedure described above. The three transducers were then calibrated dynamically for low frequency oscillations. At low frequencies the sensitivity of the transducers for the amplitude remained about the same as for static conditions. It was also seen that the phase lag for the three transducers as they were compared with each other was fairly close in value. Since it was unlikely that all three transducers would have a phase shift in the same direction with the same magnitude, it was assumed that the average phase of the three was the average of their phase lags. One of these transducers was used as the reference transducer for the calibration of the pressure transducers imbedded in the blade.

The dynamic calibration was done by connecting the compressed air to an oscillating plate that varied the pressure periodically. This oscillating pressure was applied to both the reference transducer and the transducer being calibrated. The reference transducer was embedded in a small aluminum block with a small cavity where the air tube was connected and where the sensitive portion of the transducer was located. An O-ring surrounded this cavity. Thus, when this cavity was placed over the transducer to be calibrated, a small chamber was formed in which both transducers were located and where the varying pressure could be measured. The aluminum block was pressed against the blade and the O-ring formed a seal.

Both transducers were connected to an Hewlett-Packard Signal Analyzer. The transfer function between the actual pressure and the reference transducer was already known. The Signal Analyzer determined the transfer function, amplitude and phase,

between the reference transducer and the target transducer. These points were then plotted for different frequencies of pressure oscillations. Initially, over five points were taken for the frequency range 10 Hz to 50 Hz. Later calibrations consisted of at least three points to verify that the calibration had not strayed. The amplitude transfer function was fairly constant over the frequency range. The change was about 1%. Thus, the amplitude transfer function was considered to be constant for the range of frequencies under consideration. However, the phase transfer was not constant. It was close to linear with a coherence of about 0.98. A linear change in the phase was assumed and accounted for in the data reduction program.

4. Data

This chapter will provide a general introduction to the tests conducted, as well as the methods used to analyze the data and reduce it to a usable form. Finally, the general characteristics of the results will be discussed. The plots that are presented in this and the following chapter were chosen for their clarity in showing the points being discussed. The Appendix contains the reduced test results for all test conditions. Complete results can also be obtained from the author on computer diskette.

4.1 Tests Conducted

The tests were performed for a variety of test and flow conditions, which constituted the independent variables. These are shown in Table V.

Table V: Test Conditions

angle of attack	0°,2°,4°,6°
tip clearance (mm)	1.0,2.5,3.5
Mach number	0.23,0.4,0.6
blade frequency (Hz)	20,30,40

These independent variables were systematically changed to test all possible combinations. The dependent variables that were measured include the unsteady pressure

amplitude, expressed as the unsteady pressure coefficient, the phase lag of the pressure oscillations, and the coherence of the pressure oscillations with the blade vibrations.

The combination of Mach numbers and blade frequencies resulted in reduced frequencies ranging from 0.03 to 0.15. This is well below the range where one would normally expect unsteady influences. However, it is not too far from the region where flutter in the first bending mode begins, a reduced frequency of 0.3 (Bölcs, 1992).

4.2 Signal Analysis

Some assumptions were made to simplify the analysis of the pressure signals. The pressure signals were assumed to be ergodic and stationary. The signals were assumed to have been taken simultaneously, as opposed to sequentially. An analysis indicated that for high sampling rates, compared to the signal being investigated, that this is an acceptable assumption. The amplitude of the blade vibration was assumed to be constant and the blade signal was only used to obtain information about the phase between the blade vibration and the pressure signals.

The following steps were performed for each scan independently. The FORTRAN program REDUCE.FOR, found in Appendix III, was used to analyze the data and determine the unsteady pressure coefficients and phase angles for the different pressure transducers. The first step in analysis of the data was to subtract the mean value from both the blade and pressure signals. This did not affect the needed information from the blade signal. The desired information from the pressure signal was the phase and amplitude of vibration. A Fast Fourier Transform was done on the data. A total of fifteen FFTs were done each with 1024 points and a 50% overlap between data sets. This was done to enable averaging to be done for each scan. Autospectrums were calculated for the blade signal

and all the pressure signals as well as the cross spectrum for each pressure. These were then used to determine the transfer and coherence functions. The output of the program gave the following information for each run number: angle of attack, Mach number, vibration frequency, reduced frequency, and tip gap. In addition for each pressure transducer the following results were given for the first harmonic, or blade frequency: pressure amplitude, standard deviation of pressure amplitude, unsteady pressure coefficient, standard deviation of unsteady pressure coefficient, phase lag, standard deviation of phase lag, and coherence.

4.3 Results

The series of tests and the data reduction program produced a large set of data. The entire set of reduced data is shown in Appendix I, organized by Mach number, angle of attack and blade vibration frequency. The nomenclature used in the data plots is as follows: the variable tau is the nondimensional tip clearance; the reference length is the blade chord, c; the unsteady pressure coefficient, uCp, is used as previously defined; phi represents the phase lag of the pressure oscillation at the blade frequency. The coherence between the pressure signal and the blade is a representation of how well the pressure signal is related to the blade signal (Stearns and Hush, 1990). A coherence of 1.0 is perfect correlation between the two signals. Some trends were visible in the data, and are discussed with reference to typical plots in the following Analysis and Discussion section.

5. Analysis and Discussion

The analysis and discussion chapter is divided into three different sections. The first section will deal with general trends and conclusions that can be drawn from the data and that do not appear to be dependent on either the tip clearance or the angle of attack. The second section will concern results and conclusions dealing with changes in the tip clearance. The third section identifies conclusions that can be drawn dependent on the angle of attack.

5.1 General Results

Following are selected figures which show trends or similarities in the data, and serve as a basis for discussion.

Figure 10 is a plot of unsteady pressure coefficient along the chord of the vibrating blade, and is typical of these plots. On the suction side (top) of the plate, there is always a peak at about 20% chord, which rapidly decreases and is fairly constant at a low value along the rest of the blade chord. The unsteady pressure on the pressure side is reasonably constant at all chord positions. On a similar blade, a separation bubble has been seen on the suction side just after the curvature of the leading edge (Bölcs, 1993). It has been theorized that the bubble moves with the plate vibration.

For some cases, there appears another increase on the suction side near 80% chord. This additional increase was also reported by Triebstein (1976) for the case of a single blade oscillating in a cascade.

The coherence of the pressure signal with the blade signal decreases beyond about 50% of chord, as seen in Figure 13. This occurred for almost all flow conditions, angles of

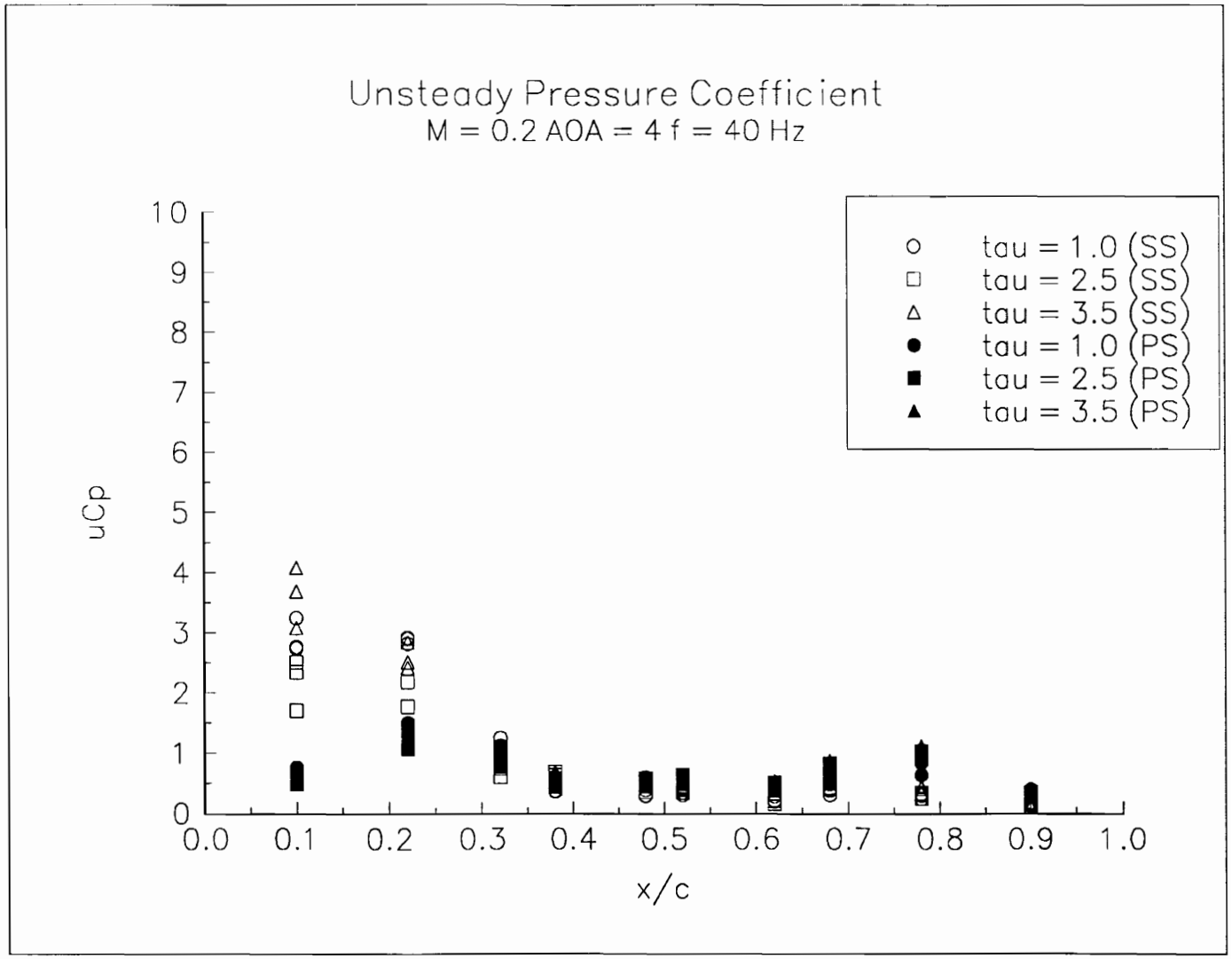

Figure 10: Typical Unsteady Pressure Coefficient Profile

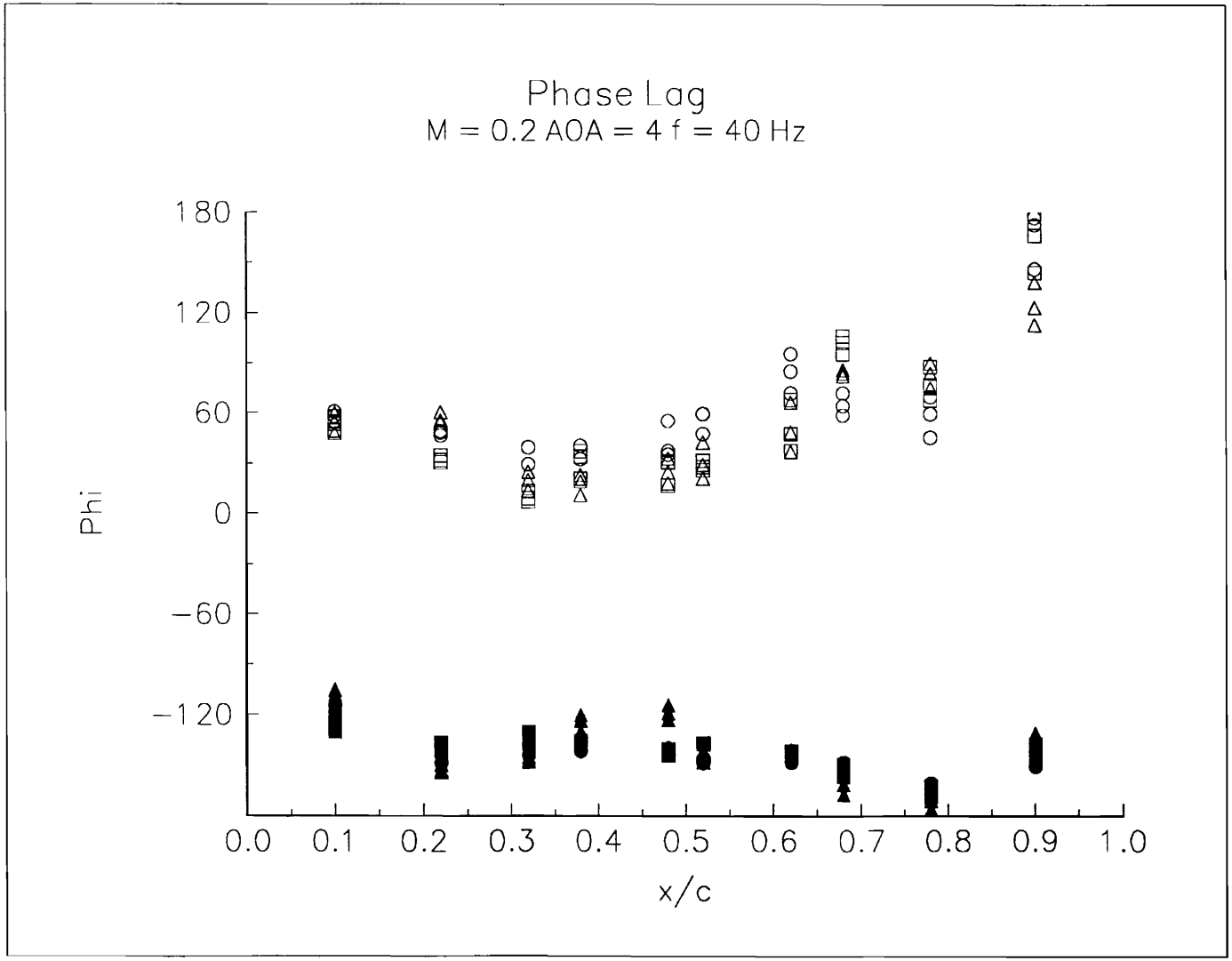

Figure 11 : Typical Phase Lags

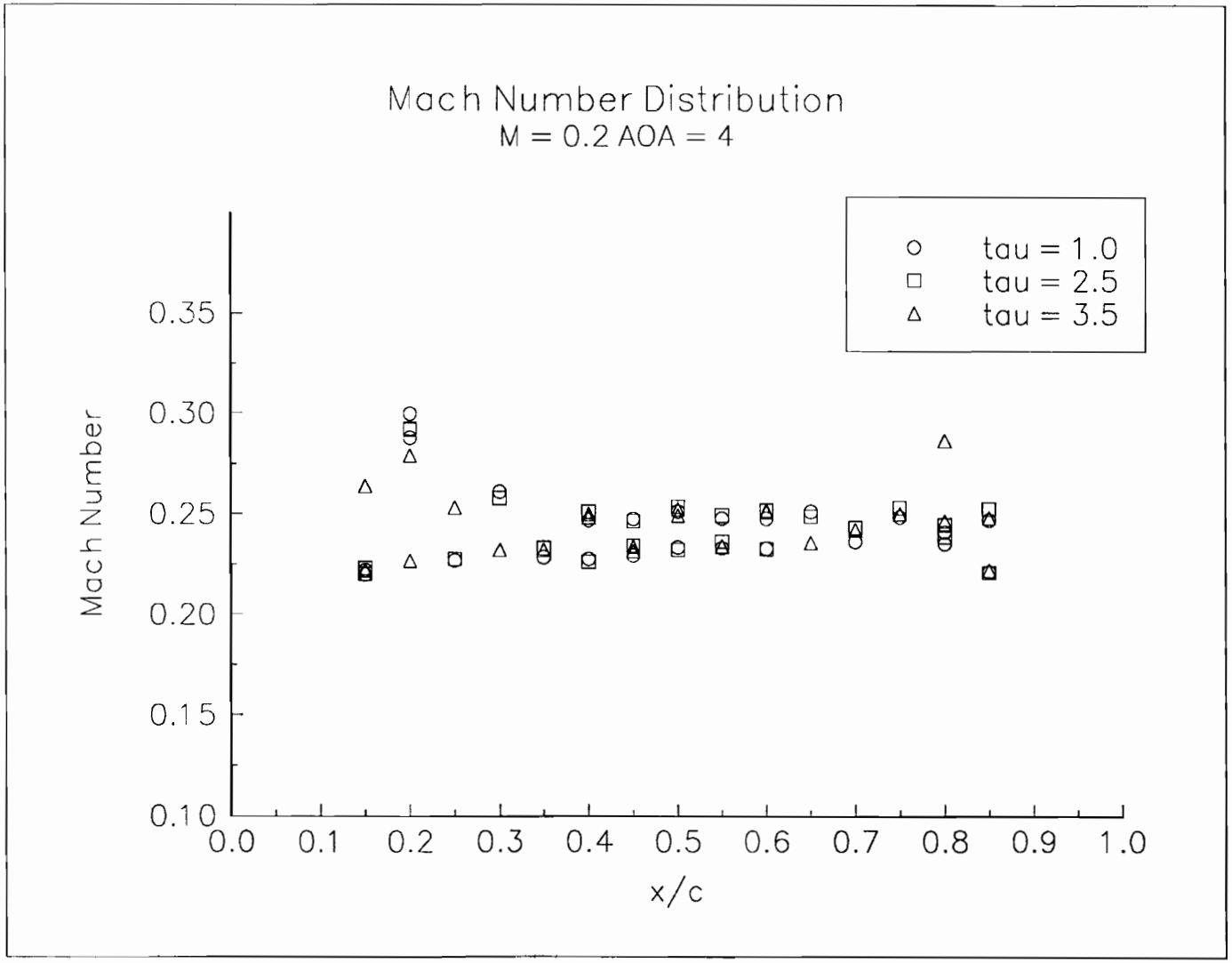

Figure 12: Typical Mach Number Distribution

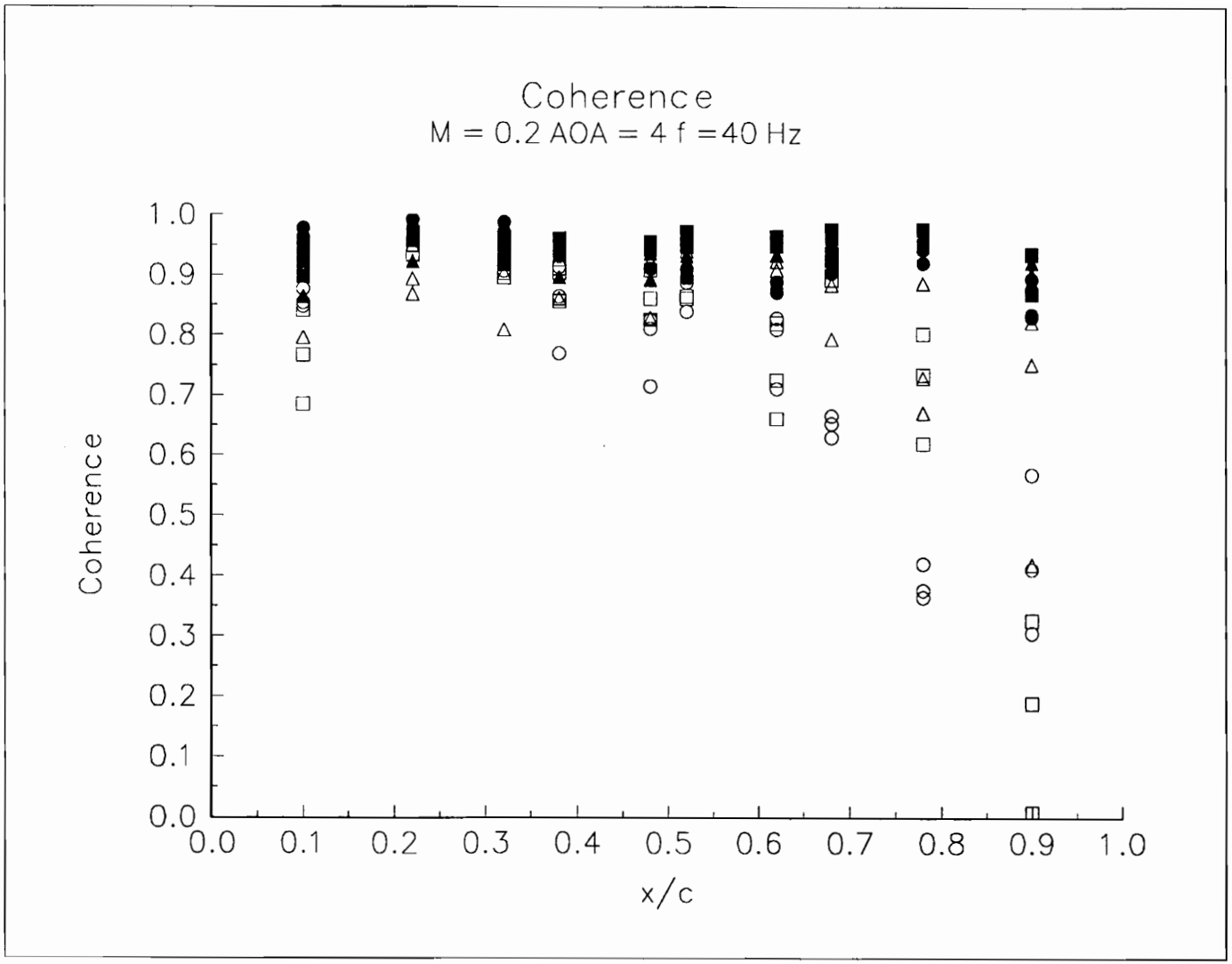

Figure 13: Typical Coherence Profile

attack, tip clearances and vibrational frequencies. A high coherence can be interpreted as indicating stable flow structures that are oscillating with the same frequency as the blade. Low coherence can be interpreted to indicate regions where there is turbulence or no coherent flow structures. This could indicate an increase in the level of turbulence over the latter portion of the blade chord. This decrease in the coherence over the second half of the blade can also be seen in work done by Triebstein and Voss (1984). They did not comment on this result.

Another trend that appeared was a dependence of coherence on the blade frequency. The coherence dropped off over the latter part of the blade and over the leading part of the chord as the frequency was decreased, as seen in Figure 14. This effect was also seen for most flow conditions. It could be suggested that high frequency blade oscillations produce more organized flow disturbances, and thus reduced turbulence.

No major influences on the parameters of the pressure side of the plate were seen. Changing the tip clearance and angle of attack had no apparent effect upon either the unsteady pressure or the phase.

5.2 Effects of Tip Clearance

From the tests conducted, the following observations can be made concerning the effect of tip clearance on various unsteady flow parameters. The size of the tip clearance does not affect either the unsteady pressure coefficient or the phase lag on the *pressure side* at mid-span. This result is to be expected, since tip clearance flows do not have much influence upon the pressure side, especially at mid-span. However, it would be possible for there to be slight influences near the tip itself.

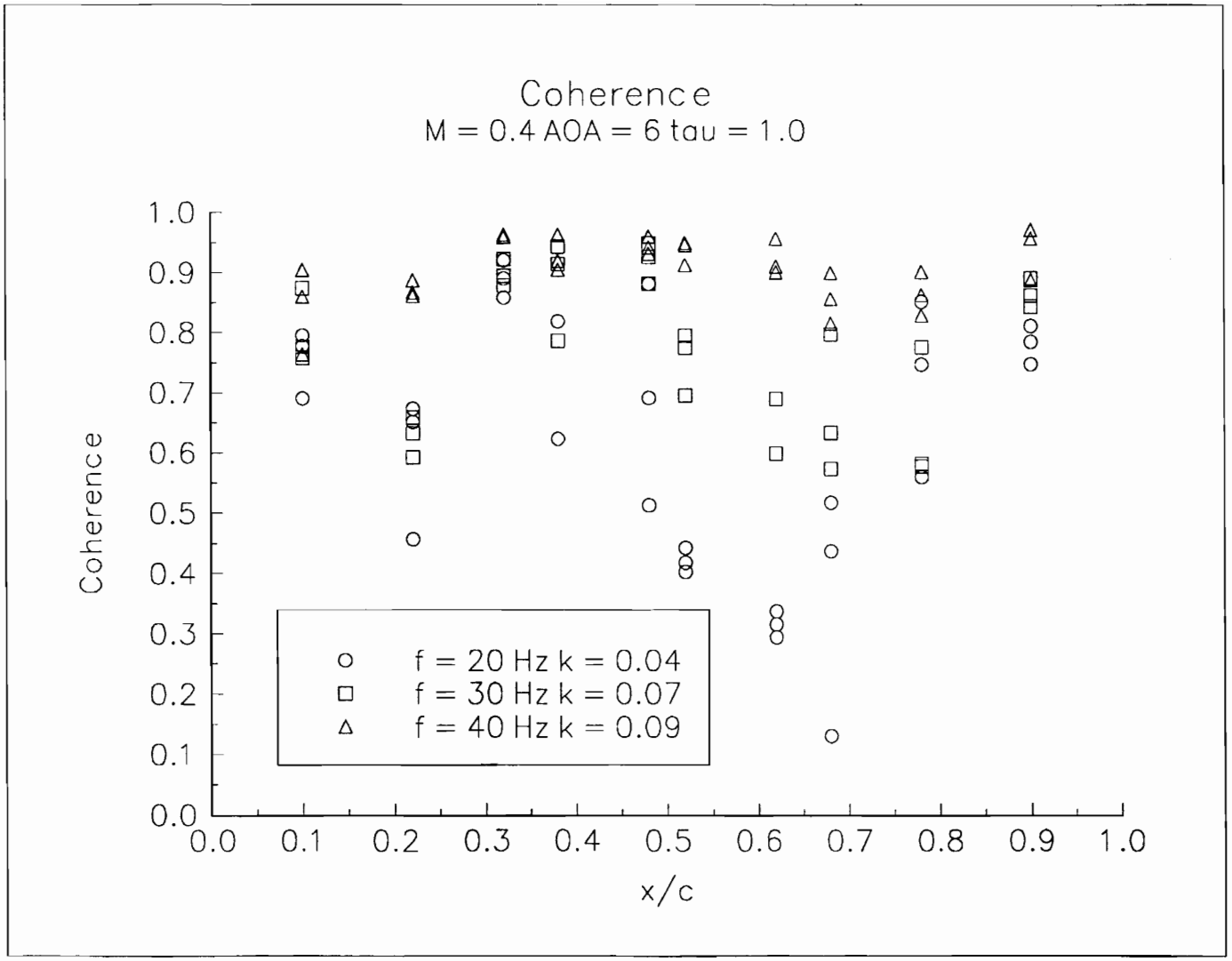

Figure 14: Coherence Dependence on Blade Frequency

If there were to be effects of the tip clearance to be seen, one would expect these effects to exist upon the *suction side* of a profile. As was noted in the literature review, effects due to the tip clearance have been seen as much as 8 to 10 tip clearance distances down the blade. For these tests however, the measurements were conducted at mid-span, a distance of 15 to 50 tip clearances down the blade, since one of the goals of these experiments was to determine how the tip clearances were affecting mid-span measurements done during flutter tests.

On the suction side effects due to the tip clearance were seen at a 6° angle of attack when the flow was approaching complete separation along the blade. This influence of tip clearance was limited to a small area of the blade near 20% to 30% of chord. For the smaller angles of attack there was no significant difference between the different tip clearances. Figure 15 shows the unsteady pressure coefficient as a function of tip clearance at 22% of chord with a frequency of 40 Hz. The error bands show a 95% confidence interval based on the total of 45 averages of the test data. One can see that the increasing tip clearance leads to an increasing unsteady pressure coefficient for the largest Mach number flow. At lower Mach numbers the change with respect to tip clearance is negligible. The dependence upon tip clearance diminishes at lower frequencies as seen in Figure 16, which shows the same flow conditions with a frequency of 20 Hz.

The phase lag for the suction side does not appear to change for different values of tip clearance. However, the phase lag is seen to increase along the chord of the blade, shown in Figure 17. This rate of increase is greater for larger angles of attack and for smaller Mach numbers. The phase lag increases along the blade because of the period of time it takes for the pressure wave to reach the end of the blade. This time period translates into a phase lag. This rate increases at lower Mach numbers since the flow speed

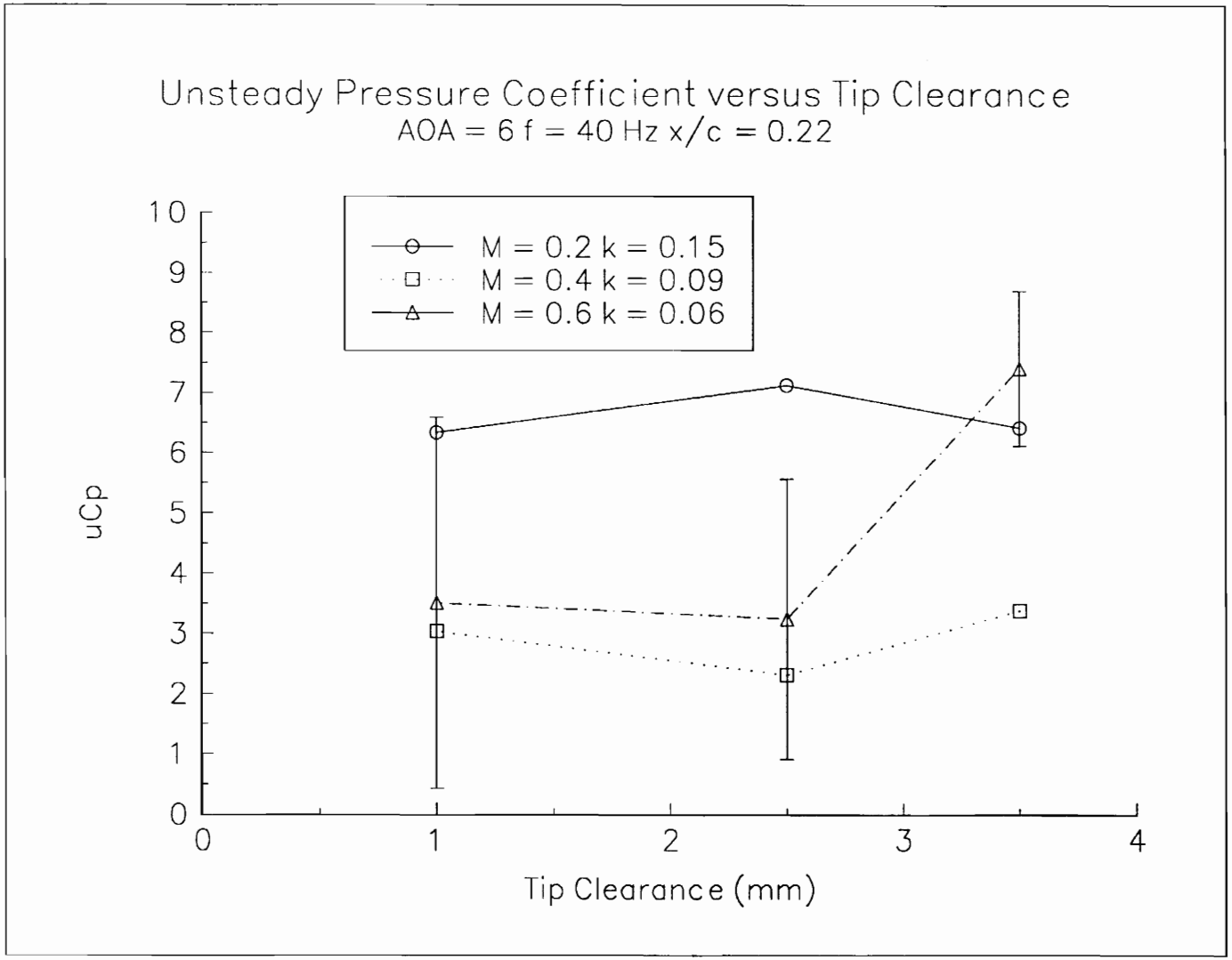

Figure 15: Effect of Tip Clearance on Unsteady Pressure Coefficient at High Frequency

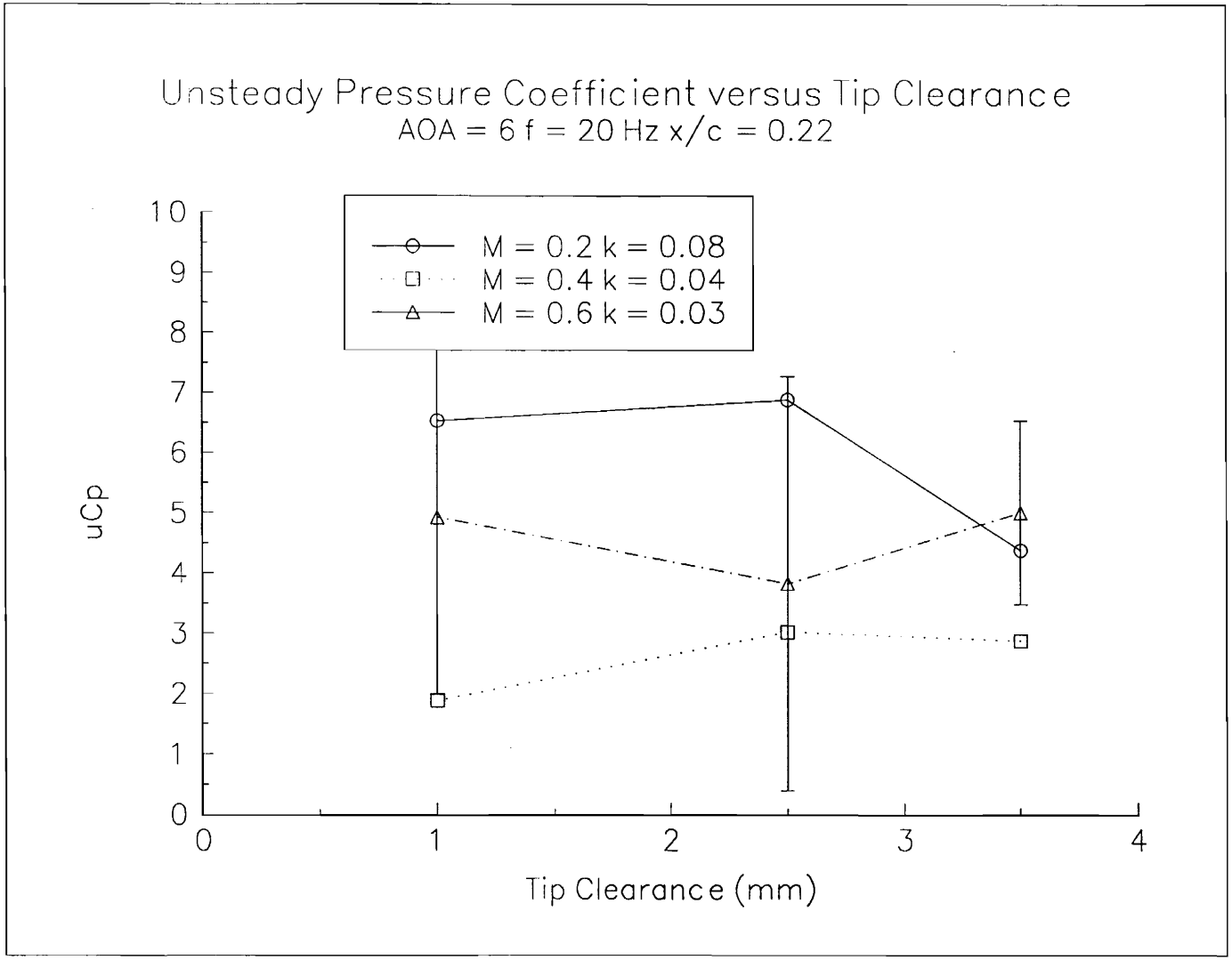

Figure 16: Effect of Tip Clearance on Unsteady Pressure Coefficient at Low Frequency

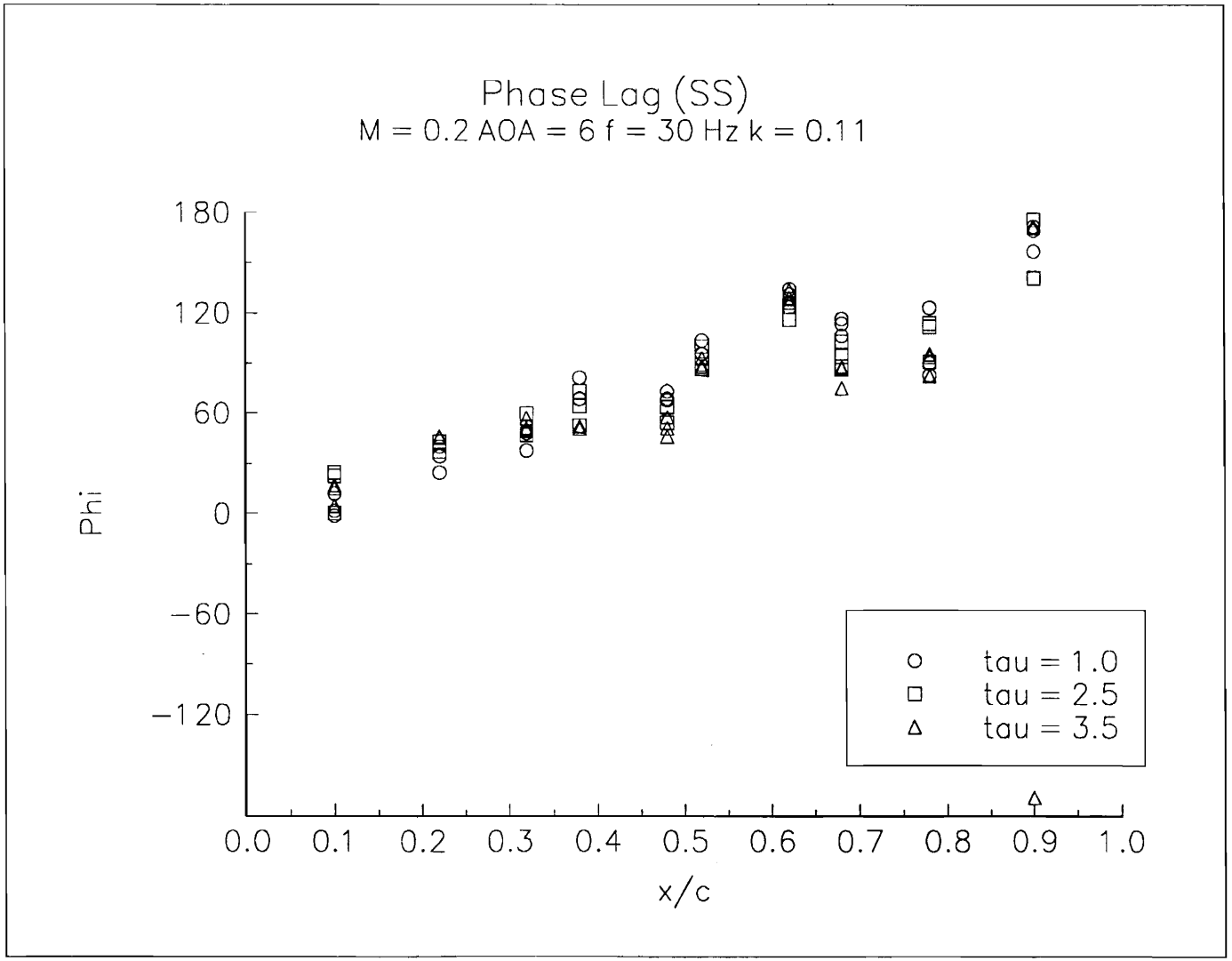

Figure 17: Increase in Phase along Blade Chord

is lower and thus the time for the wave to reach a given point on the blade is longer, and the phase lag greater.

5.3 Effects of Angle of Attack

For a 6° angle of attack there was a very noticeable change in the unsteady pressure coefficient profile along the suction side of the plate, as compared to smaller angles of attack. This is seen in Figure 18. Between about 20% and 40% of chord the unsteady pressure coefficient is much greater for this angle of attack. The basic profile of the coefficient is the same; it is the peak values which have increased. This is perhaps due to a separation bubble, or reattachment of a separation bubble. If there were separation, and the size of the separation depended on the vibration, there would be a strong correlation between the pressure measured in the region of reattachment and the vibration as the reattachment point oscillated. This would also cause a large amplitude of vibration, which is also seen at this point along the blade. For some cases the unsteady pressure coefficients for the 4° angle of attack approach that for the 6° angle of attack.

Another interesting observation may be made when comparing the results between the plots for the different tip clearances. For the larger tip clearances, 2.5 mm and 3.5 mm, the coefficients are increased up until about 40% of chord; by 50% of chord there is no discernible difference between the different angles of attack. However, for the smallest tip clearance, 1.0 mm seen in Figure 19, the unsteady pressure coefficients at a 6° angle of attack remain larger than for the other angles of attack until about 50% of chord, and sometimes further along the blade.

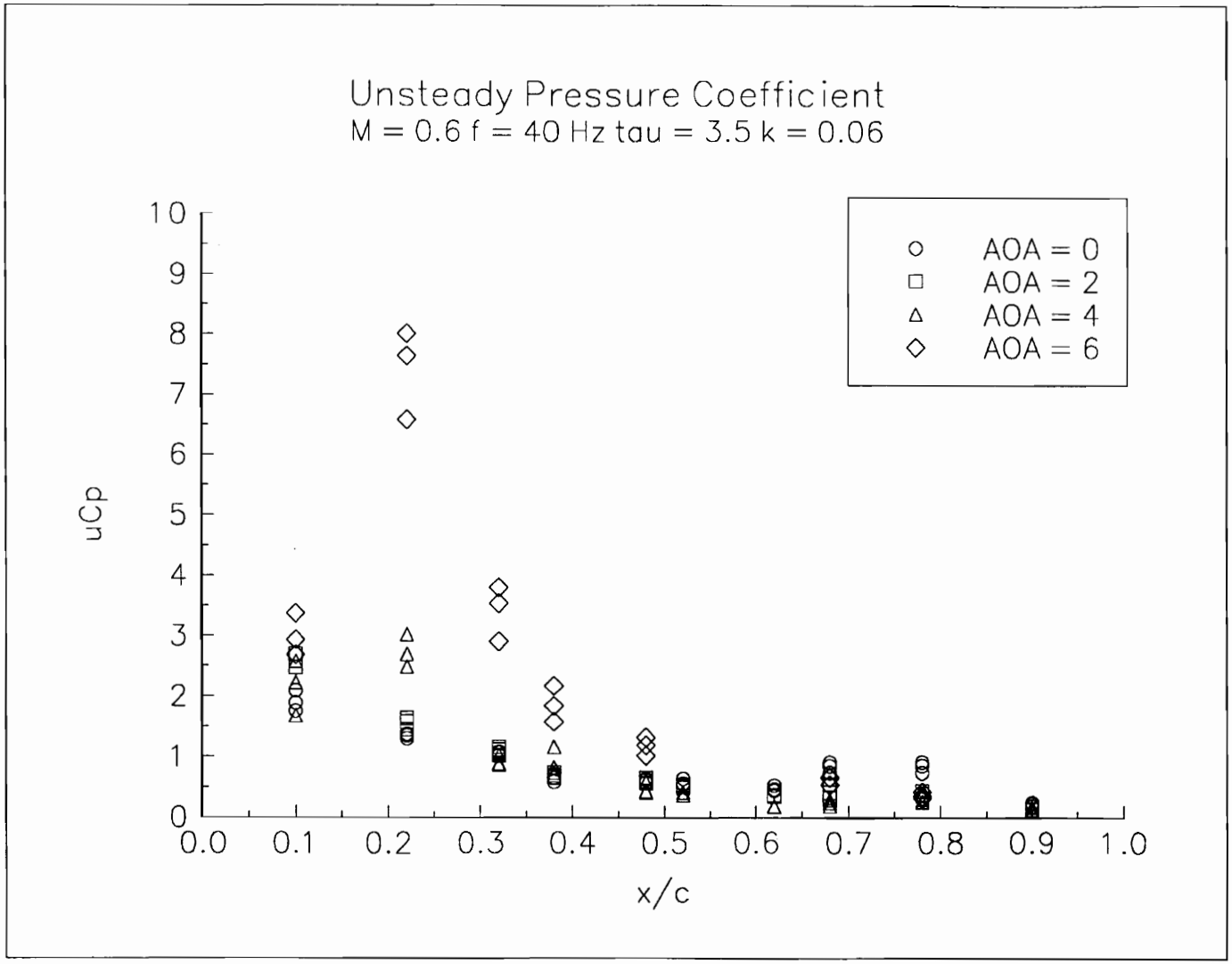

Figure 18: Effect of Angle of Attack on Unsteady Pressure Coefficient at Large Tip Clearance

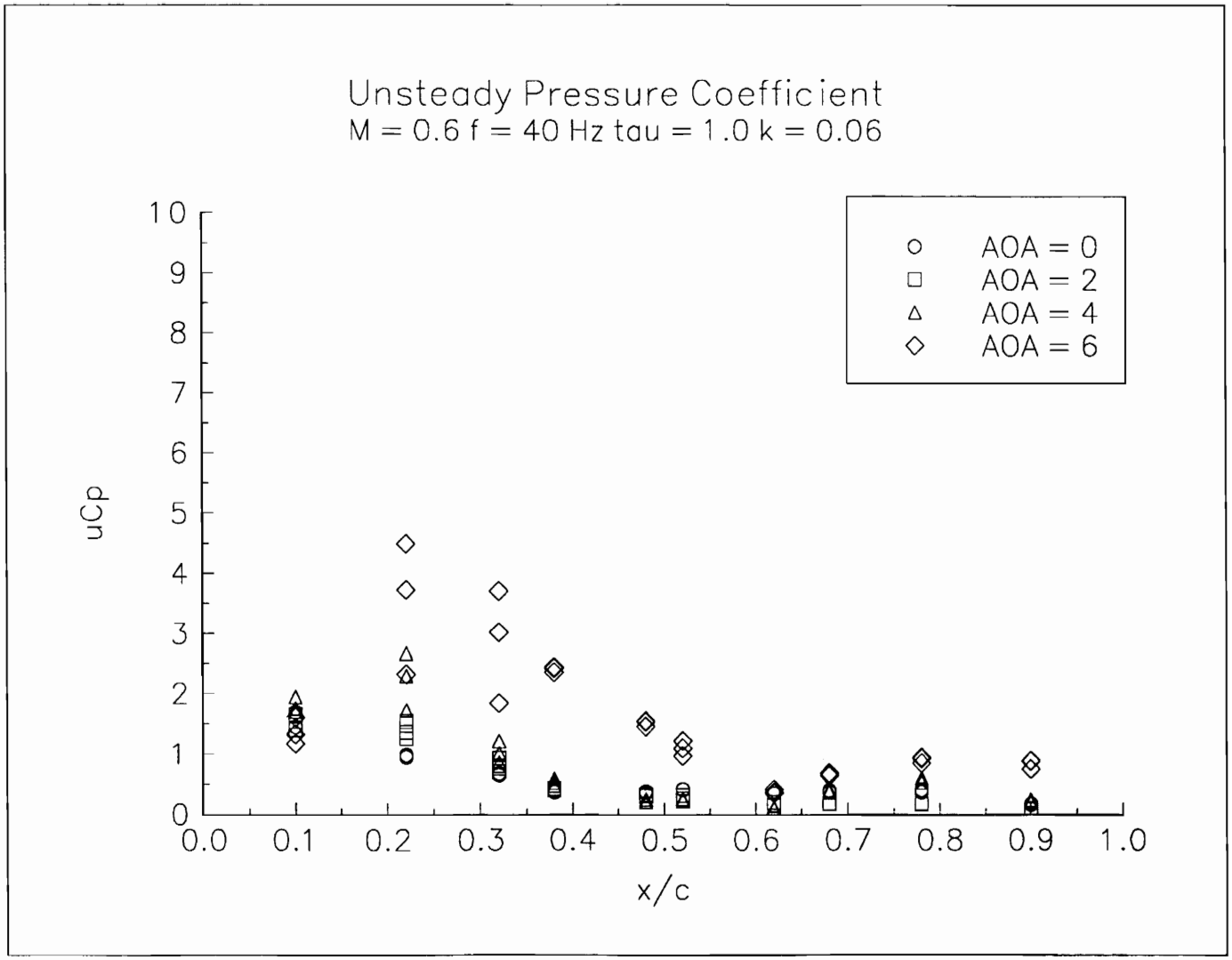

Figure 19: Effect of Angle of Attack on Unsteady Pressure Coefficient at Small Tip Clearance

6. Conclusions and Recommendations for Future Work

6.1 Conclusions

Tests were conducted on an flat plate vibrating in translation, simulating the first bending mode, to determine the influence of tip clearance and angle of attack upon the unsteady pressure measured at mid-span.

In the reported tests, it was observed that the effect of increasing tip clearance, from 1% to 3.5% of chord, was to locally increase the amplitude of the measured unsteady pressure oscillations by approximately 100% at a 6° angle of attack, a Mach number of 0.6 and a frequency of 40 Hz on the suction side of the plate. From these flat plate tests, it is inferred that tip clearance may have an effect on unsteady cascade measurements.

It was also observed that at a 6° angle of attack, for all flow cases and tip clearances, that the unsteady pressure coefficient on the suction side was locally much greater, up to 250%, than for lower angles of attack. At this angle of attack it was also observed that the region of increase amplitude vibrations was longer for the smallest tip clearance.

No changes in the response of the pressure side of the plate due to either tip clearance or angle of attack were observed.

6.2 Recommendations

Future investigations in this field are desirable. Some possible avenues of research are mentioned below.

1. Different blade profiles need to be investigated to determine how the tip clearance influences their unsteady reaction. The flat plate is a simple profile. Cambered blades would provide additional phenomena to be considered.

2. Having seen the effects of tip clearance at the mid-span, where no previous steady influences had been observed, an investigation of unsteady effects closer to the tip gap should also be conducted.

3. Testing should also be conducted at higher reduced frequencies. It has been theorized that unsteady phenomena become more important as the reduced frequency increases.

4. A more detailed study into why there is an effect due to tip clearance in the area where reattachment of a separation bubble is occurring.

References

Bindon, J. P. (1988) "The Measurement and Formation of Tip Clearance Loss." ASME Journal of Turbomachinery. Volume 111, Number 3, July 1989. p.256-263. ASME 88 - GT - 203.

Bölcs, A. (1993) Personal communication.

Bölcs, A. (1992) "Turbomachines Thermiques: Volume II" Laboratoire de Thermique Appliquée et de Turbomachines, Ecole Polytechnique Fédérale de Lausanne, Switzerland. 1992.

Bölcs, A., Fransson, T. H., and Schläfli, D. (1989) "Aerodynamic Superposition Principle in Vibrating Turbine Cascades" AGARD, 74th Specialists' Meeting of the Propulsion and Energetics Panel on Unsteady Aerodynamic Phenomena in Turbomachines, Luxembourg, August 28 - September 1989.

Dishart, P. T., and Moore, J. (1989) "Tip Leakage Losses in a Linear Turbine Cascade." Gas Turbine and Aeroengine Congress and Exposition, Toronto, Canada, June 1989. ASME 89 - GT - 56.

Fransson, T. H. (1991) "Aeroelasticity in Axial-Flow Turbomachines: A Brief Introduction in the Form of Lecture Notes." Part of a Lecture Series given at Ecole Polytechnique Fédérale de Lausanne, Switzerland, and Ecole Centrale de Lyon, France, January 1991.

Fransson, T. H. (1990) Analysis of Experimental Time-Dependent Blade Surface Pressures from an Oscillating Turbine Cascade with the Influence-Coefficient Technique."

Gas Turbine and Aeroengine Congress and Exposition, Brussels, Belgium, June, 1990. ASME 90 - GT - 255.

Fung, Y. C. (1969) An Introduction to The Theory of Aeroelasticity. Dover Publications, New York, New York. 1969.

Heyes, F. J. G., Hodson, H. P., and Dailey, G. M. (1991) "The Effect of Blade Tip Geometry on the Tip Leakage Flow in Axial Turbine Cascades." International Gas Turbine and Aeroengine Congress and Exposition, Orlando, Florida, June 1991. ASME 91 - GT - 135.

Moore, J., and Tilton, J. S. (1987) "Tip Leakage Flow in a Linear Turbine Cascade." Gas Turbine Conference and Exhibition, Anaheim, California, June 1987. ASME 87 - GT - 222.

Moore, J., Moore, J. G., Henry, G. S., and Chaudhry, U. (1988) "Flow and Heat Transfer in Turbine Tip Gaps." ASME Journal of Turbomachinery. Volume 111, Number 3, July 1989. P. 301 - 309. ASME 88 - GT - 188.

Platzer, M. F. (1990) "Aeroelasticity: Lecture Notes" Ecole Polytechnique Fédérale de Lausanne, Switzerland. 1990.

Senoo, Y. (1987) "Pressure Losses and Flow Field Distortion Induced by Tip Clearance of Centrifugal and Axial Compressors." JSME International Journal. Volume 30, Number 261. p.375-385.

Sjolander, S. A., and Amrud, K. K. (1986) "Effects of Tip Clearance on Blade Loading in a Planar Cascade of Turbine Blades." ASME Journal of Turbomachinery. volume 109, April 1987. p.237-245. ASME 86 - GT - 245.

Stearns, S., and Hush, D. R. (1990) Digital Signal Analysis, Second Edition.. Prentice Hall, Inc. New Jersey.

Triebstein, H. (1976) "Unsteady Pressures on a Harmonically Oscillating Staggered Cascade in Incompressible and Compressible Flow." Revue Française de Mécanique Symposium I. U. T. A. M. sur L'Aéroélasticité dans les Turbomachines, Paris, 1976 p. 115-122

Triebstein, H., and Voss, R. (1984) "Transonic Pressure Distribution on a Two-Dimensional 0012 and Supercritical MBB-A3 Profile Oscillating in Heave and Pitch." AGARD Conference Proceedings No. 374 Transonic Unsteady Aerodynamics and its Aeroelastic Applications. 59th Meeting of the Structures and Materials Panel, Toulouse, France, September 1984.

Watanabe, T., and Kaji, S. (1987) "Unsteady Aerodynamic Characteristics of Oscillating Cascade with Tip Clearance." Unsteady Aerodynamics and Aeroelasticity of Turbomachines and Propellers, Proceedings of the Fourth International Symposium. Aachen, West Germany, 6-10 September 1987. Editors H. E. Gallus and S. Servaty. p. 405-435.

Yamamoto, A. (1988) "Interaction Mechanisms Between Tip Leakage Flow and the Passage Vortex in a Linear Turbine Cascade." ASME Journal of Turbomachinery. Volume 110, Number 3, July 1988. p. 329-338.

Yamamoto, A. (1988) "Endwall Flow/Loss Mechanisms in a Linear Turbine Cascade with Blade Tip Clearance." ASME Journal of Turbomachinery. Volume 111, Number 3, July 1989. p. 264-275. ASME 88 - GT - 235.

Yaras, M., and Sjolander, S. A. (1989) "Development of the Tip-Leakage Flow Downstream of a Planar Cascade of Turbine Blades: Vorticity Field." Gas Turbine and Aeroengine Congress and Exposition, Toronto, Canada, June, 1989. ASME 89 - GT - 55.

Yaras, M., and Sjolander, S. A. (1990) "Prediction of Tip-Leakage Losses in Axial Turbines." Gas Turbine and Aeroengine Congress and Exposition, Brussels, Belgium, June, 1990. ASME 90 - GT - 154.

Yaras, M. I., and Sjolander, S. A. (1991) "Effects of Simulated Rotation on Tip Leakage in a Planar Cascade of Turbine Blades Part I: Tip Gap Flow." International Gas Turbine and Aeroengine Congress and Exposition, Orlando, Florida, June, 1991. ASME - GT - 127.

Yaras, M. I., Sjolander, S. A., and Kind, R. J. (1991) "Effects of Simulated Rotation on Tip Leakage in a Planar Cascade of Turbine Blades Part I: Downstream Flow Field and Blade Loading." International Gas Turbine and Aeroengine Congress and Exposition, Orlando, Florida, June, 1991. ASME - GT - 128.

Yaras, M., Yingkang, Z., and Sjolander, S. A. (1988) "Flow Field in the Tip Gap of a Planar Cascade of Turbine Blades." ASME Journal of Turbomachinery. Volume 111, Number 3, July 1989. p. 276-283. ASME 88 - GT - 29.

Appendix I

This appendix contains plots of all the data collected during the series of experiments. Each page shows plots of unsteady pressure coefficient, phase lag, Mach number distribution, and coherence along the blade for a given Mach number, Angle of Attack and Frequency. All three tip clearances are shown on each graph. The plots showing Mach number distribution do not change for varying frequency, since the static pressure was not found to be dependent on the frequency of oscillation. The graphs are arranged as follows: first, the Mach number and angle of attack are held constant as the frequency is increased, then the angle of attack is increased, and finally, the Mach number is increased.

There are some items to be noted for the data taken at an angle of attack of 0°. It was assumed that the results from one side would be equal to the other. This is why there is only one set of data for the measurements. Due to this assumption the graphs depicting the phase lag have some data points with lags of about 0° and other data points with phase lags of 180°, since two of the five unsteady pressure measurements were taken on the opposite side.

Those interested in the full data set, both steady and unsteady, can contact the author for a diskette of the data.

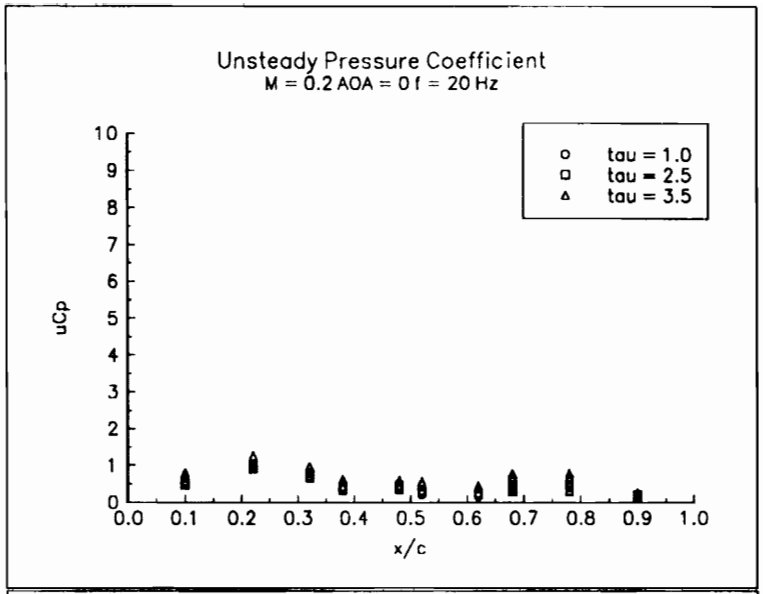
Unsteady Pressure Coefficient
M = 0.2 AOA = 0 f = 20 Hz
tau = 1.0
tau = 2.5
tau = 3.5
uCp
x/c

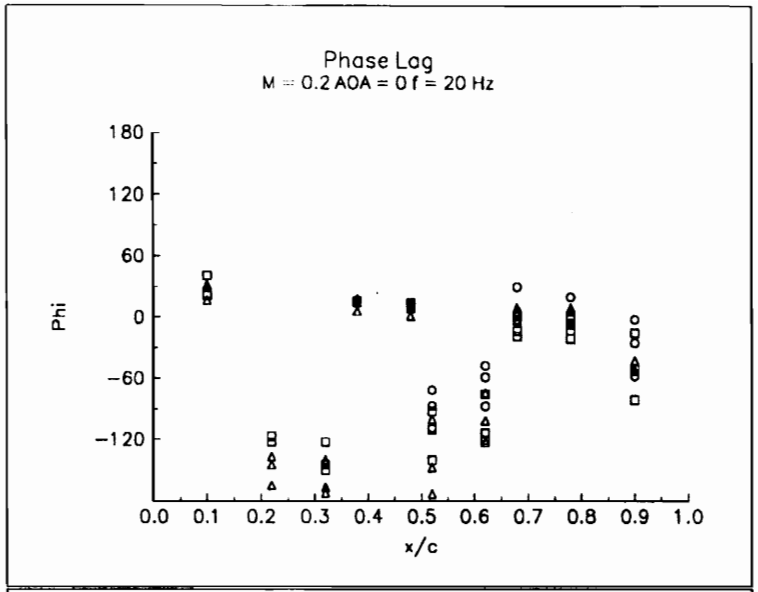
Phase Lag
M = 0.2 AOA = 0 f = 20 Hz
Phi
x/c

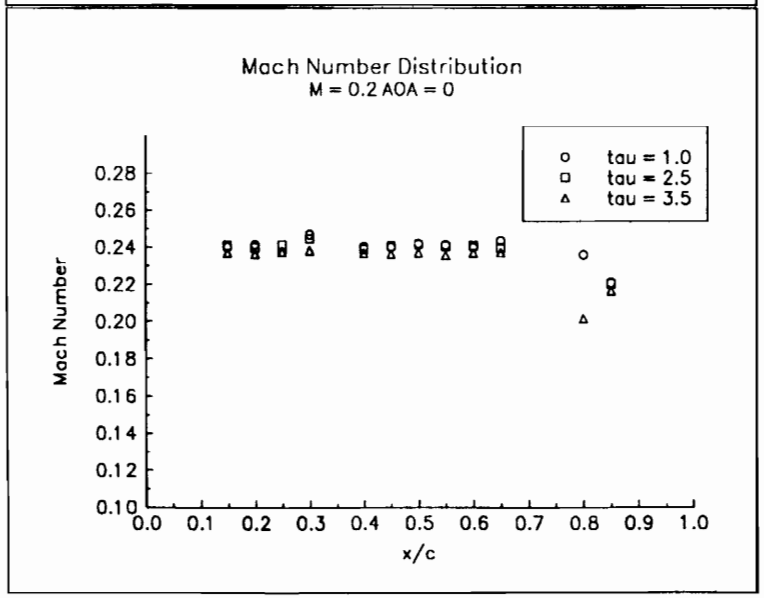
Mach Number Distribution
M = 0.2 AOA = 0
tau = 1.0
tau = 2.5
tau = 3.5
Mach Number
x/c

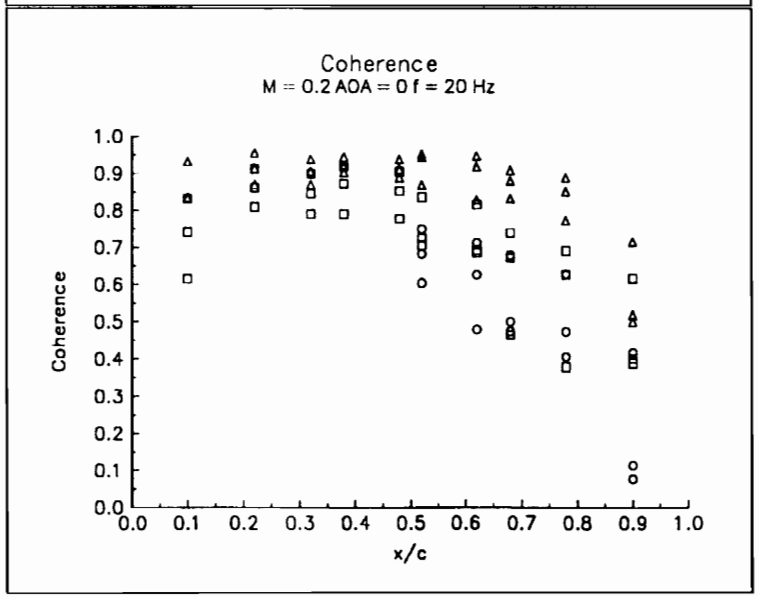
Coherence
M = 0.2 AOA = 0 f = 20 Hz
Coherence
x/c

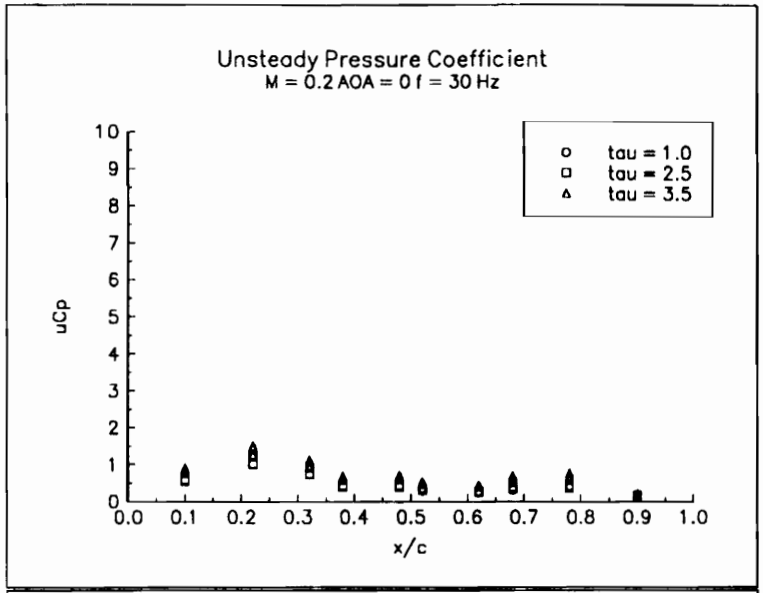
Unsteady Pressure Coefficient
M = 0.2 AOA = 0 f = 30 Hz
tau = 1.0
tau = 2.5
tau = 3.5
uCp
x/c

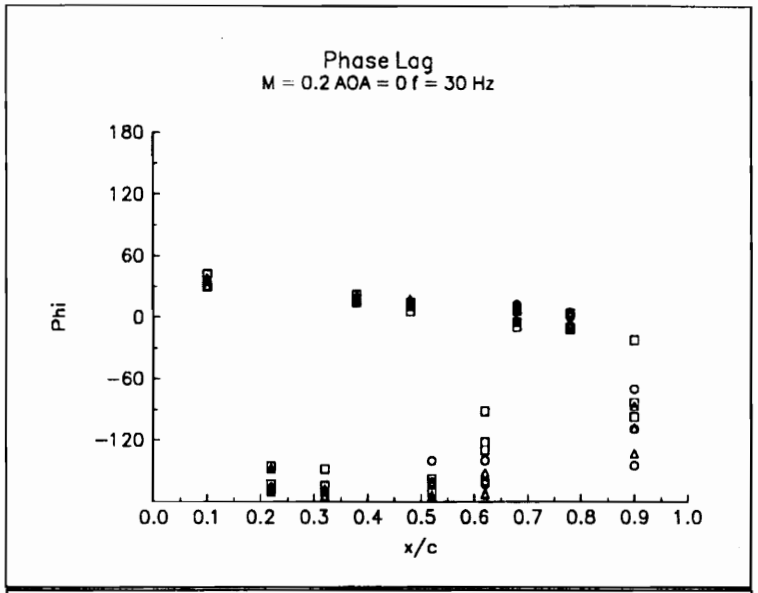
Phase Lag
M = 0.2 AOA = 0 f = 30 Hz
Phi
x/c

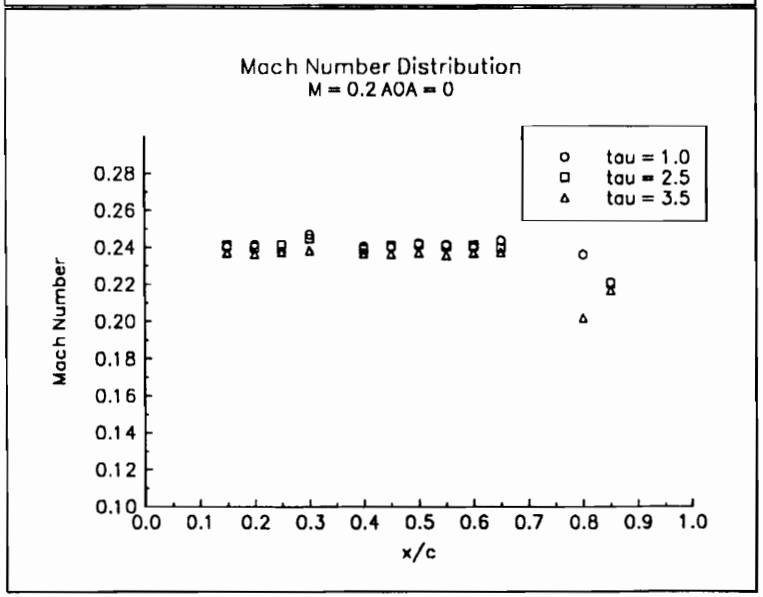
Mach Number Distribution
M = 0.2 AOA = 0
tau = 1.0
tau = 2.5
tau = 3.5
Mach Number
x/c

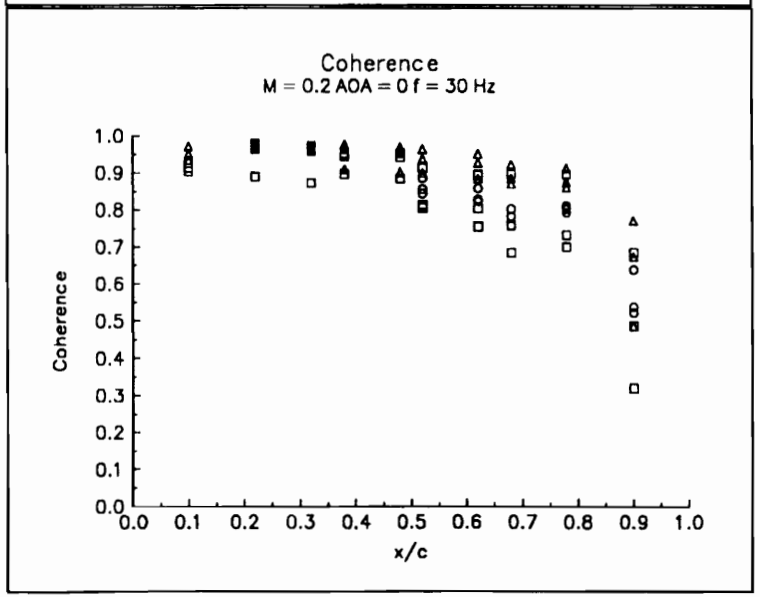
Coherence
M = 0.2 AOA = 0 f = 30 Hz
Coherence
x/c

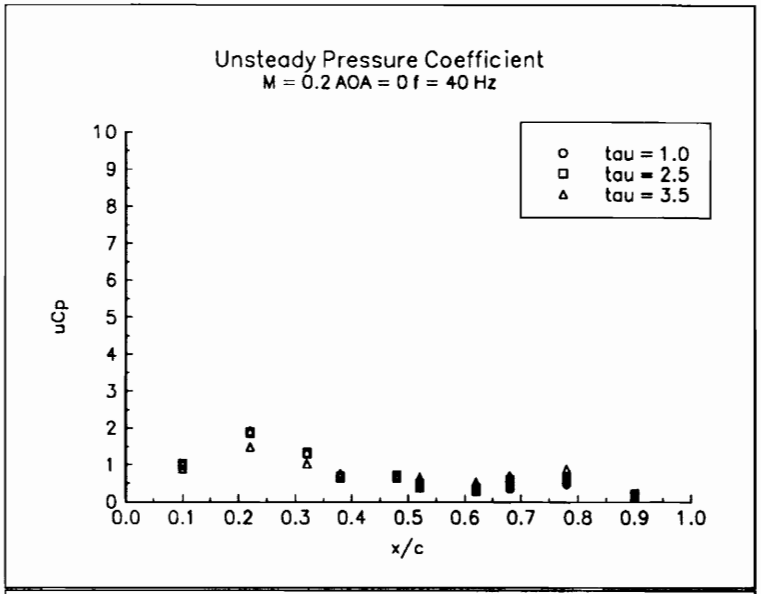
Unsteady Pressure Coefficient
M = 0.2 AOA = 0 f = 40 Hz
tau = 1.0
tau = 2.5
tau = 3.5
uCp
x/c

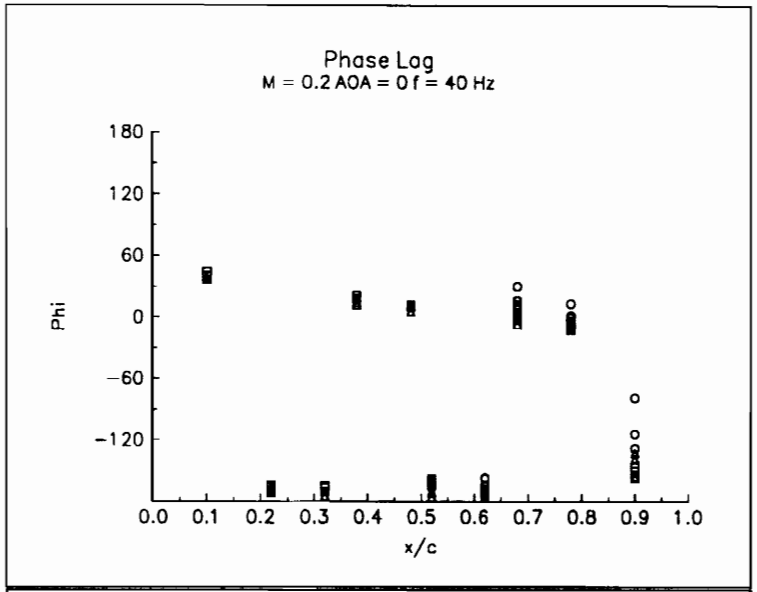
Phase Lag
M = 0.2 AOA = 0 f = 40 Hz
Phi
x/c

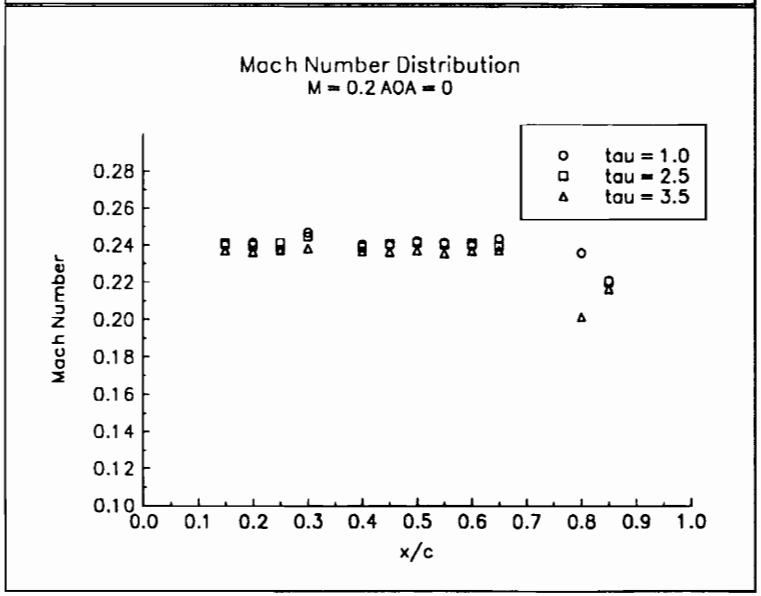
Mach Number Distribution
M = 0.2 AOA = 0
tau = 1.0
tau = 2.5
tau = 3.5
Mach Number
x/c

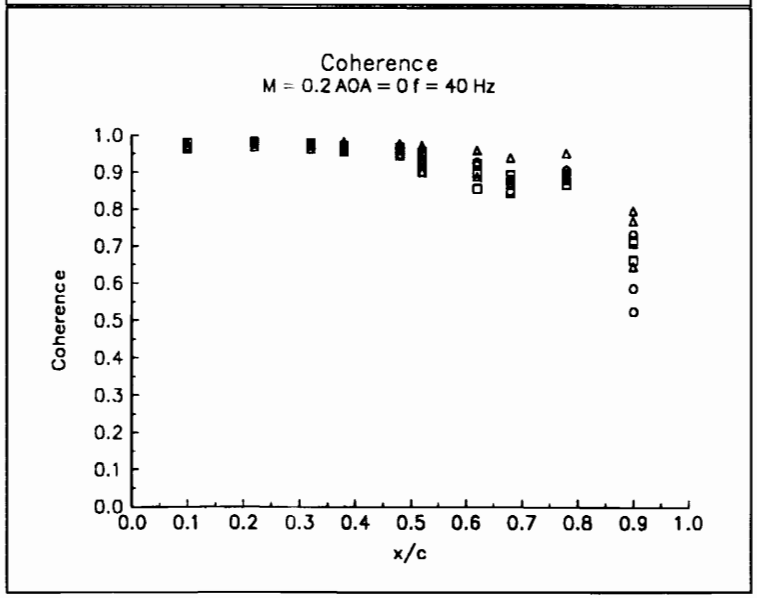
Coherence
M = 0.2 AOA = 0 f = 40 Hz
Coherence
x/c

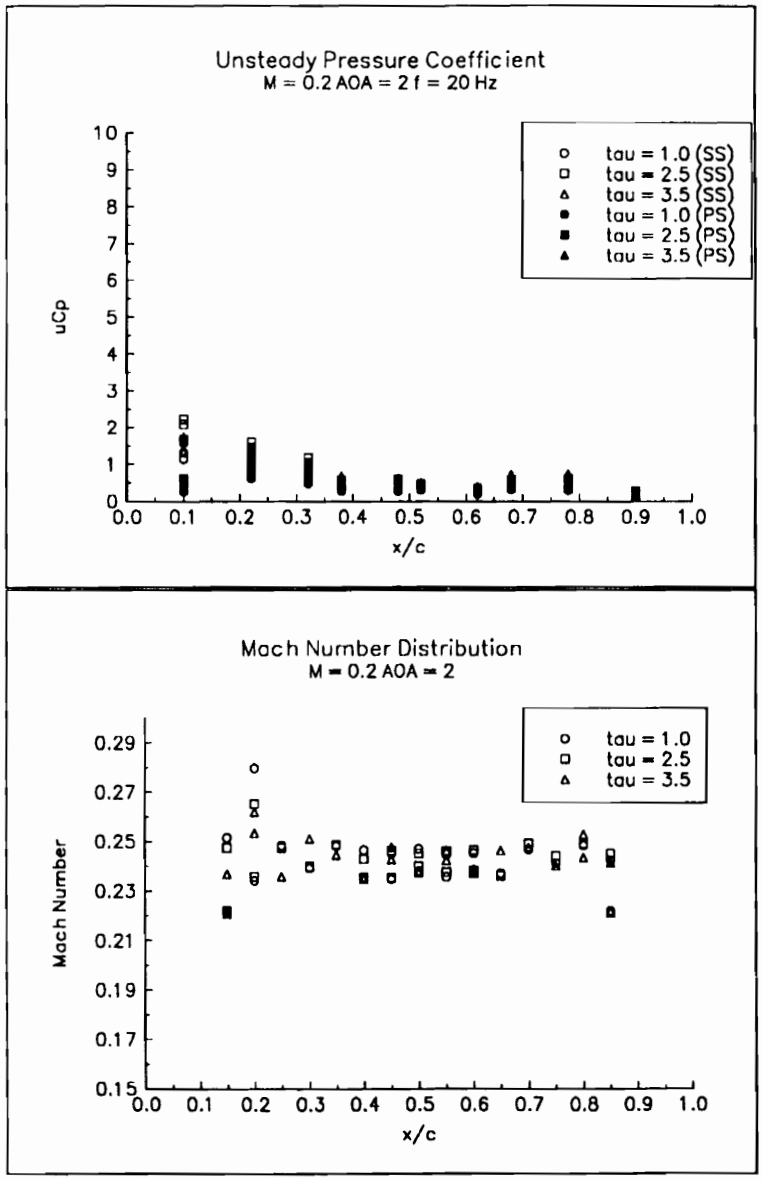
Unsteady Pressure Coefficient
M = 0.2 AOA = 2 f = 20 Hz
uCp
x/c
tau = 1.0 (SS)
tau = 2.5 (SS)
tau = 3.5 (SS)
tau = 1.0 (PS)
tau = 2.5 (PS)
tau = 3.5 (PS)
Phase Lag
M = 0.2 AOA = 2 f = 20 Hz
Phi
x/c
Mach Number Distribution
M = 0.2 AOA = 2
Mach Number
x/c
tau = 1.0
tau = 2.5
tau = 3.5
Coherence
M = 0.2 AOA = 2 f = 20 Hz
Coherence
x/c

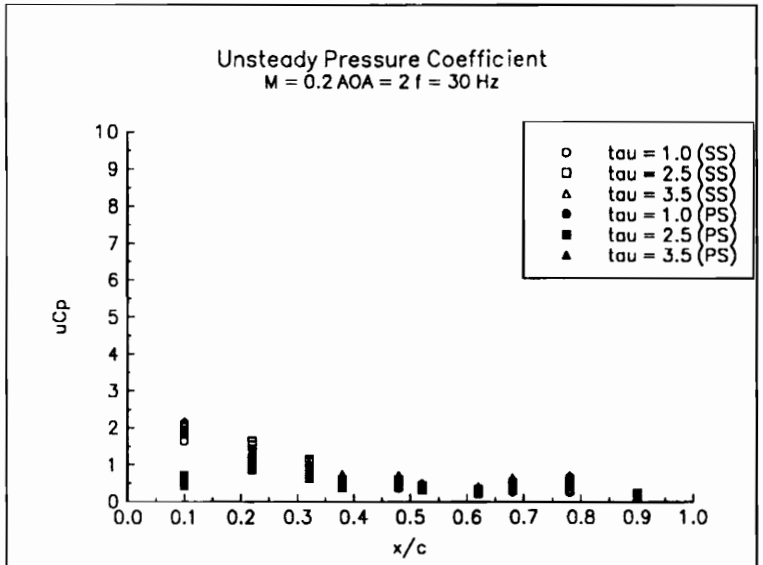
Unsteady Pressure Coefficient
M = 0.2 AOA = 2 f = 30 Hz
tau = 1.0 (SS)
tau = 2.5 (SS)
tau = 3.5 (SS)
tau = 1.0 (PS)
tau = 2.5 (PS)
tau = 3.5 (PS)
uCp
x/c

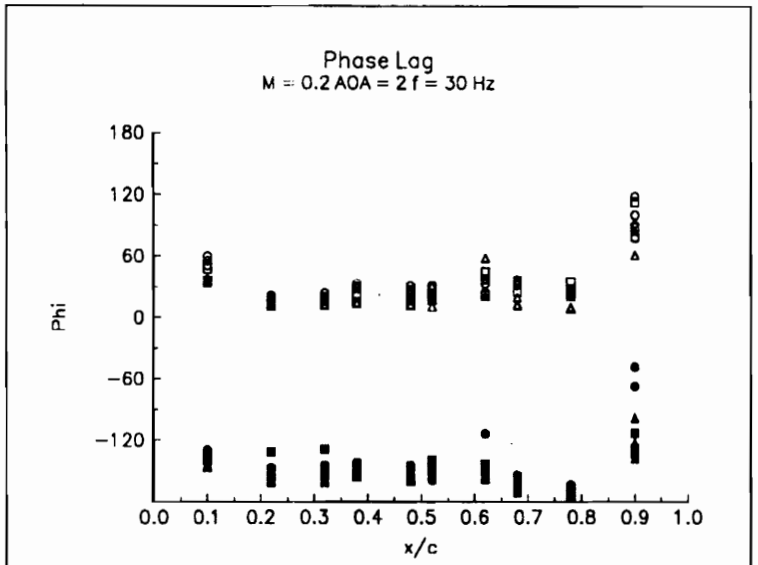
Phase Lag
M = 0.2 AOA = 2 f = 30 Hz
Phi
x/c

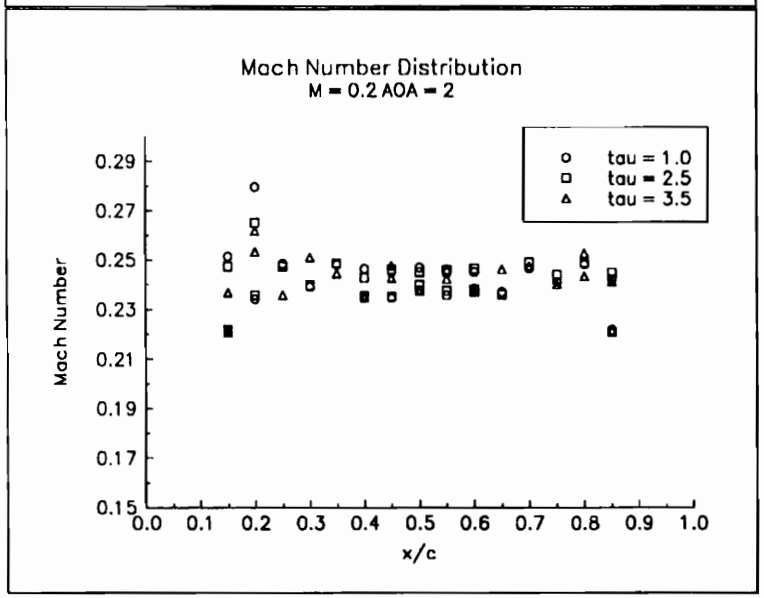
Mach Number Distribution
M = 0.2 AOA = 2
tau = 1.0
tau = 2.5
tau = 3.5
Mach Number
x/c

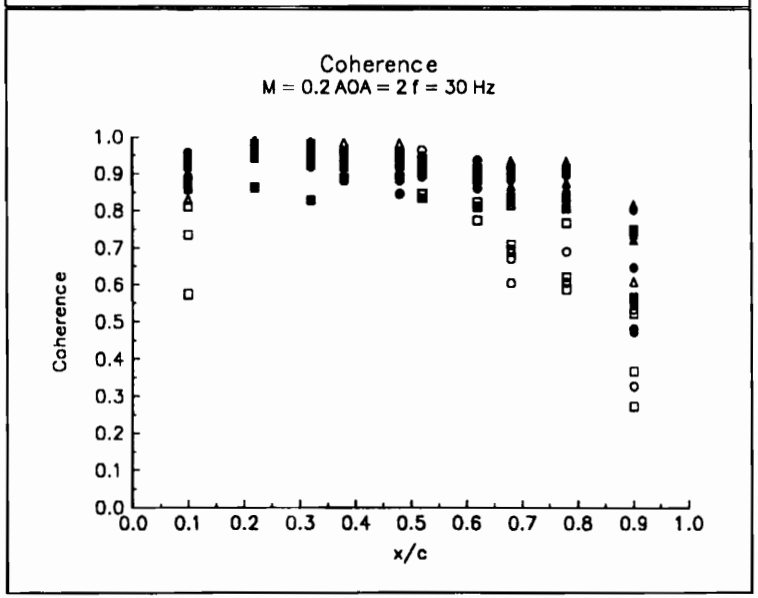
Coherence
M = 0.2 AOA = 2 f = 30 Hz
Coherence
x/c

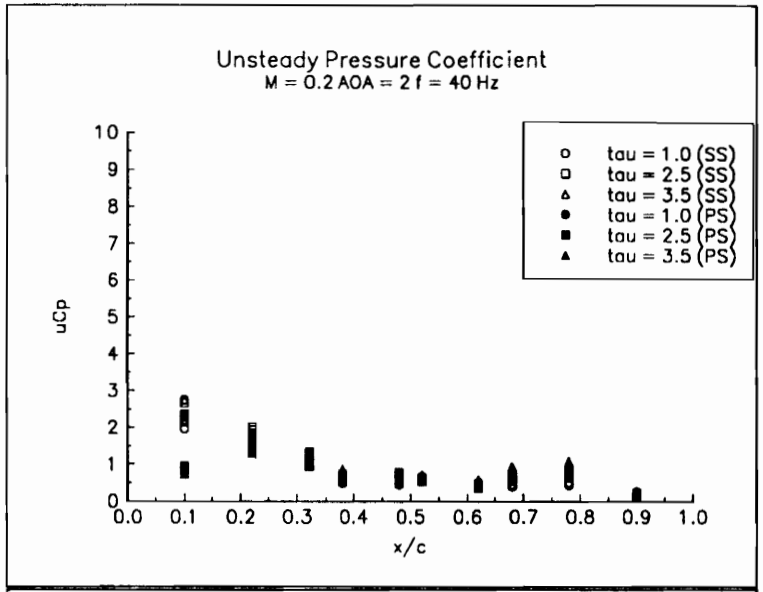
Unsteady Pressure Coefficient
M = 0.2 AOA = 2 f = 40 Hz
uCp
x/c
tau = 1.0 (SS)
tau = 2.5 (SS)
tau = 3.5 (SS)
tau = 1.0 (PS)
tau = 2.5 (PS)
tau = 3.5 (PS)

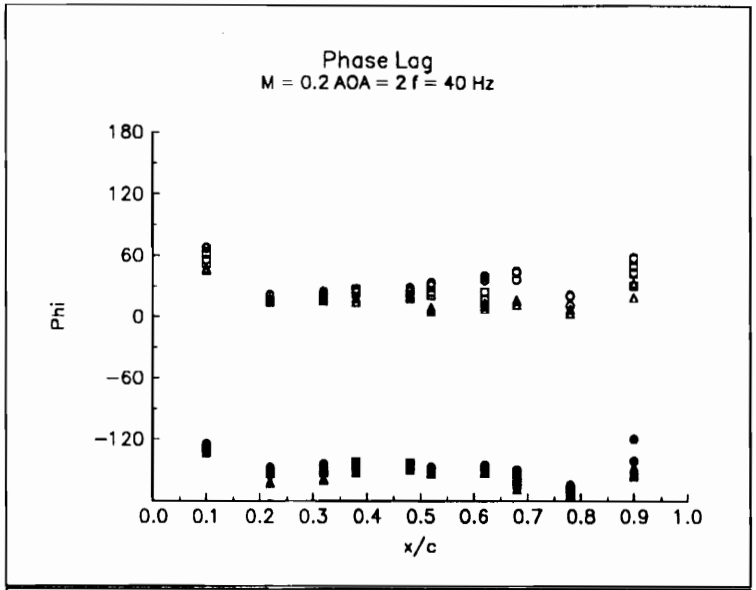
Phase Lag
M = 0.2 AOA = 2 f = 40 Hz
Phi
x/c

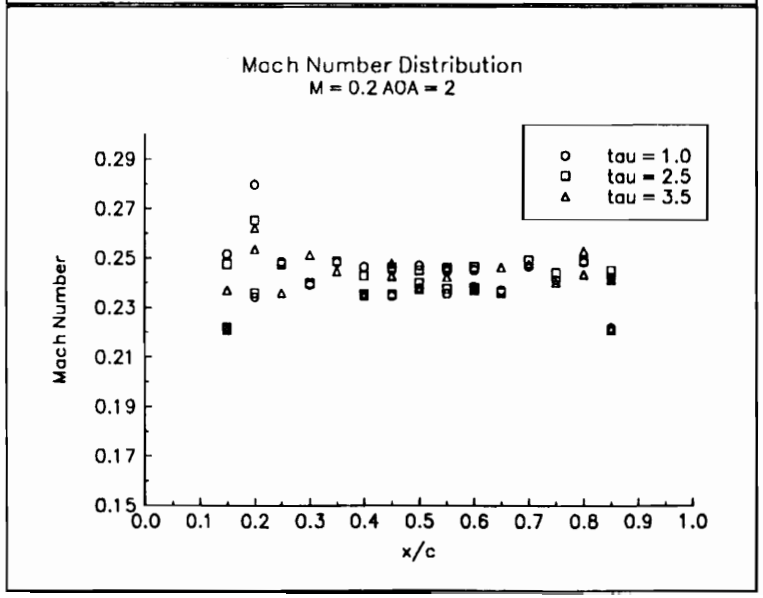
Mach Number Distribution
M = 0.2 AOA = 2
Mach Number
x/c
tau = 1.0
tau = 2.5
tau = 3.5

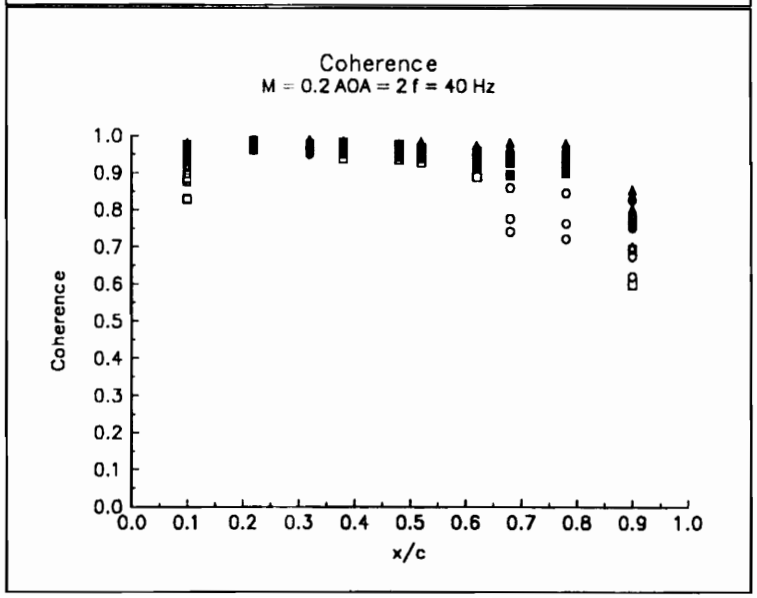
Coherence
M = 0.2 AOA = 2 f = 40 Hz
Coherence
x/c

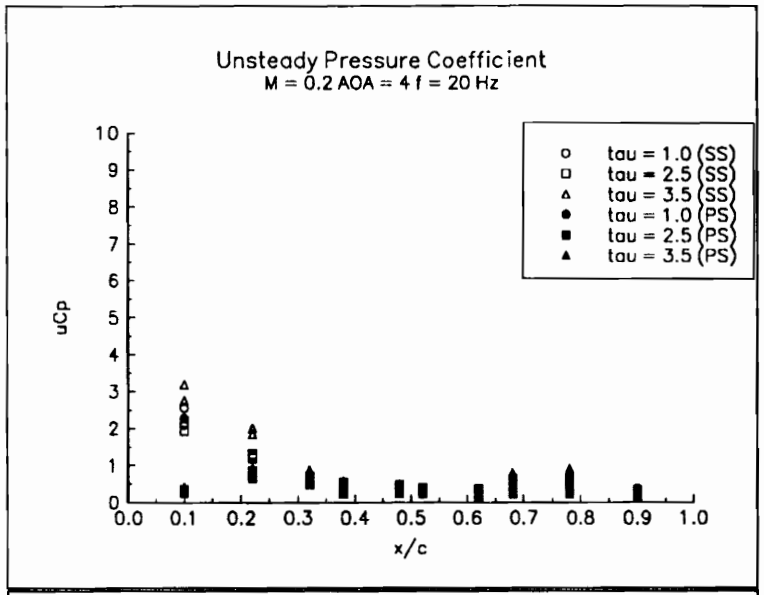
Unsteady Pressure Coefficient
M = 0.2 AOA = 4 f = 20 Hz
tau = 1.0 (SS)
tau = 2.5 (SS)
tau = 3.5 (SS)
tau = 1.0 (PS)
tau = 2.5 (PS)
tau = 3.5 (PS)
uCp
x/c

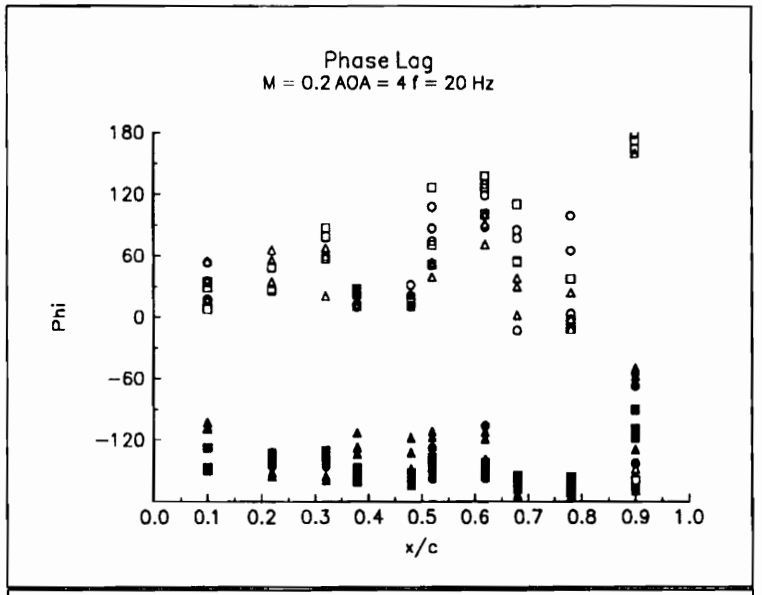
Phase Lag
M = 0.2 AOA = 4 f = 20 Hz
Phi
x/c

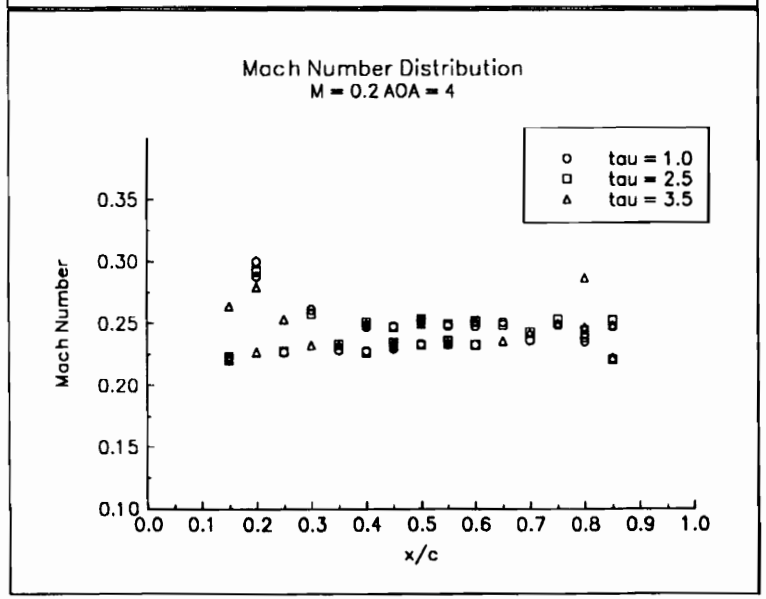
Mach Number Distribution
M = 0.2 AOA = 4
tau = 1.0
tau = 2.5
tau = 3.5
Mach Number
x/c

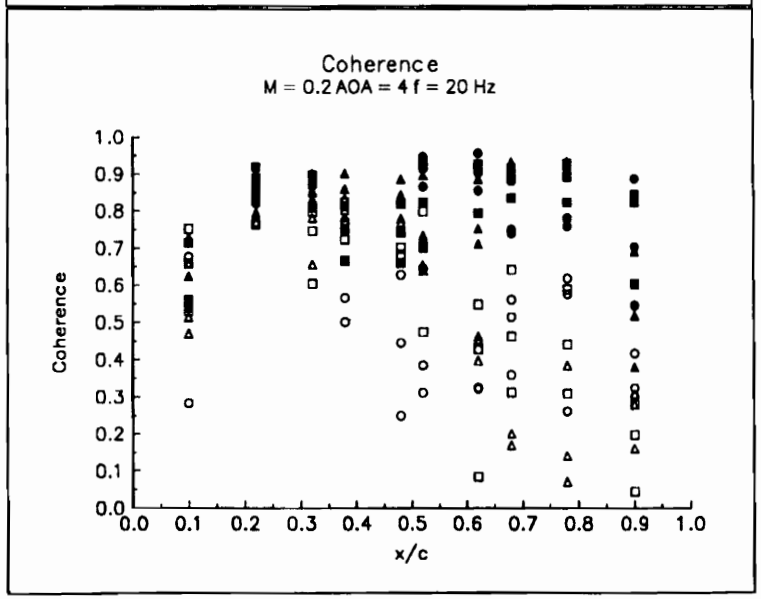
Coherence
M = 0.2 AOA = 4 f = 20 Hz
Coherence
x/c

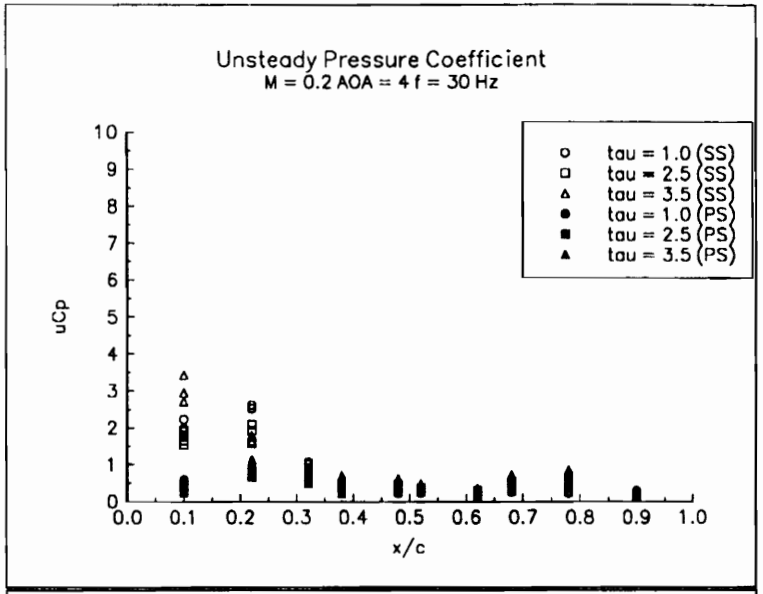
Unsteady Pressure Coefficient
M = 0.2 AOA = 4 f = 30 Hz
tau = 1.0 (SS)
tau = 2.5 (SS)
tau = 3.5 (SS)
tau = 1.0 (PS)
tau = 2.5 (PS)
tau = 3.5 (PS)
uCp
x/c

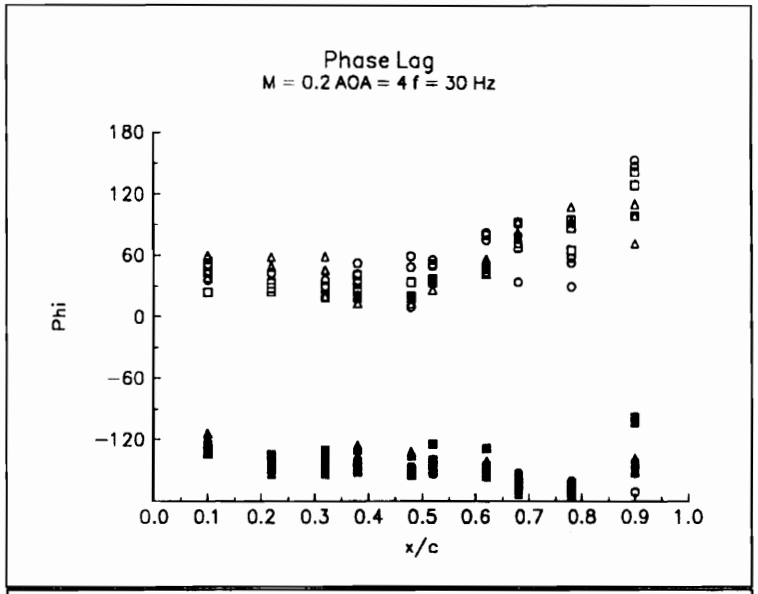
Phase Lag
M = 0.2 AOA = 4 f = 30 Hz
Phi
x/c

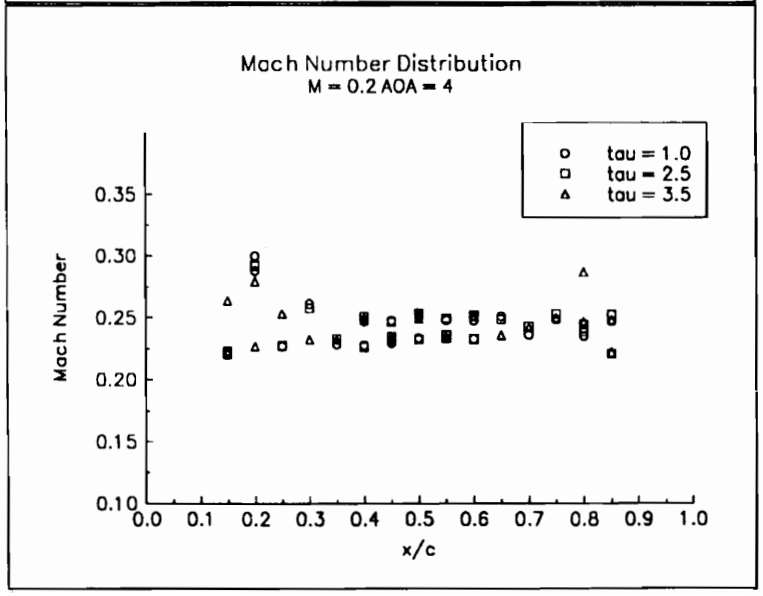
Mach Number Distribution
M = 0.2 AOA = 4
tau = 1.0
tau = 2.5
tau = 3.5
Mach Number
x/c

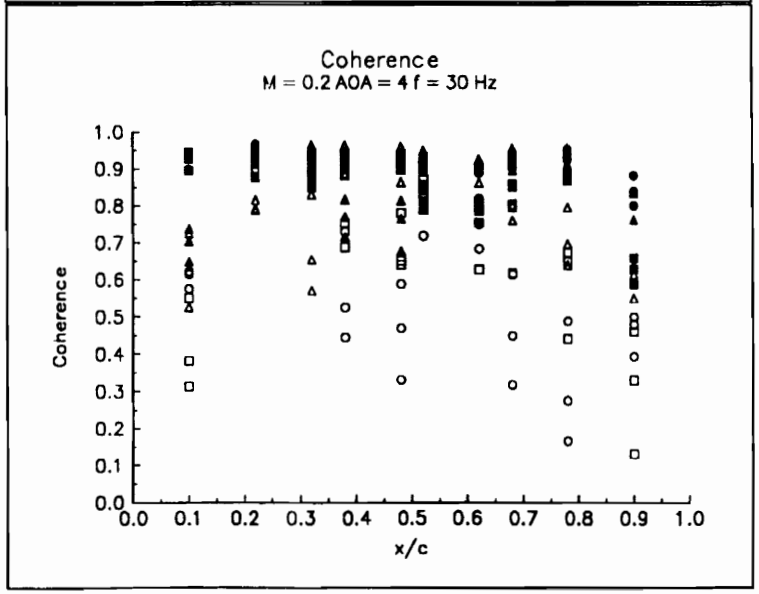
Coherence
M = 0.2 AOA = 4 f = 30 Hz
Coherence
x/c

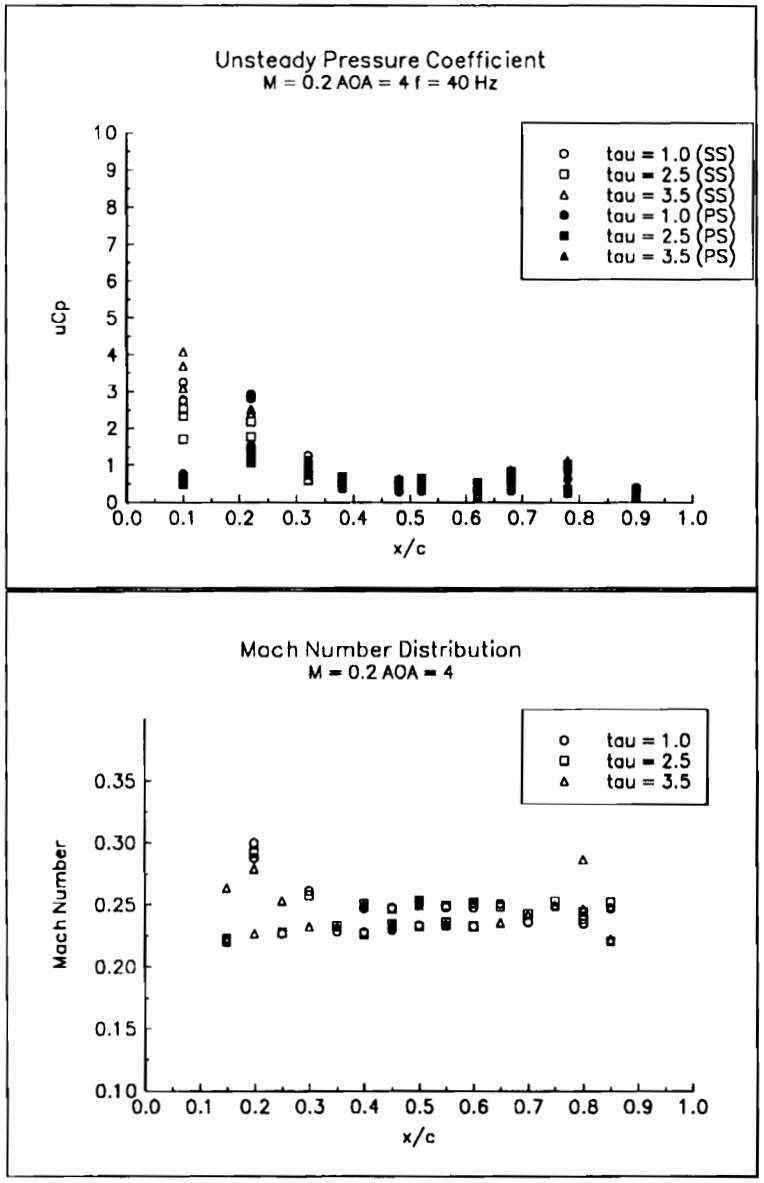
Unsteady Pressure Coefficient
M = 0.2 AOA = 4 f = 40 Hz
tau = 1.0 (SS)
tau = 2.5 (SS)
tau = 3.5 (SS)
tau = 1.0 (PS)
tau = 2.5 (PS)
tau = 3.5 (PS)
uCp
x/c

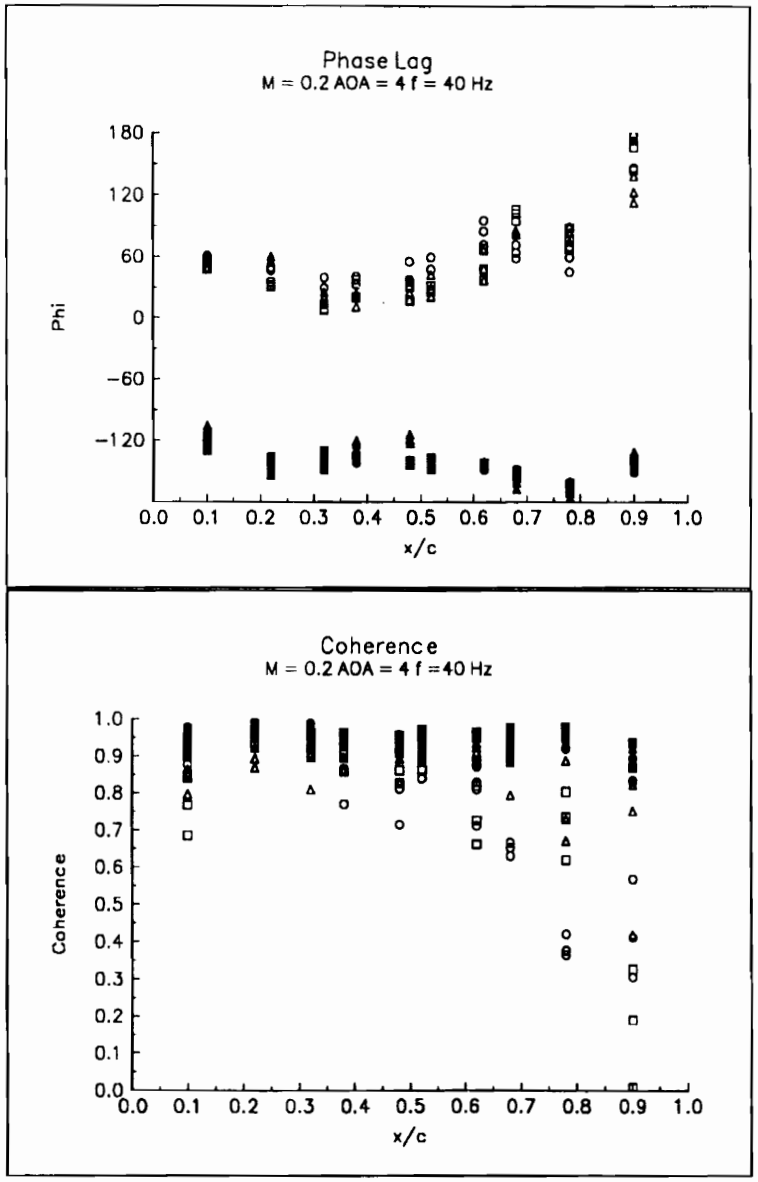
Phase Lag
M = 0.2 AOA = 4 f = 40 Hz
Phi
x/c

Mach Number Distribution
M = 0.2 AOA = 4
tau = 1.0
tau = 2.5
tau = 3.5
Mach Number
x/c

Coherence
M = 0.2 AOA = 4 f = 40 Hz
Coherence
x/c

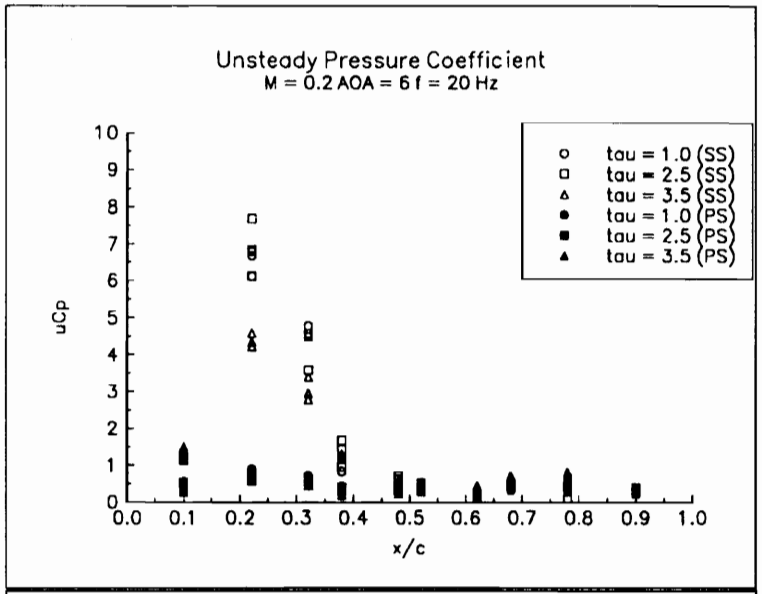
Unsteady Pressure Coefficient
M = 0.2 AOA = 6 f = 20 Hz
tau = 1.0 (SS)
tau = 2.5 (SS)
tau = 3.5 (SS)
tau = 1.0 (PS)
tau = 2.5 (PS)
tau = 3.5 (PS)
uCp
x/c

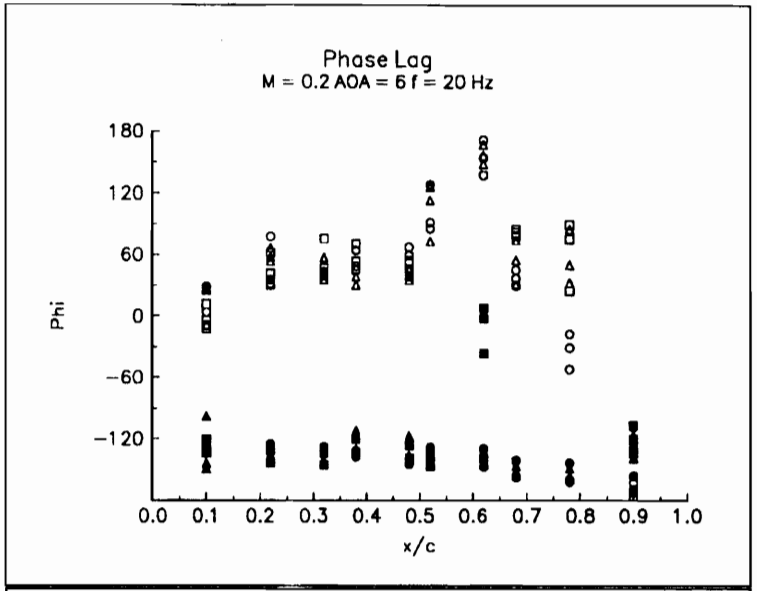
Phase Lag
M = 0.2 AOA = 6 f = 20 Hz
Phi
x/c

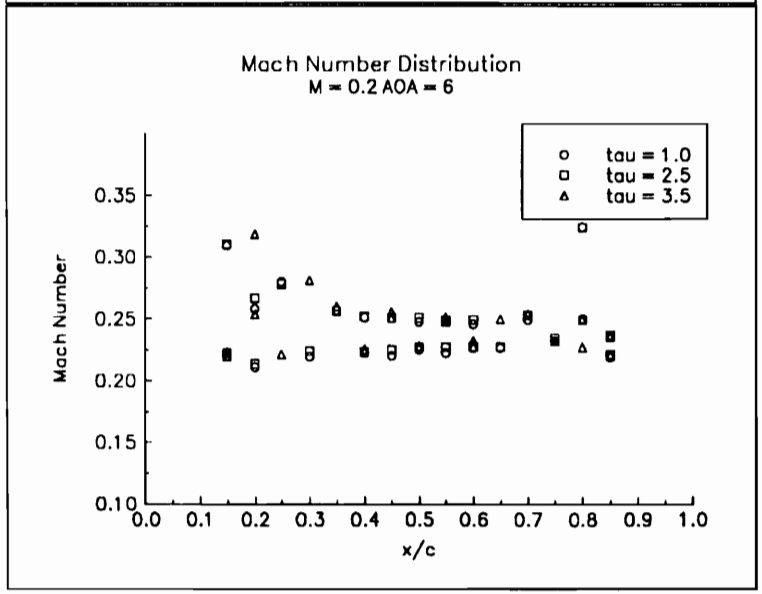
Mach Number Distribution
M = 0.2 AOA = 6
tau = 1.0
tau = 2.5
tau = 3.5
Mach Number
x/c

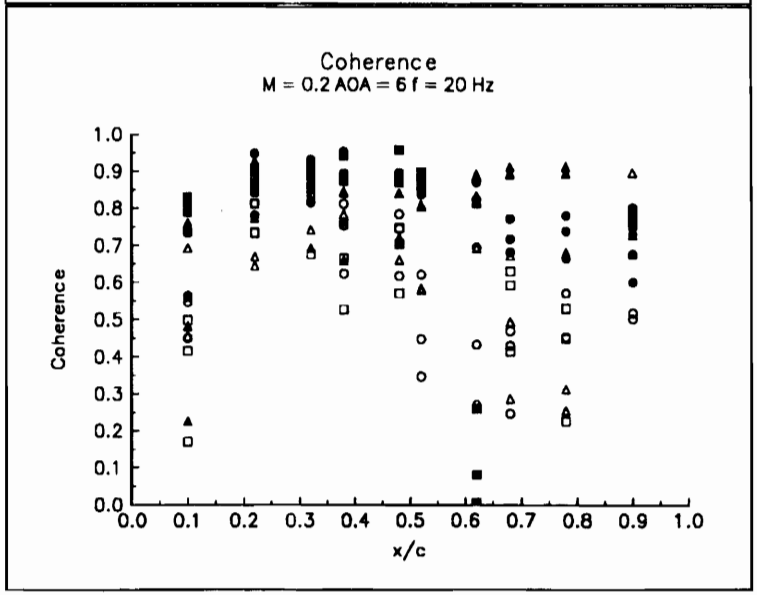
Coherence
M = 0.2 AOA = 6 f = 20 Hz
Coherence
x/c

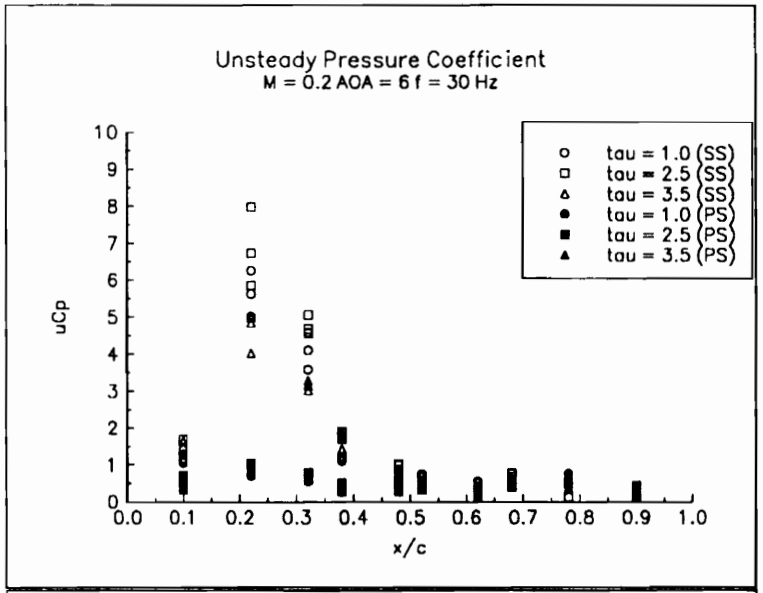
Unsteady Pressure Coefficient
M = 0.2 AOA = 6 f = 30 Hz
tau = 1.0 (SS)
tau = 2.5 (SS)
tau = 3.5 (SS)
tau = 1.0 (PS)
tau = 2.5 (PS)
tau = 3.5 (PS)
uCp
x/c

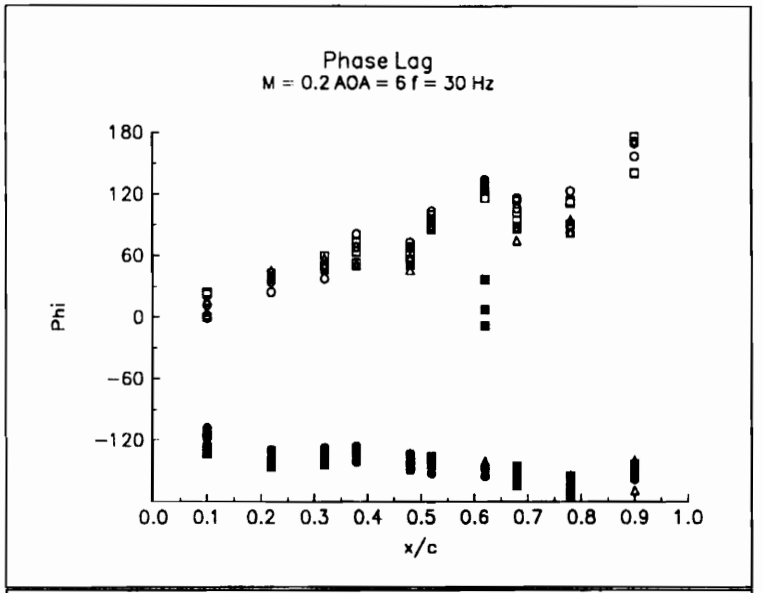
Phase Lag
M = 0.2 AOA = 6 f = 30 Hz
Phi
x/c

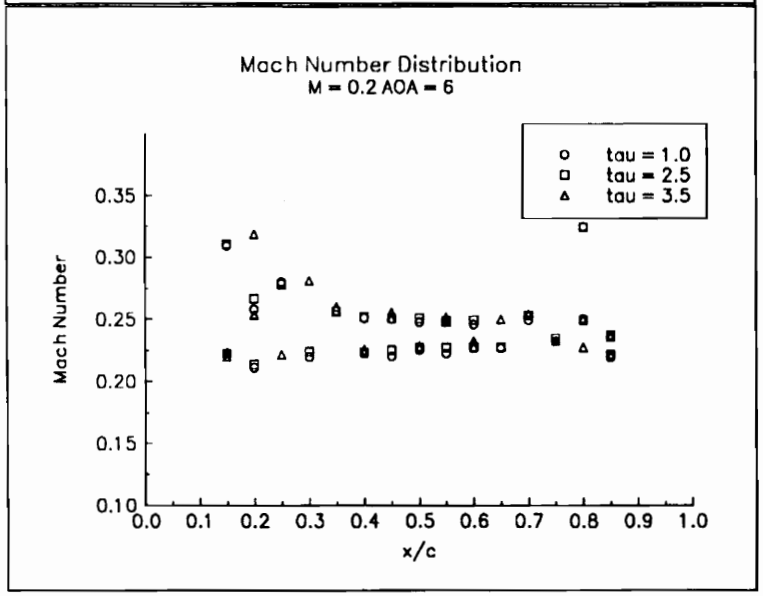
Mach Number Distribution
M = 0.2 AOA = 6
tau = 1.0
tau = 2.5
tau = 3.5
Mach Number
x/c

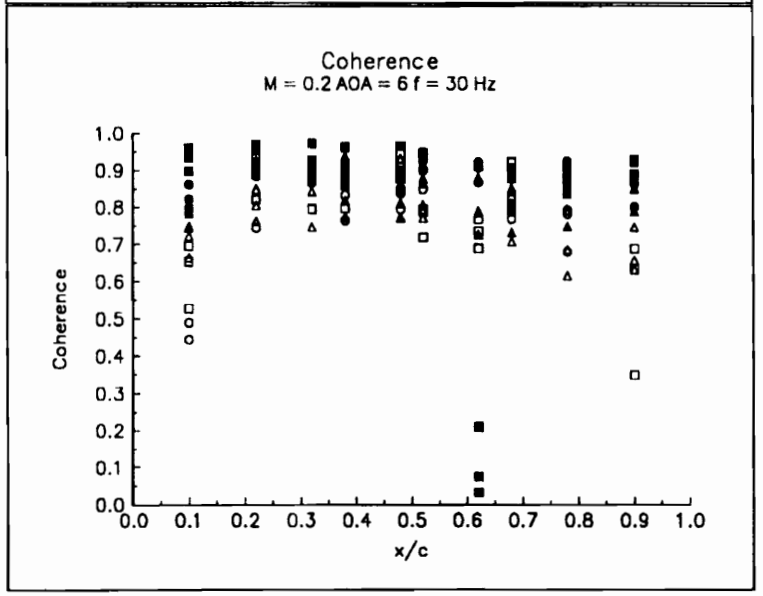
Coherence
M = 0.2 AOA = 6 f = 30 Hz
Coherence
x/c

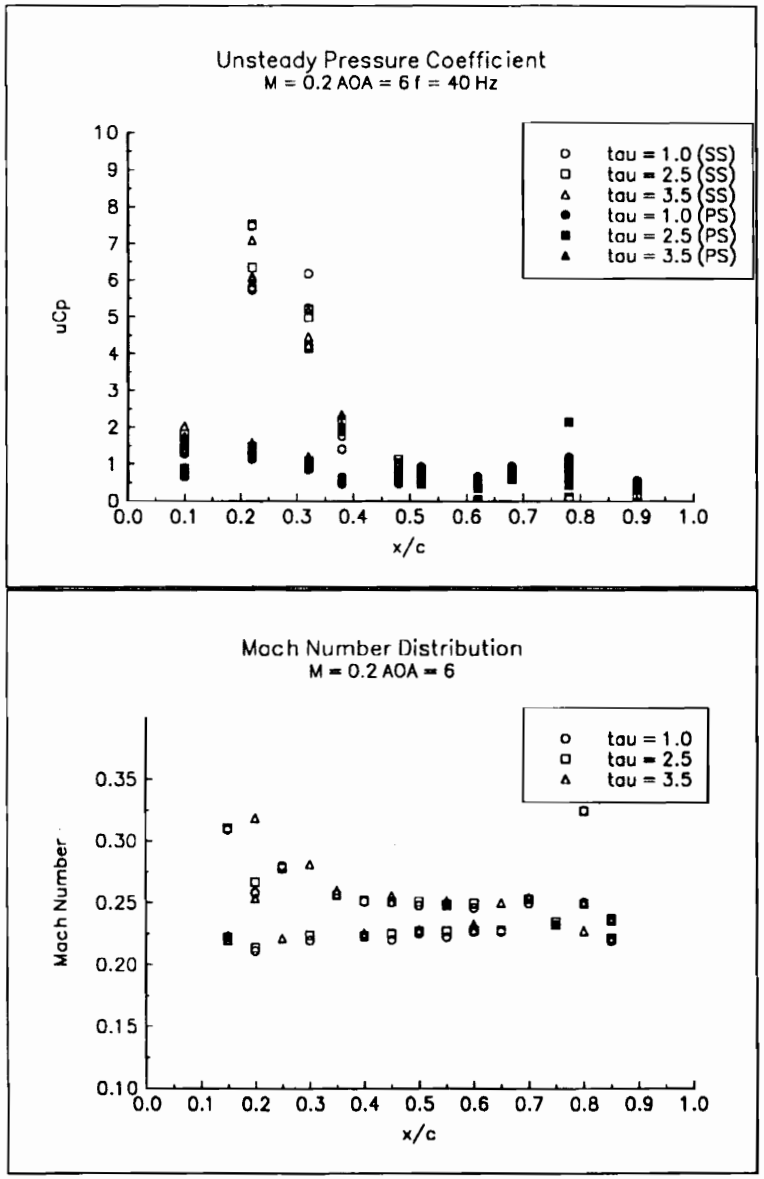
Unsteady Pressure Coefficient
M = 0.2 AOA = 6 f = 40 Hz
uCp
x/c
tau = 1.0 (SS)
tau = 2.5 (SS)
tau = 3.5 (SS)
tau = 1.0 (PS)
tau = 2.5 (PS)
tau = 3.5 (PS)
Phase Lag
M = 0.2 AOA = 6 f = 40 Hz
Phi
x/c
Mach Number Distribution
M = 0.2 AOA = 6
Mach Number
x/c
tau = 1.0
tau = 2.5
tau = 3.5
Coherence
M = 0.2 AOA = 6 f = 40 Hz
Coherence
x/c

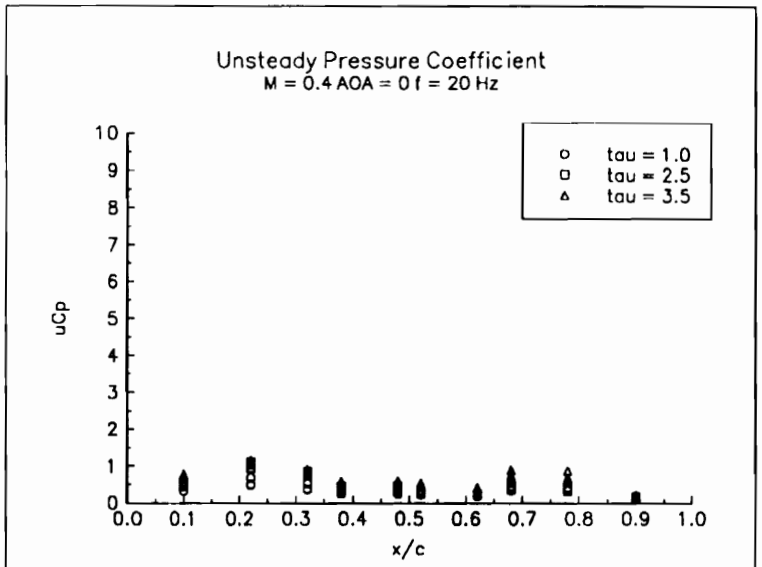
Unsteady Pressure Coefficient
M = 0.4 AOA = 0 f = 20 Hz
uCp
x/c
tau = 1.0
tau = 2.5
tau = 3.5

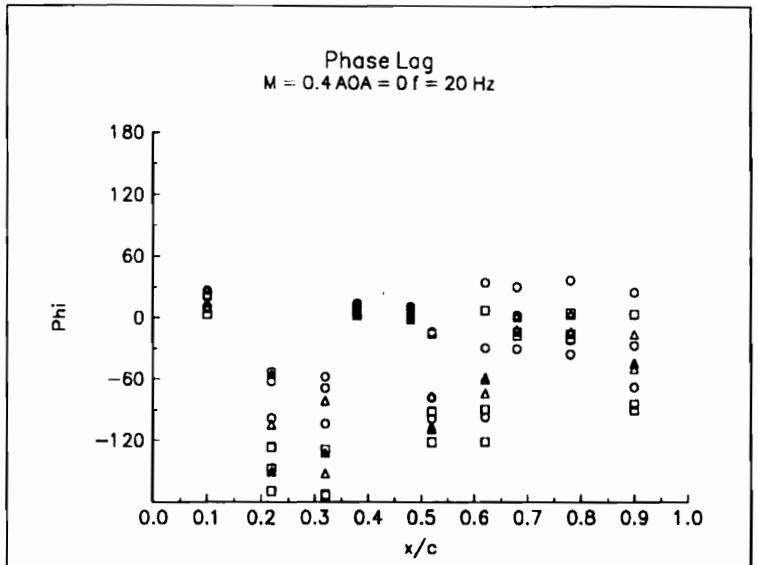
Phase Lag
M = 0.4 AOA = 0 f = 20 Hz
Phi
x/c

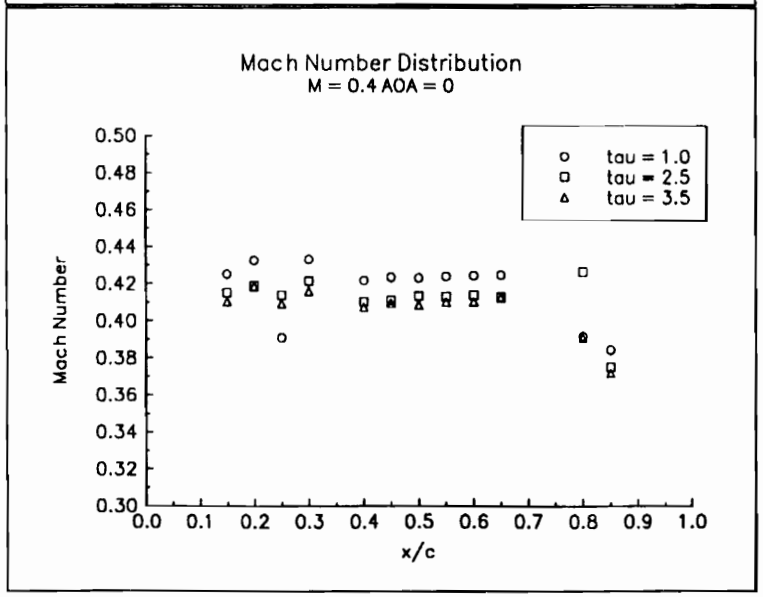
Mach Number Distribution
M = 0.4 AOA = 0
Mach Number
x/c
tau = 1.0
tau = 2.5
tau = 3.5

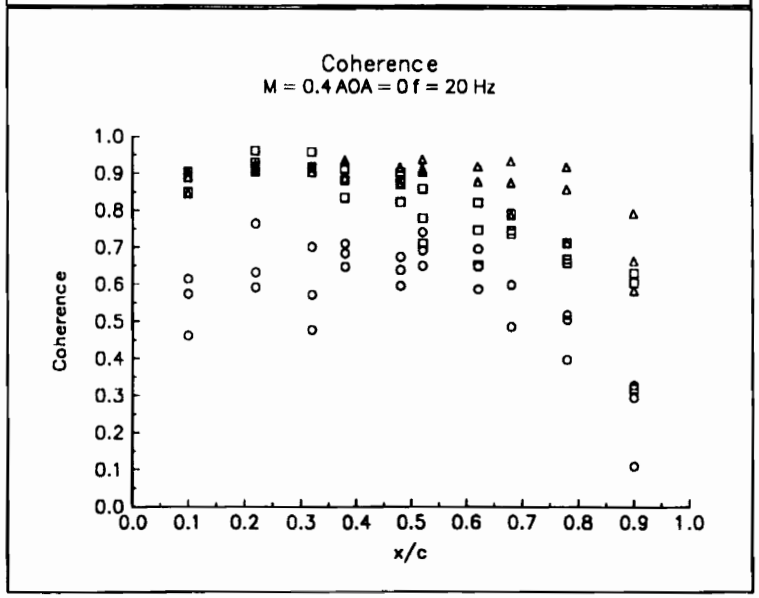
Coherence
M = 0.4 AOA = 0 f = 20 Hz
Coherence
x/c

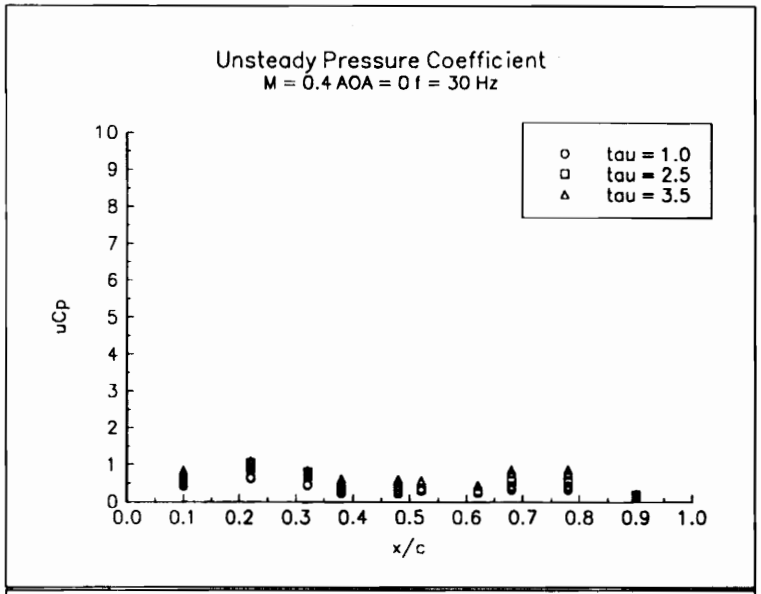
Unsteady Pressure Coefficient
M = 0.4 AOA = 0 f = 30 Hz
tau = 1.0
tau = 2.5
tau = 3.5
uCp
x/c

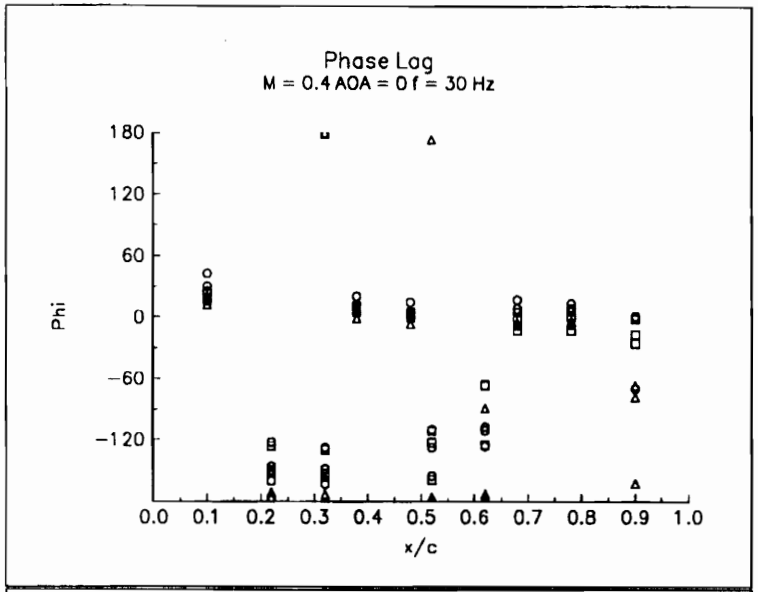
Phase Lag
M = 0.4 AOA = 0 f = 30 Hz
Phi
x/c

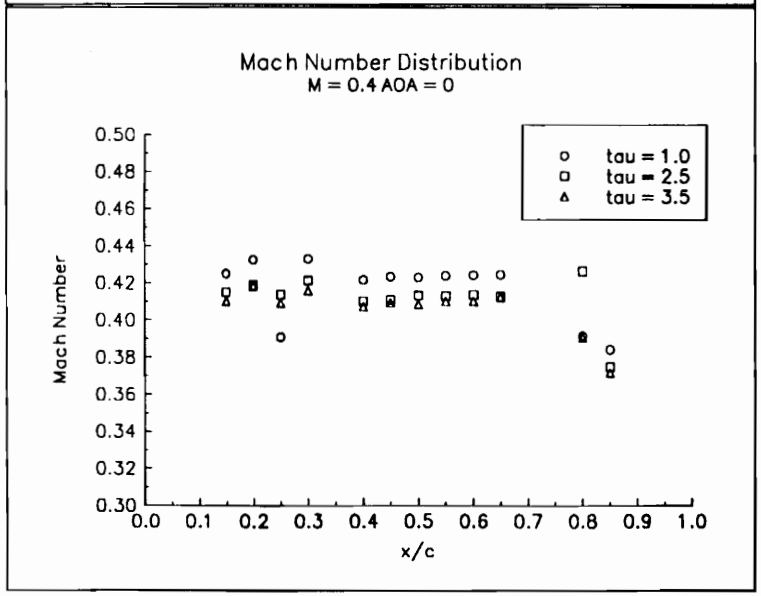
Mach Number Distribution
M = 0.4 AOA = 0
tau = 1.0
tau = 2.5
tau = 3.5
Mach Number
x/c

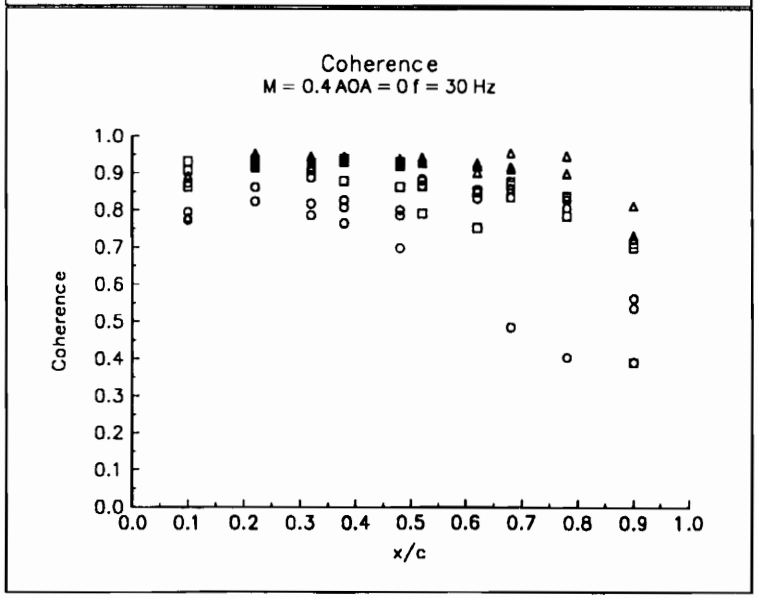
Coherence
M = 0.4 AOA = 0 f = 30 Hz
Coherence
x/c

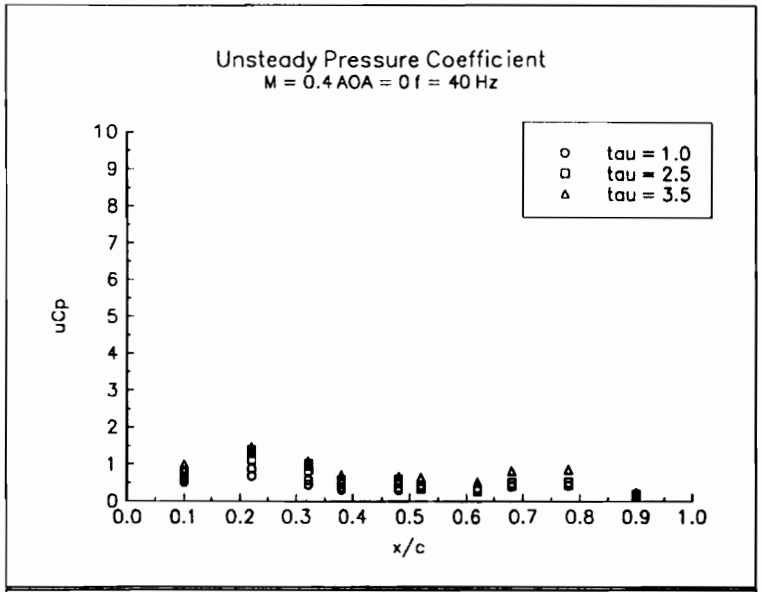
Unsteady Pressure Coefficient
M = 0.4 AOA = 0 f = 40 Hz
tau = 1.0
tau = 2.5
tau = 3.5
uCp
x/c

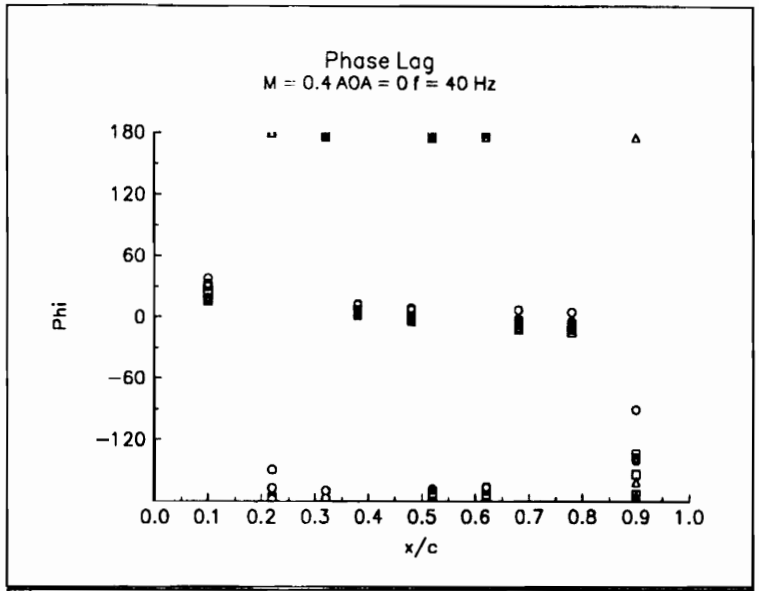
Phase Lag
M = 0.4 AOA = 0 f = 40 Hz
Phi
x/c

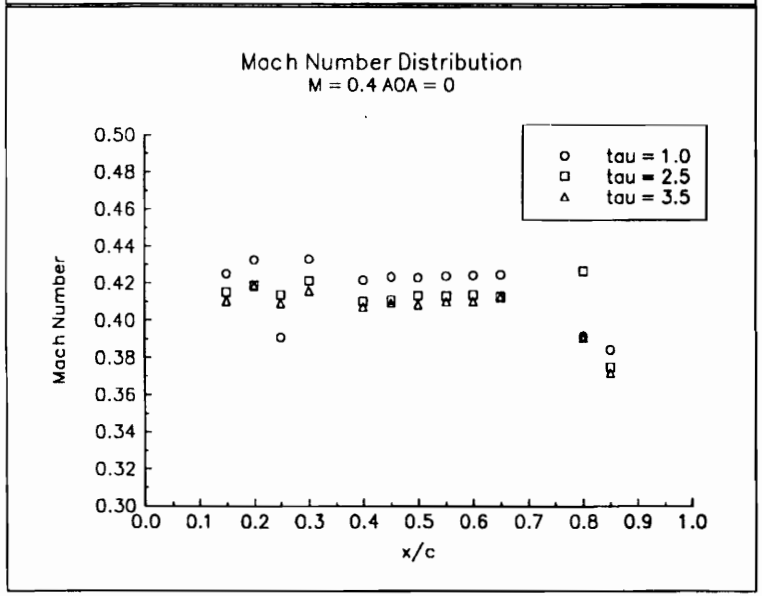
Mach Number Distribution
M = 0.4 AOA = 0
tau = 1.0
tau = 2.5
tau = 3.5
Mach Number
x/c

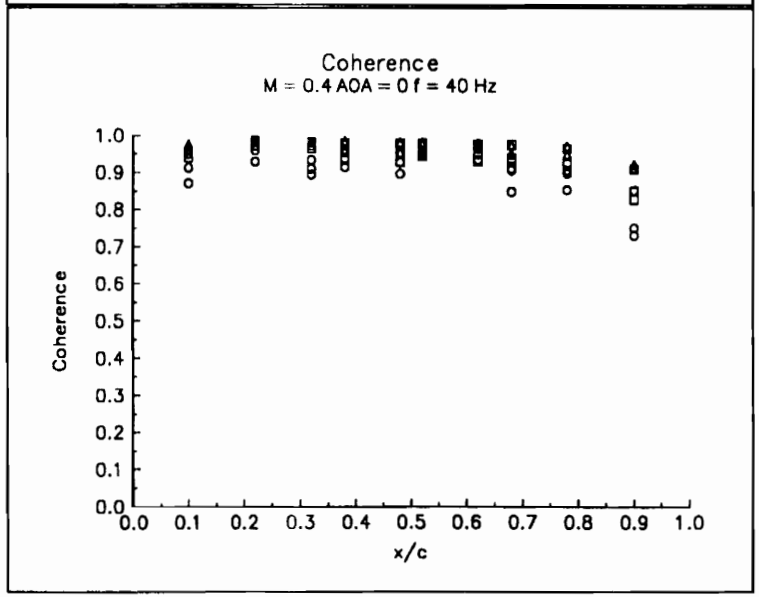
Coherence
M = 0.4 AOA = 0 f = 40 Hz
Coherence
x/c

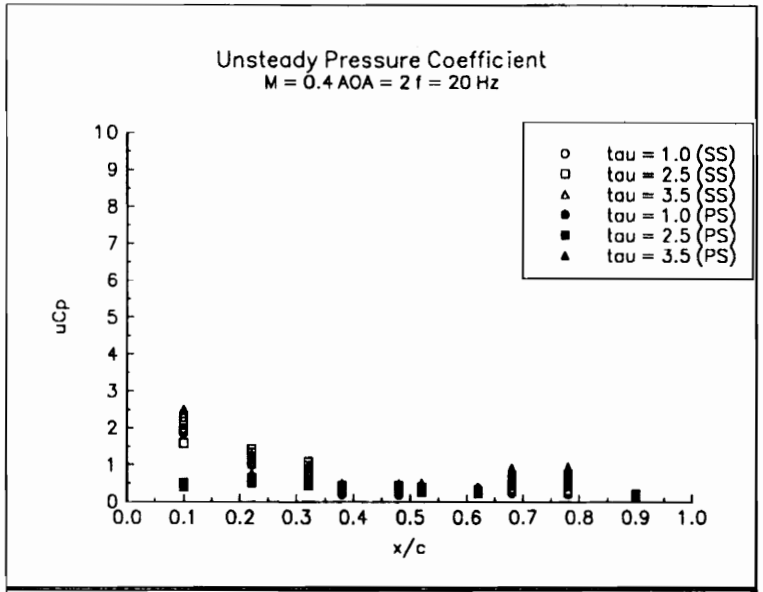
Unsteady Pressure Coefficient
M = 0.4 AOA = 2 f = 20 Hz
uCp
x/c
tau = 1.0 (SS)
tau = 2.5 (SS)
tau = 3.5 (SS)
tau = 1.0 (PS)
tau = 2.5 (PS)
tau = 3.5 (PS)

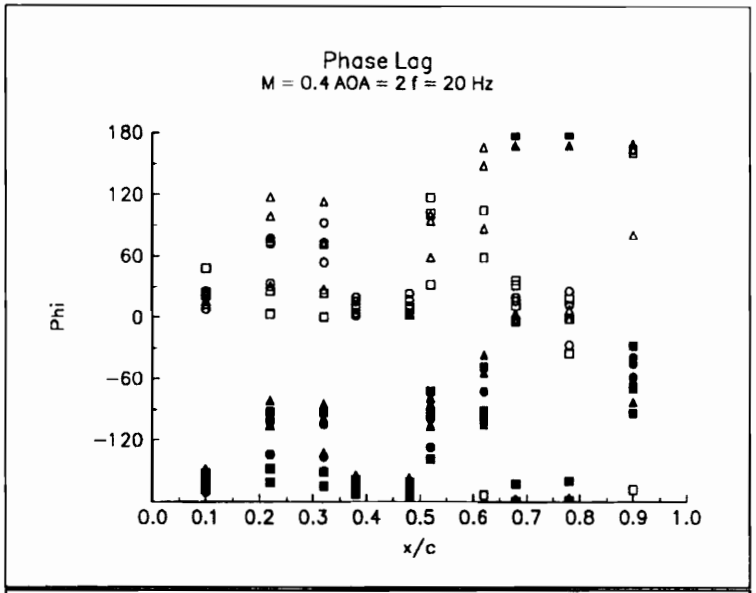
Phase Lag
M = 0.4 AOA = 2 f = 20 Hz
Phi
x/c

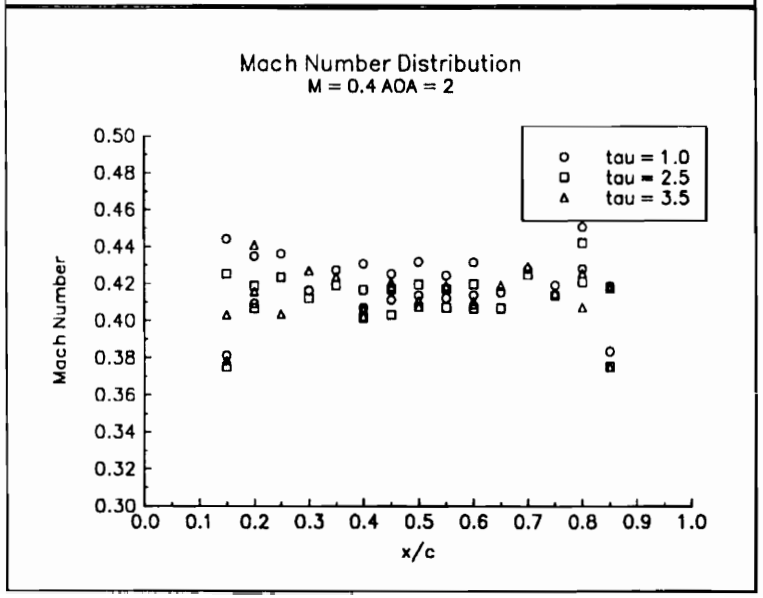
Mach Number Distribution
M = 0.4 AOA = 2
Mach Number
x/c
tau = 1.0
tau = 2.5
tau = 3.5

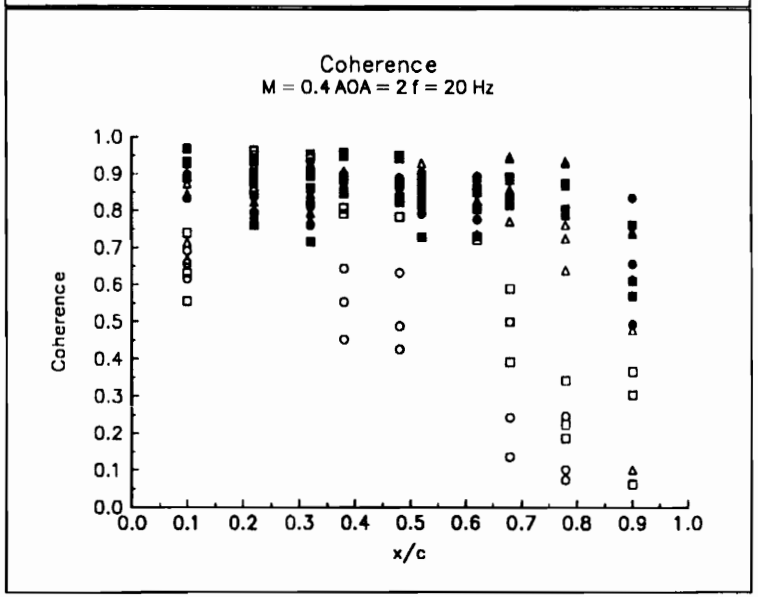
Coherence
M = 0.4 AOA = 2 f = 20 Hz
Coherence
x/c

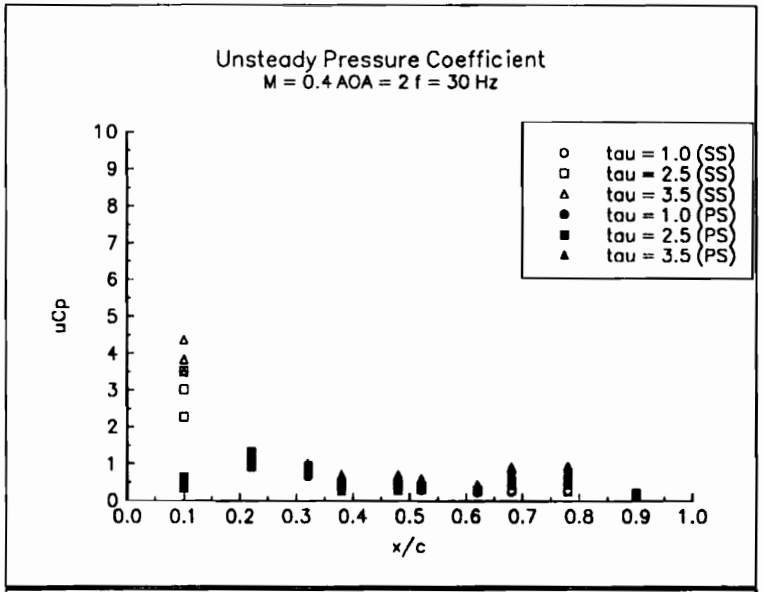
Unsteady Pressure Coefficient
M = 0.4 AOA = 2 f = 30 Hz
uCp
x/c
tau = 1.0 (SS)
tau = 2.5 (SS)
tau = 3.5 (SS)
tau = 1.0 (PS)
tau = 2.5 (PS)
tau = 3.5 (PS)

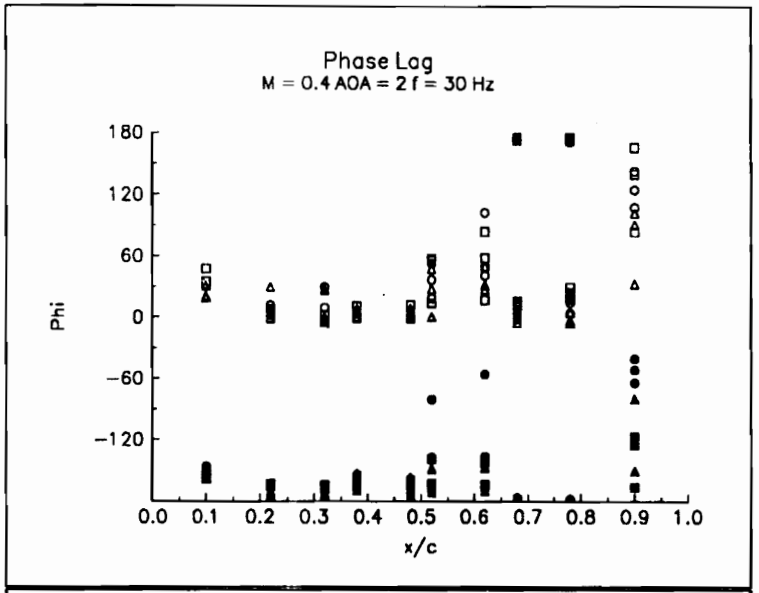
Phase Lag
M = 0.4 AOA = 2 f = 30 Hz
Phi
x/c

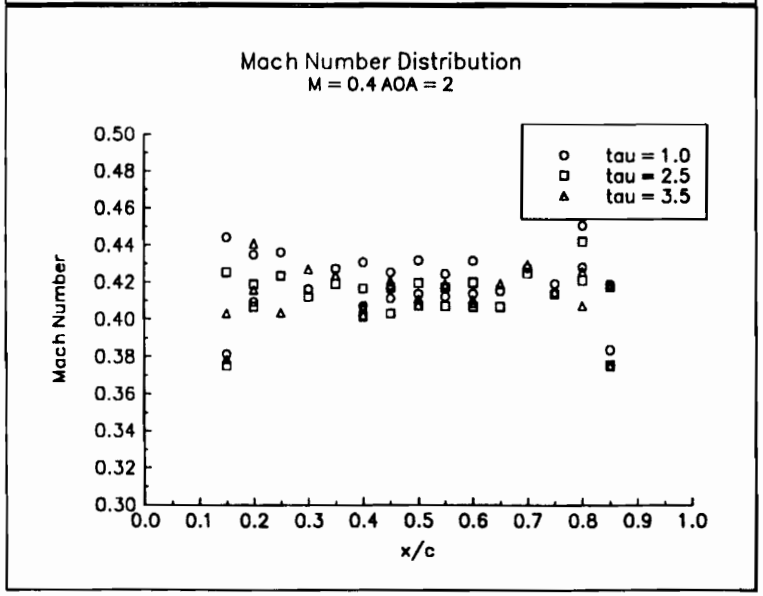
Mach Number Distribution
M = 0.4 AOA = 2
Mach Number
x/c
tau = 1.0
tau = 2.5
tau = 3.5

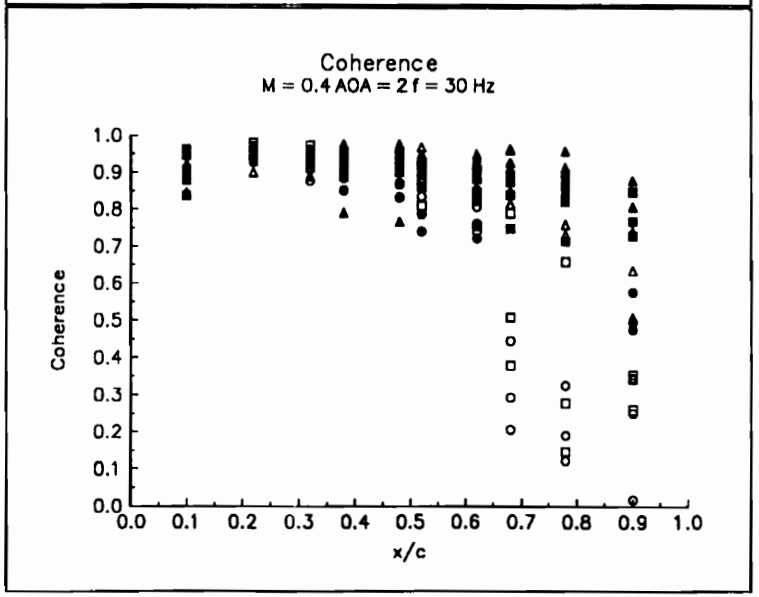
Coherence
M = 0.4 AOA = 2 f = 30 Hz
Coherence
x/c

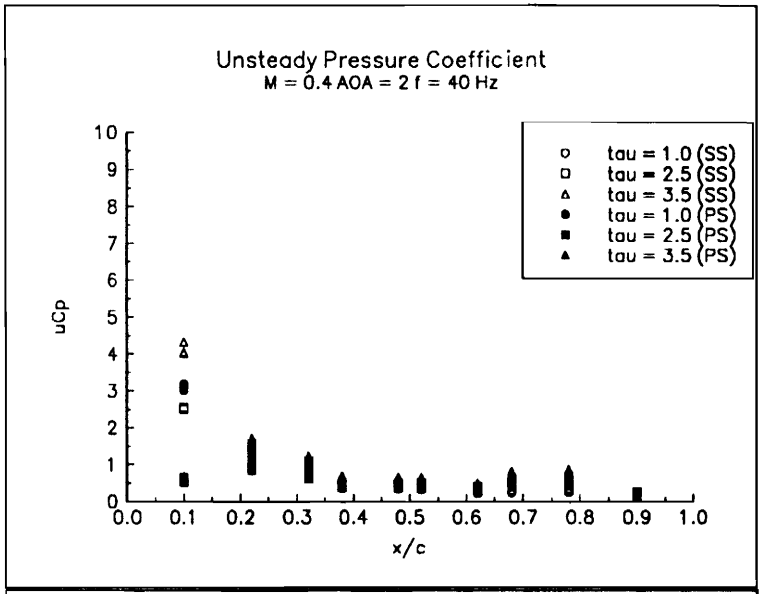
Unsteady Pressure Coefficient
M = 0.4 AOA = 2 f = 40 Hz
tau = 1.0 (SS)
tau = 2.5 (SS)
tau = 3.5 (SS)
tau = 1.0 (PS)
tau = 2.5 (PS)
tau = 3.5 (PS)
uCp
x/c

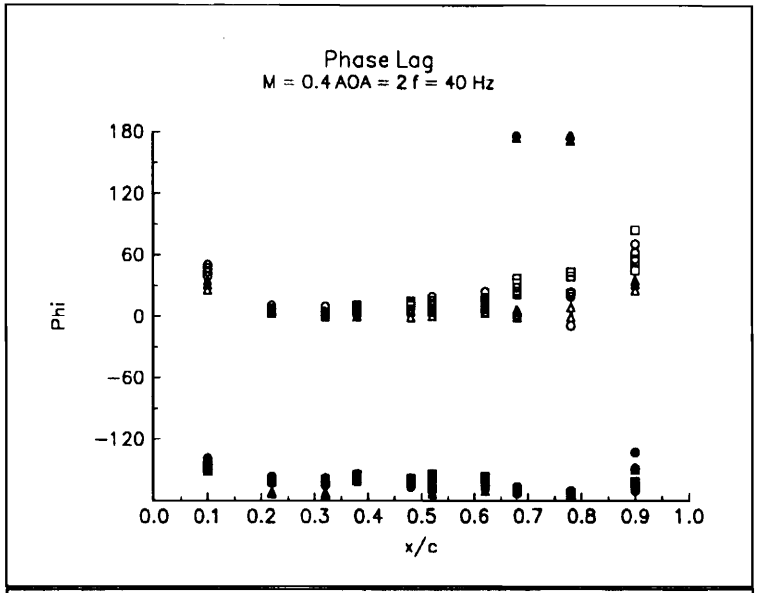
Phase Lag
M = 0.4 AOA = 2 f = 40 Hz
Phi
x/c

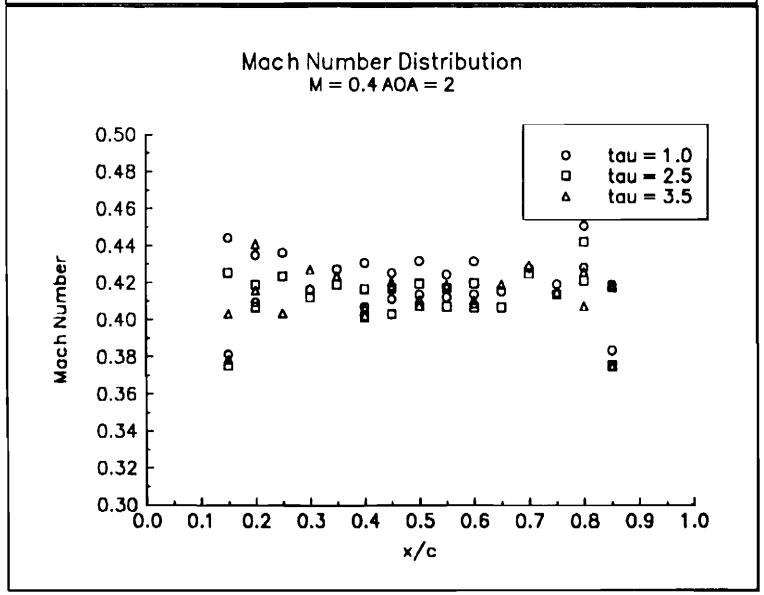
Mach Number Distribution
M = 0.4 AOA = 2
tau = 1.0
tau = 2.5
tau = 3.5
Mach Number
x/c

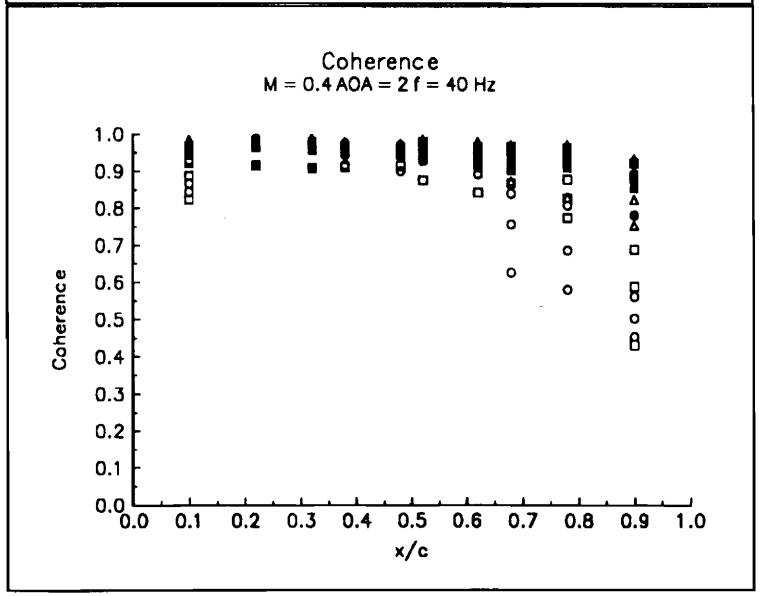
Coherence
M = 0.4 AOA = 2 f = 40 Hz
Coherence
x/c

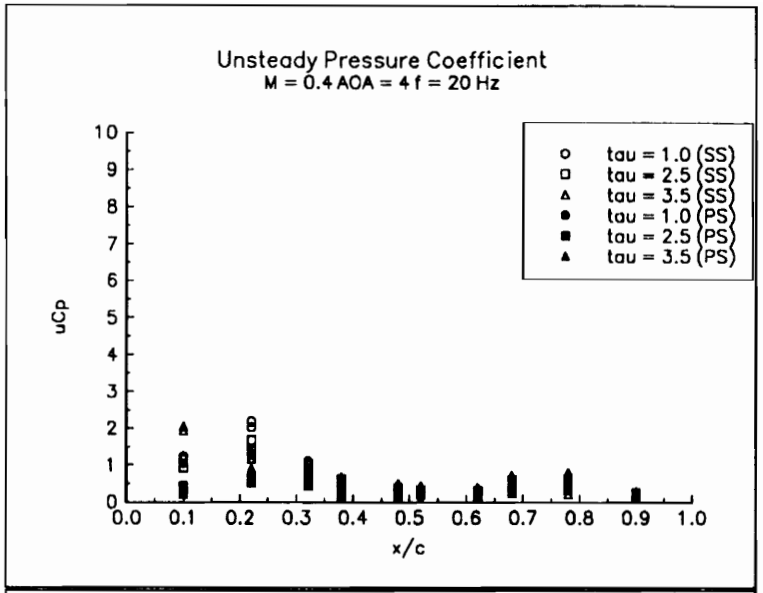
Unsteady Pressure Coefficient
M = 0.4 AOA = 4 f = 20 Hz
tau = 1.0 (SS)
tau = 2.5 (SS)
tau = 3.5 (SS)
tau = 1.0 (PS)
tau = 2.5 (PS)
tau = 3.5 (PS)
uCp
x/c

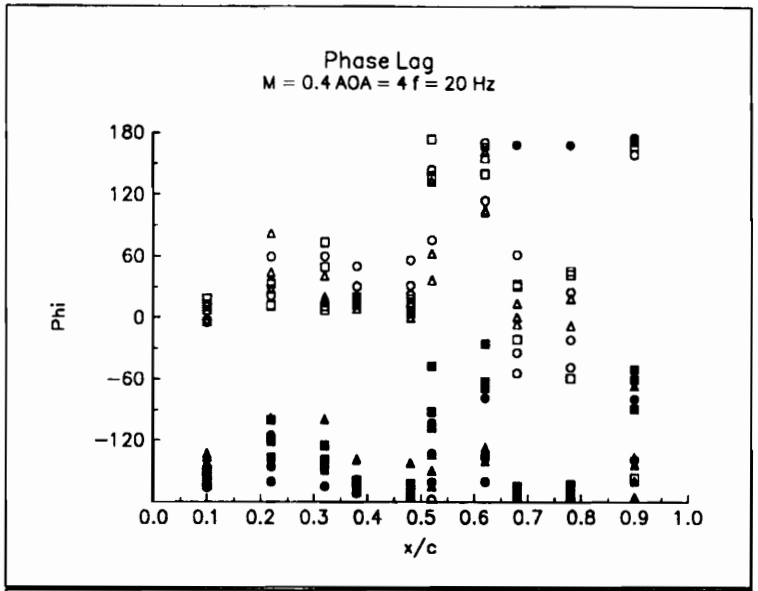
Phase Lag
M = 0.4 AOA = 4 f = 20 Hz
Phi
x/c

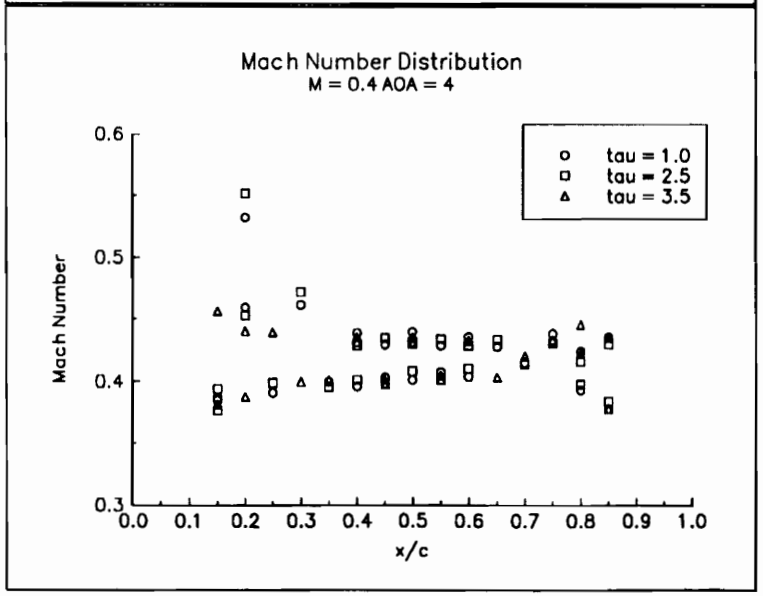
Mach Number Distribution
M = 0.4 AOA = 4
tau = 1.0
tau = 2.5
tau = 3.5
Mach Number
x/c

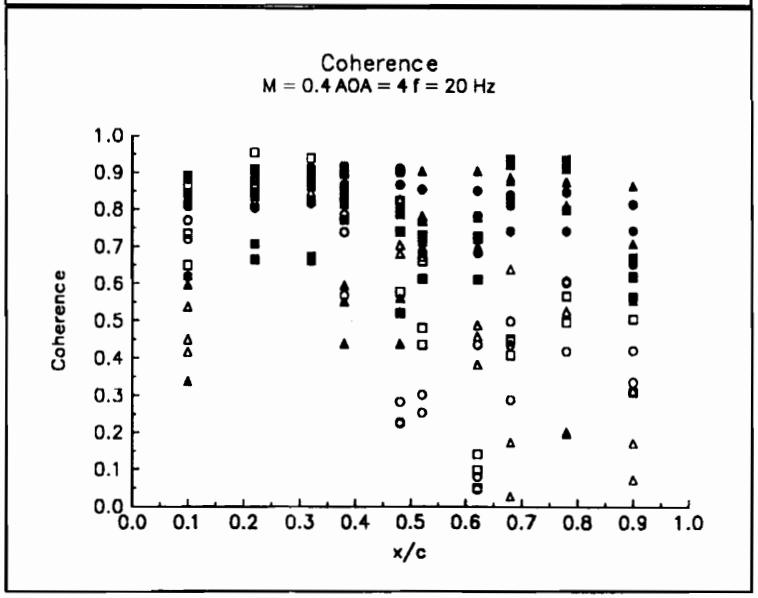
Coherence
M = 0.4 AOA = 4 f = 20 Hz
Coherence
x/c

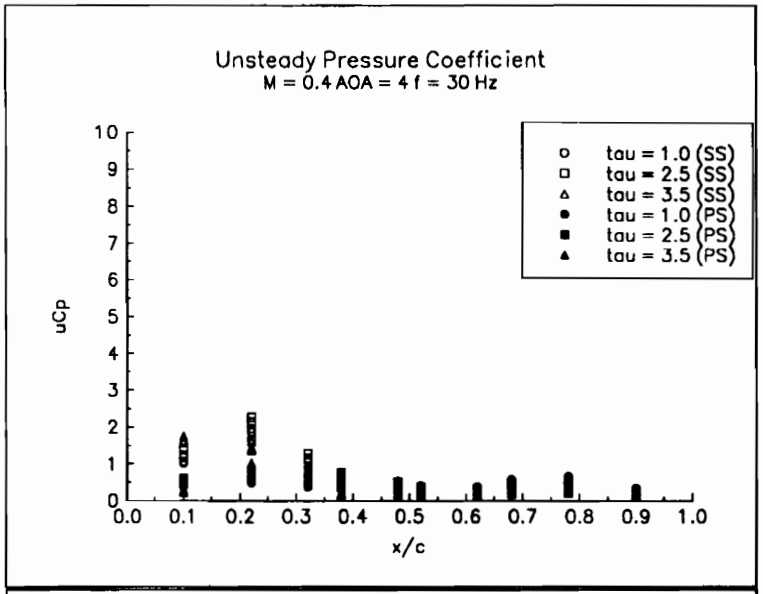
Unsteady Pressure Coefficient
M = 0.4 AOA = 4 f = 30 Hz
tau = 1.0 (SS)
tau = 2.5 (SS)
tau = 3.5 (SS)
tau = 1.0 (PS)
tau = 2.5 (PS)
tau = 3.5 (PS)
uCp
x/c

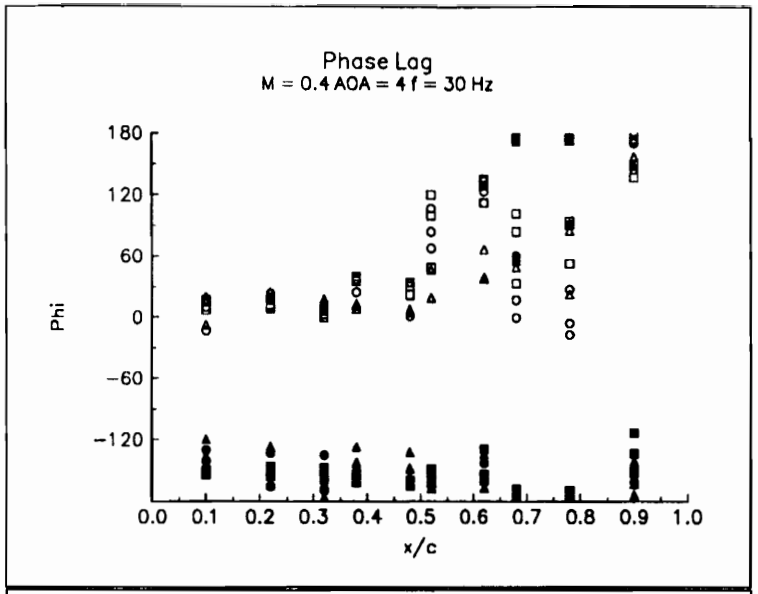
Phase Lag
M = 0.4 AOA = 4 f = 30 Hz
Phi
x/c

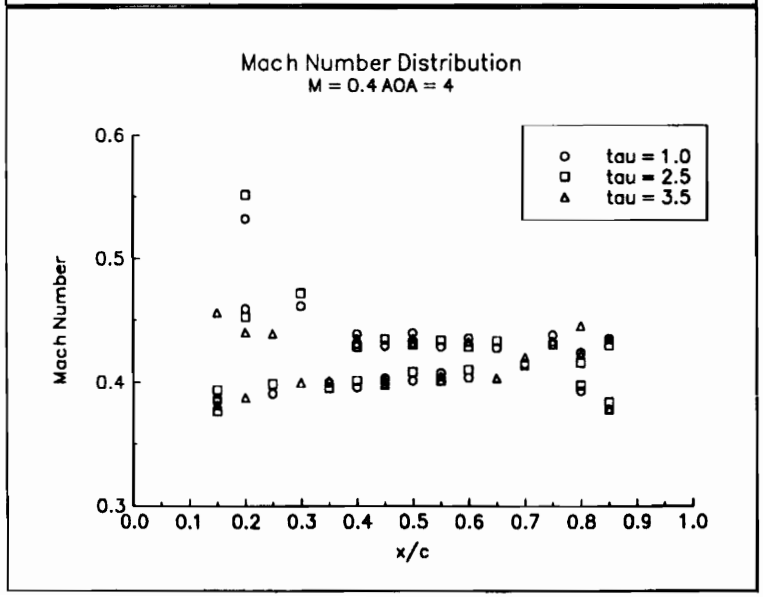
Mach Number Distribution
M = 0.4 AOA = 4
tau = 1.0
tau = 2.5
tau = 3.5
Mach Number
x/c

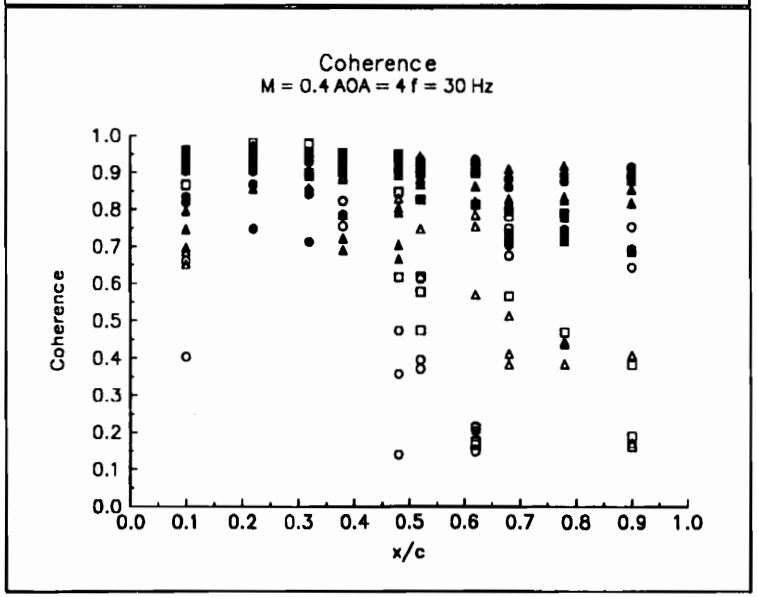
Coherence
M = 0.4 AOA = 4 f = 30 Hz
Coherence
x/c

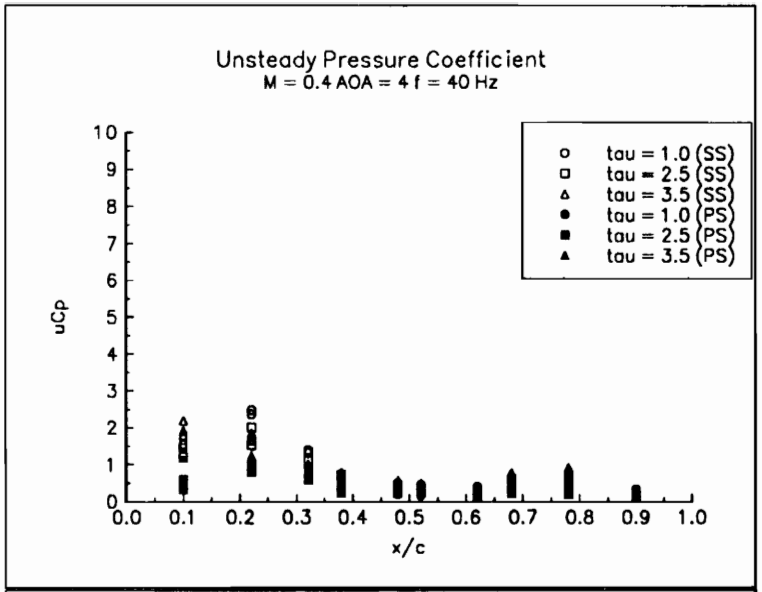
Unsteady Pressure Coefficient
M = 0.4 AOA = 4 f = 40 Hz
tau = 1.0 (SS)
tau = 2.5 (SS)
tau = 3.5 (SS)
tau = 1.0 (PS)
tau = 2.5 (PS)
tau = 3.5 (PS)
uCp
x/c

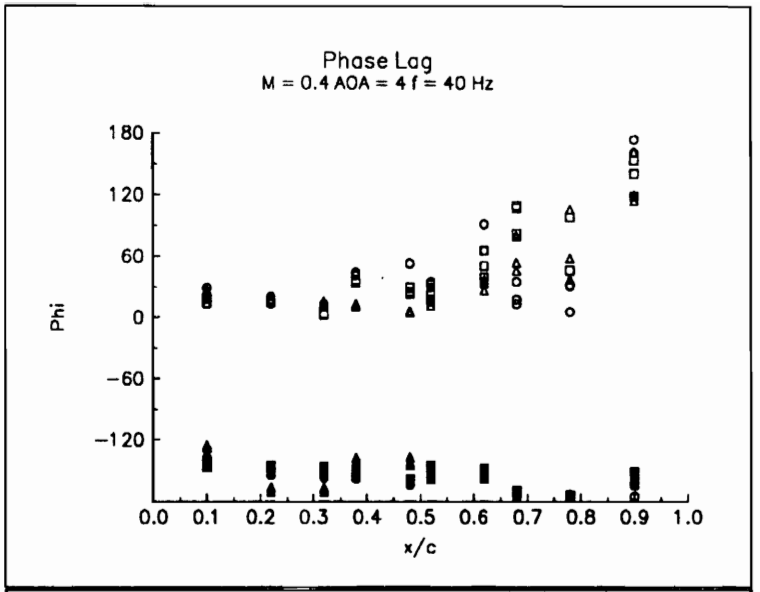
Phase Lag
M = 0.4 AOA = 4 f = 40 Hz
Phi
x/c

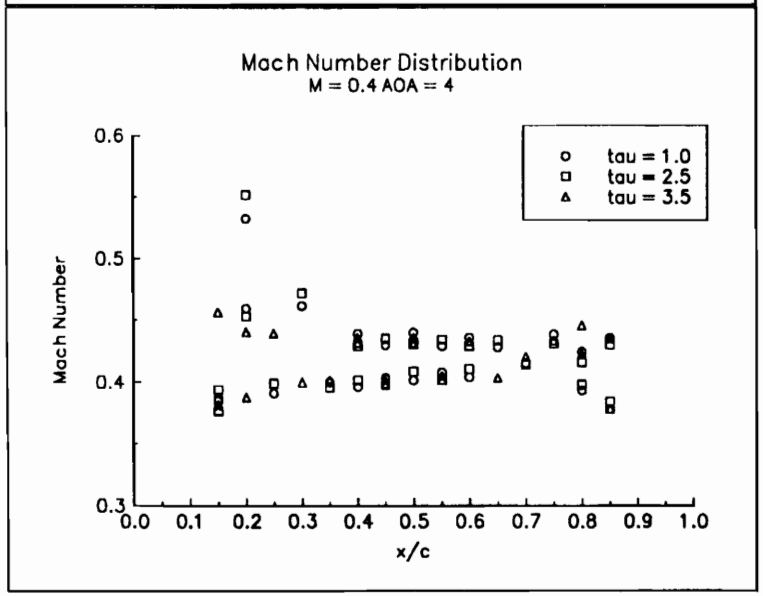
Mach Number Distribution
M = 0.4 AOA = 4
tau = 1.0
tau = 2.5
tau = 3.5
Mach Number
x/c

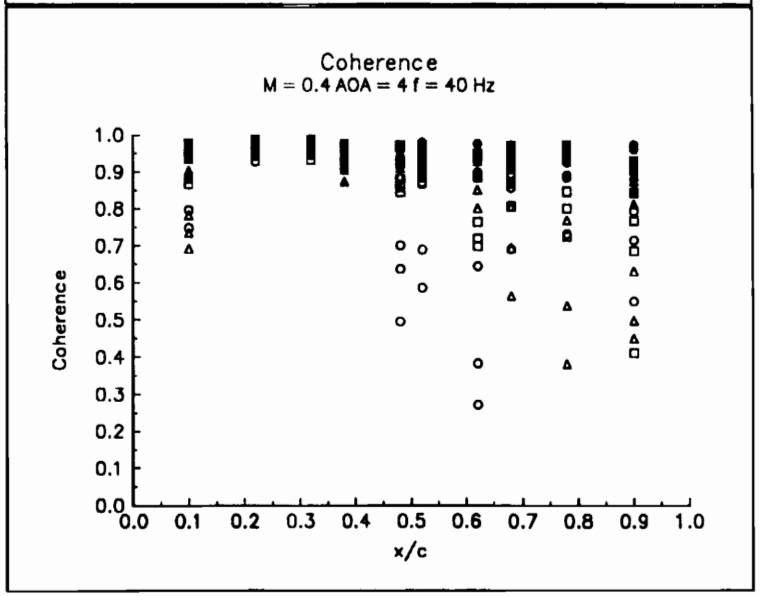
Coherence
M = 0.4 AOA = 4 f = 40 Hz
Coherence
x/c

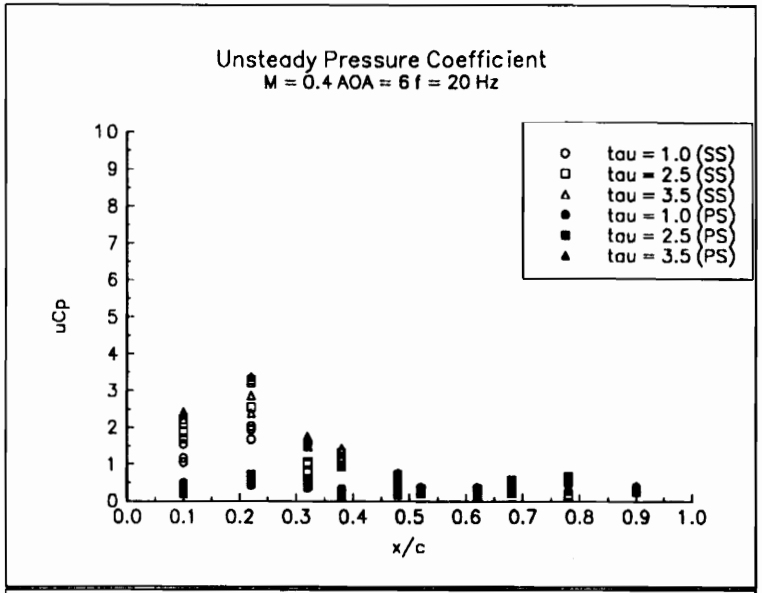
Unsteady Pressure Coefficient
M = 0.4 AOA = 6 f = 20 Hz
tau = 1.0 (SS)
tau = 2.5 (SS)
tau = 3.5 (SS)
tau = 1.0 (PS)
tau = 2.5 (PS)
tau = 3.5 (PS)
uCp
x/c

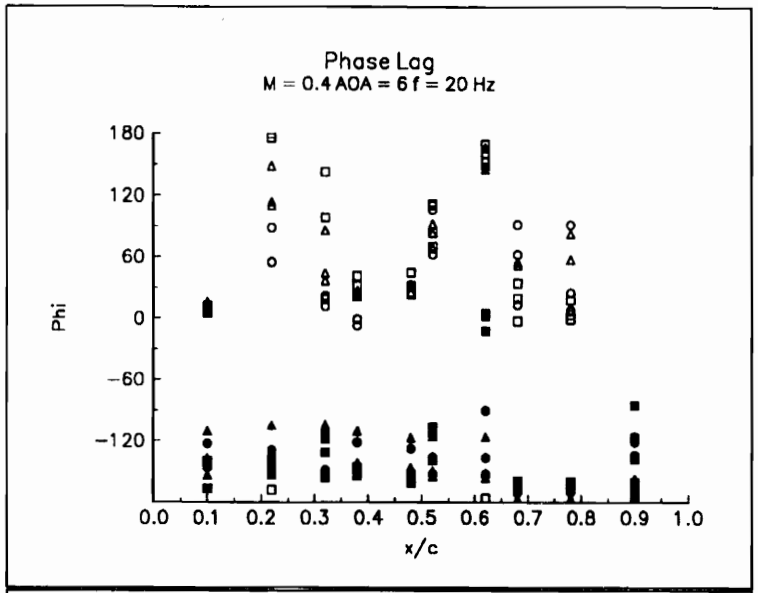
Phase Lag
M = 0.4 AOA = 6 f = 20 Hz
Phi
x/c

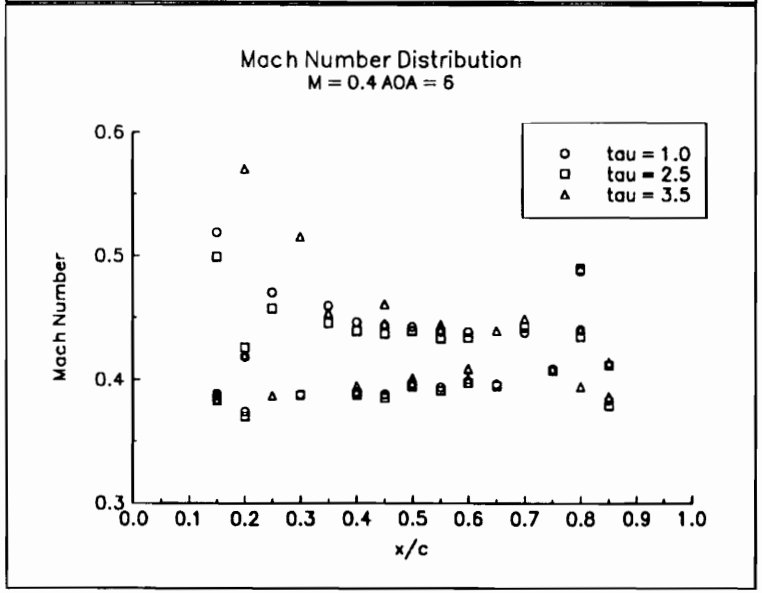
Mach Number Distribution
M = 0.4 AOA = 6
tau = 1.0
tau = 2.5
tau = 3.5
Mach Number
x/c

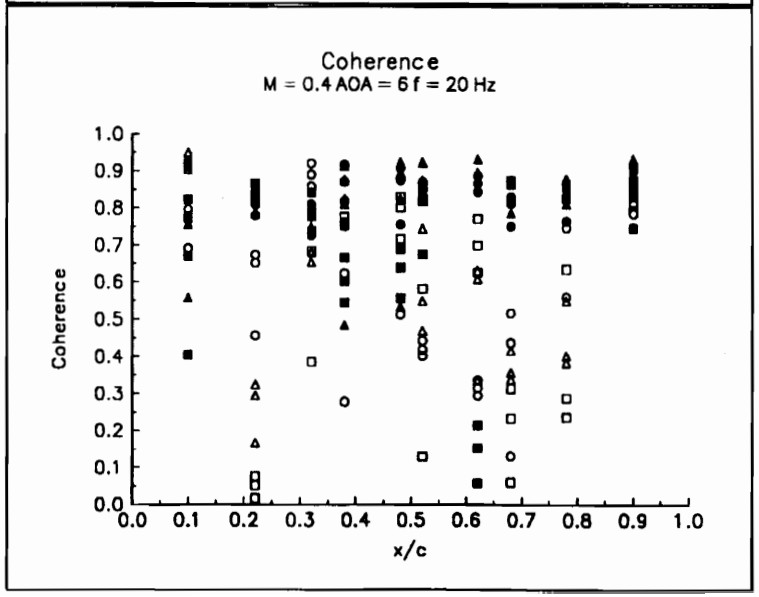
Coherence
M = 0.4 AOA = 6 f = 20 Hz
Coherence
x/c

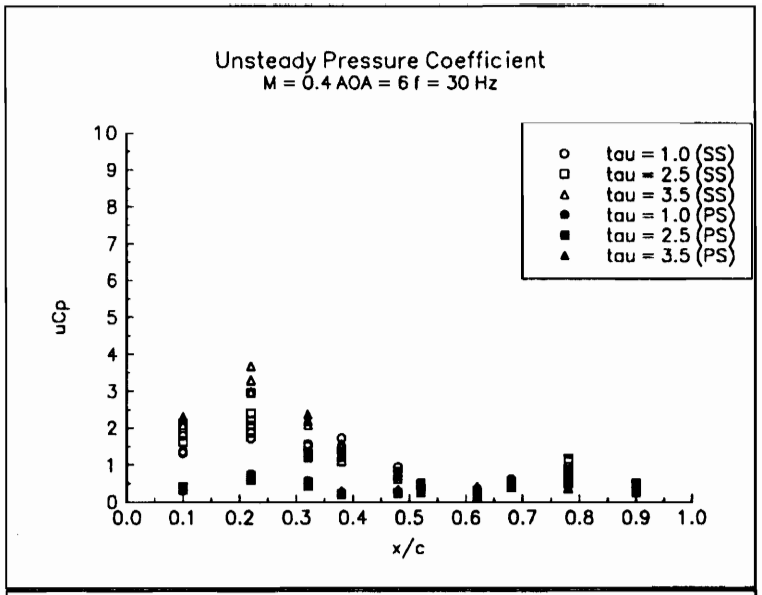
Unsteady Pressure Coefficient
M = 0.4 AOA = 6 f = 30 Hz
uCp
x/c
tau = 1.0 (SS)
tau = 2.5 (SS)
tau = 3.5 (SS)
tau = 1.0 (PS)
tau = 2.5 (PS)
tau = 3.5 (PS)

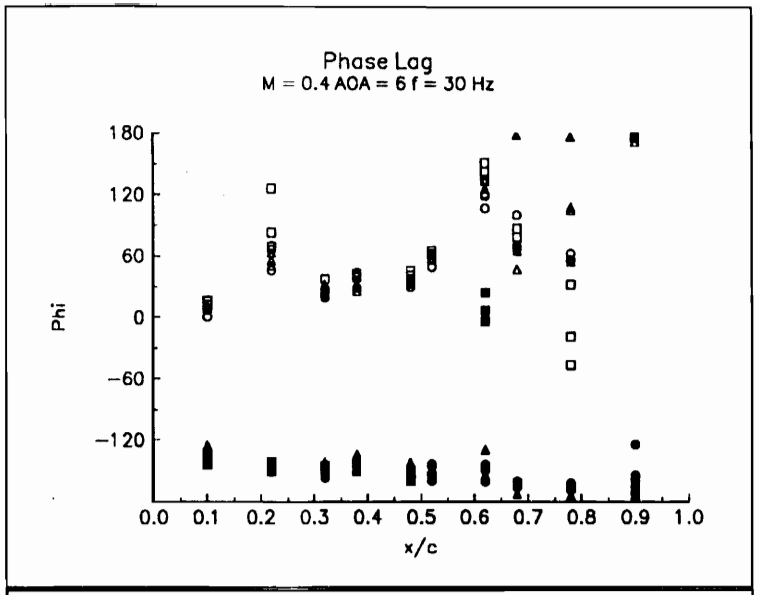
Phase Lag
M = 0.4 AOA = 6 f = 30 Hz
Phi
x/c

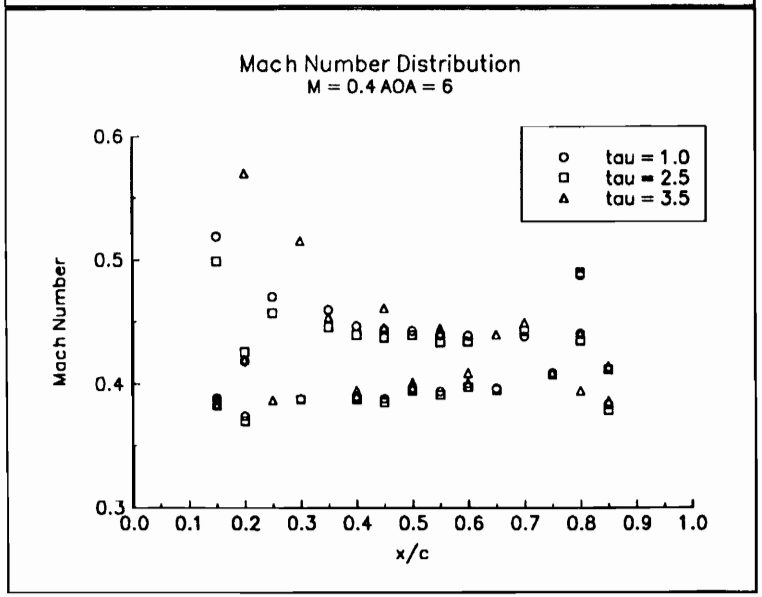
Mach Number Distribution
M = 0.4 AOA = 6
Mach Number
x/c
tau = 1.0
tau = 2.5
tau = 3.5

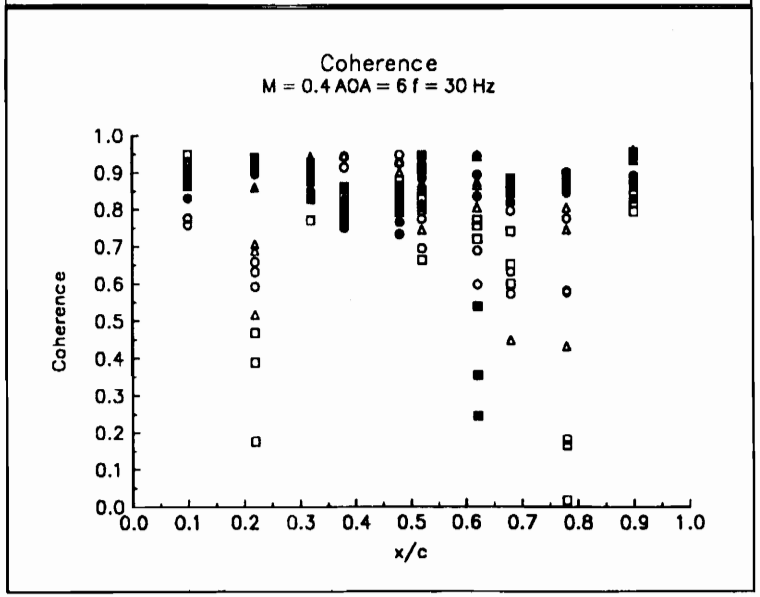
Coherence
M = 0.4 AOA = 6 f = 30 Hz
Coherence
x/c

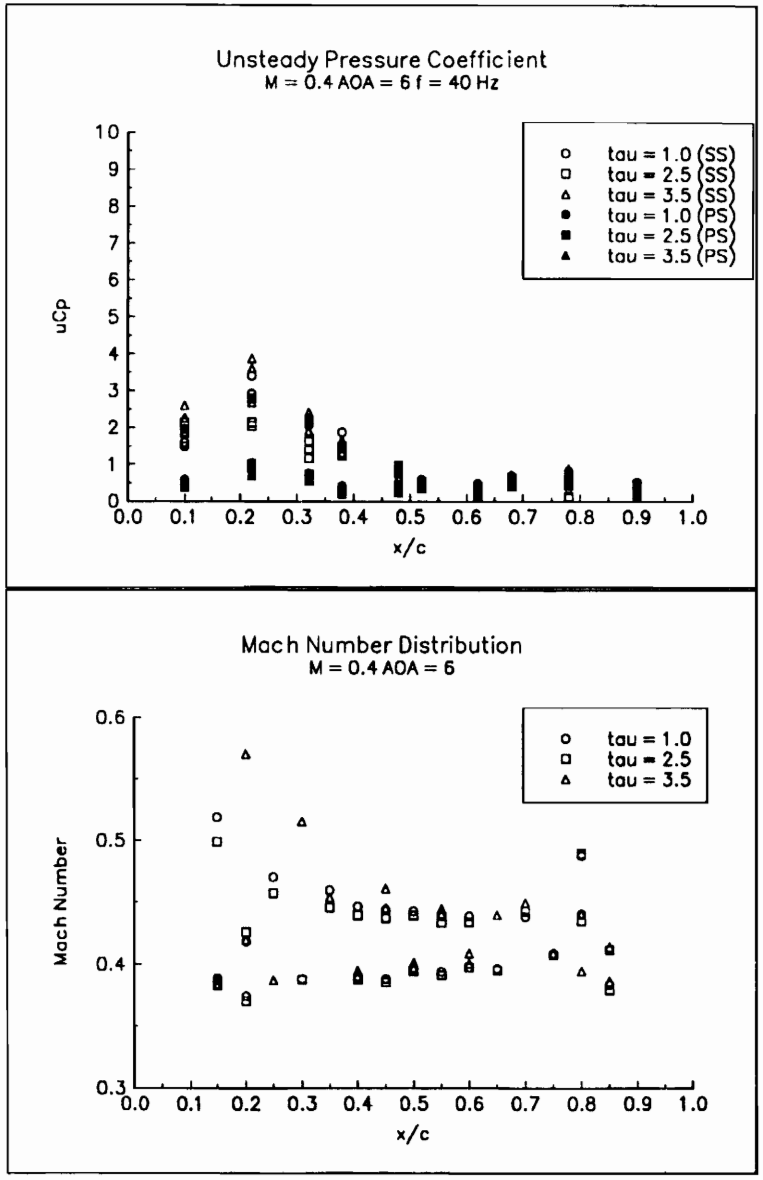
Unsteady Pressure Coefficient
M = 0.4 AOA = 6 f = 40 Hz
uCp
x/c
tau = 1.0 (SS)
tau = 2.5 (SS)
tau = 3.5 (SS)
tau = 1.0 (PS)
tau = 2.5 (PS)
tau = 3.5 (PS)
Phase Lag
M = 0.4 AOA = 6 f = 40 Hz
Phi
x/c
Mach Number Distribution
M = 0.4 AOA = 6
Mach Number
x/c
tau = 1.0
tau = 2.5
tau = 3.5
Coherence
M = 0.4 AOA = 6 f = 40 Hz
Coherence
x/c

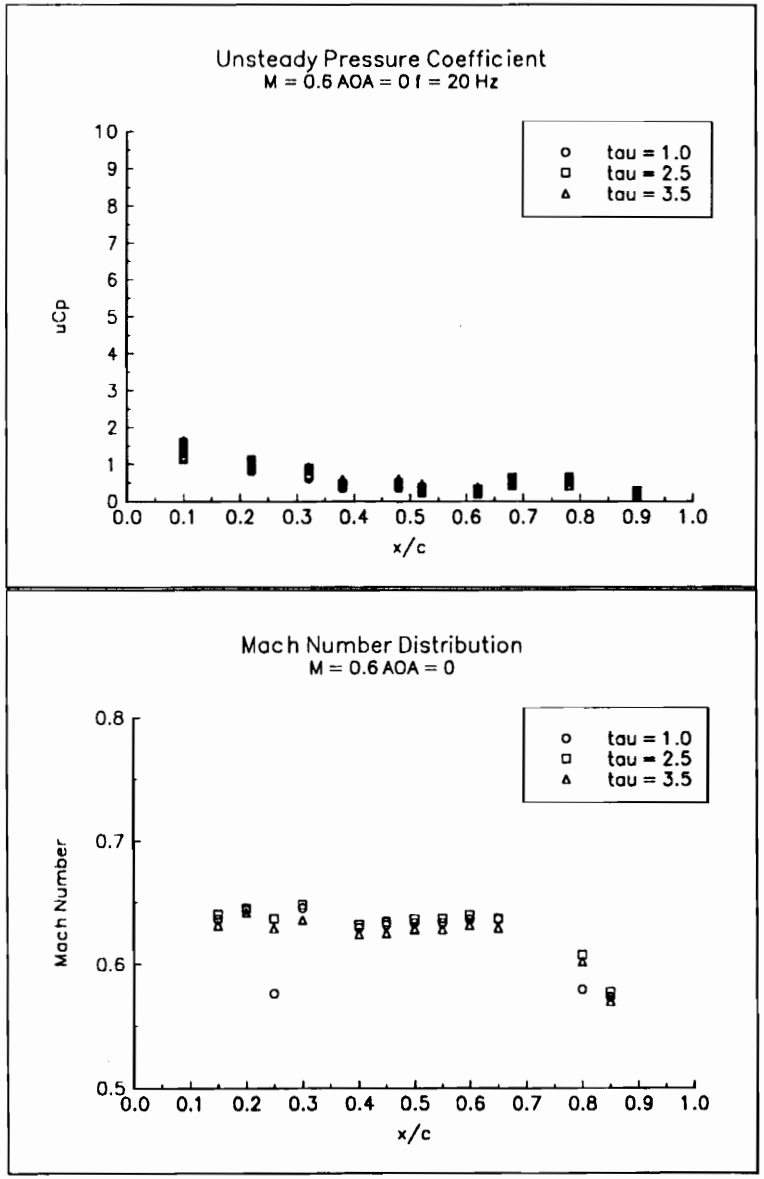
Unsteady Pressure Coefficient
M = 0.6 AOA = 0 f = 20 Hz
tau = 1.0
tau = 2.5
tau = 3.5
uCp
x/c

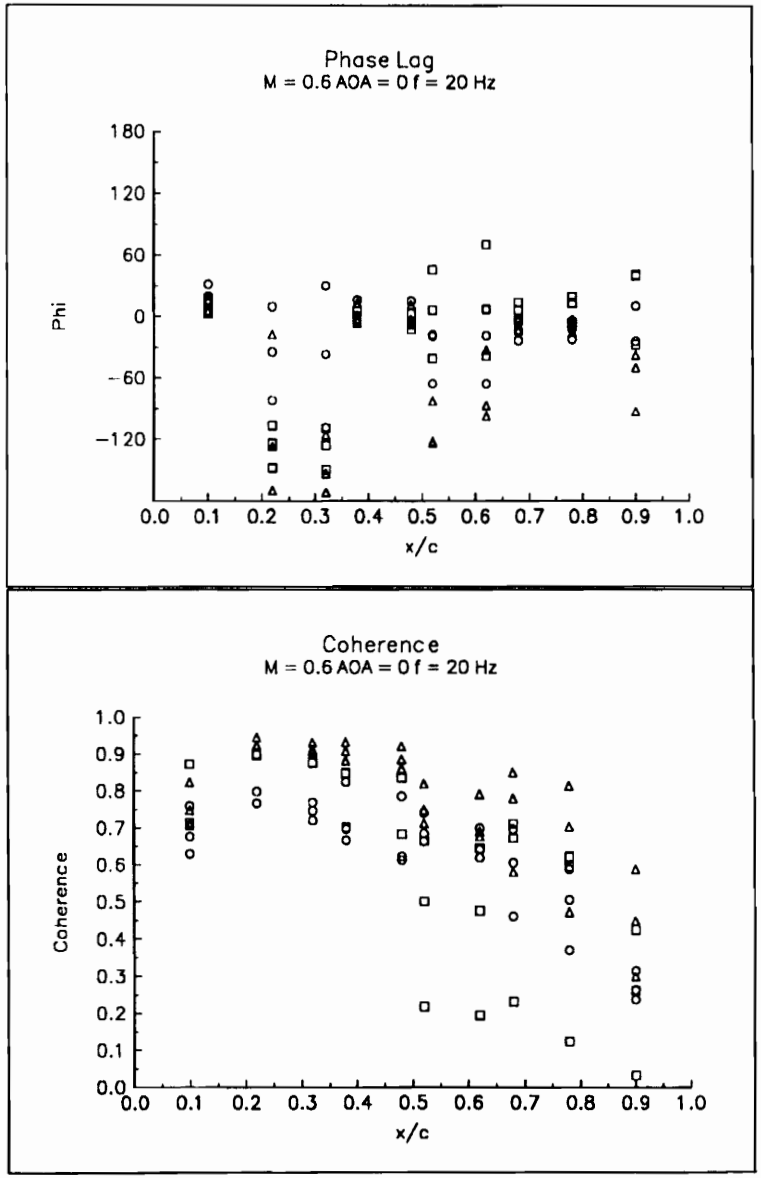
Phase Lag
M = 0.6 AOA = 0 f = 20 Hz
Phi
x/c

Mach Number Distribution
M = 0.6 AOA = 0
tau = 1.0
tau = 2.5
tau = 3.5
Mach Number
x/c

Coherence
M = 0.6 AOA = 0 f = 20 Hz
Coherence
x/c

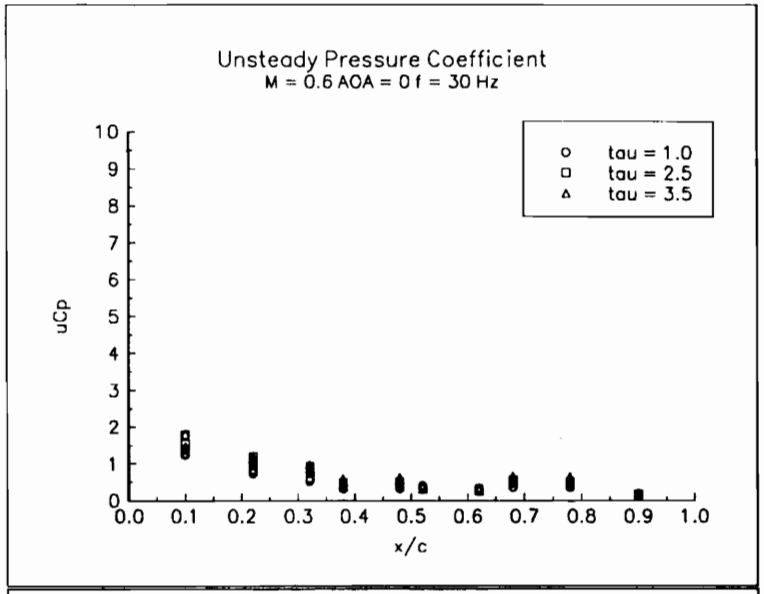
Unsteady Pressure Coefficient
M = 0.6 AOA = 0 f = 30 Hz
tau = 1.0
tau = 2.5
tau = 3.5
uCp
x/c

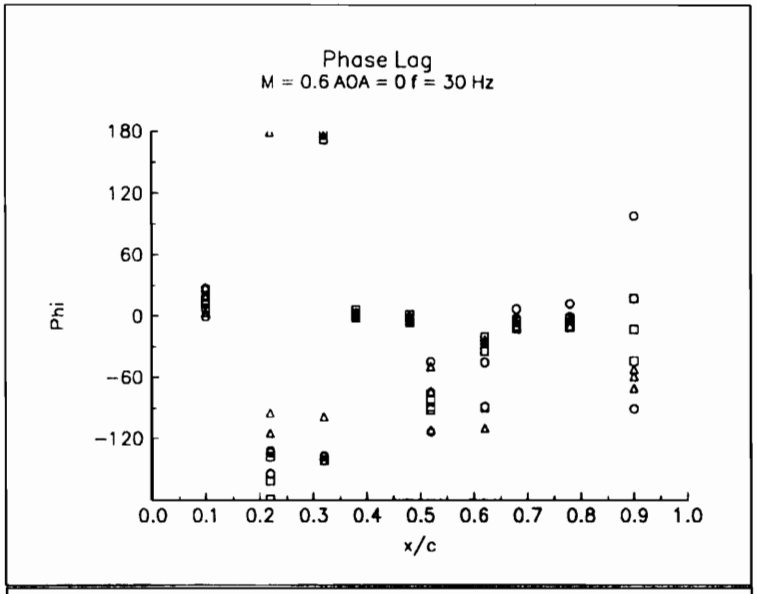
Phase Lag
M = 0.6 AOA = 0 f = 30 Hz
Phi
x/c

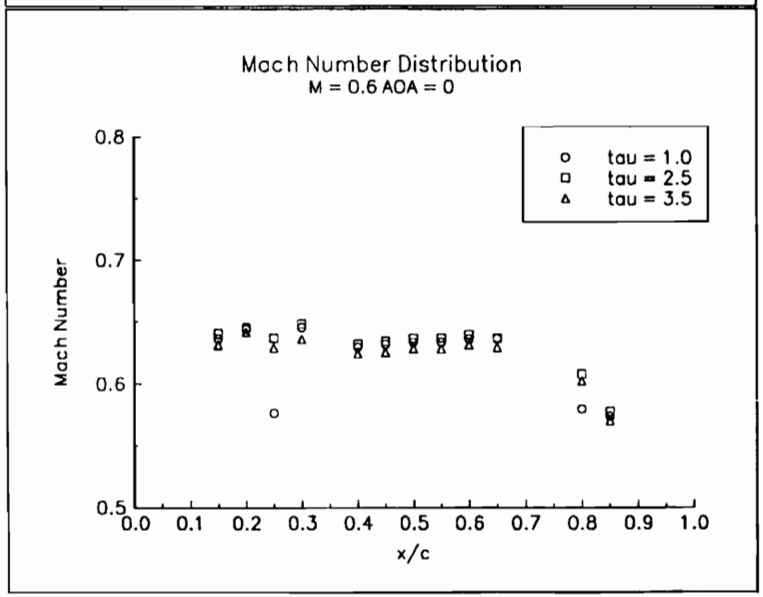
Mach Number Distribution
M = 0.6 AOA = 0
tau = 1.0
tau = 2.5
tau = 3.5
Mach Number
x/c

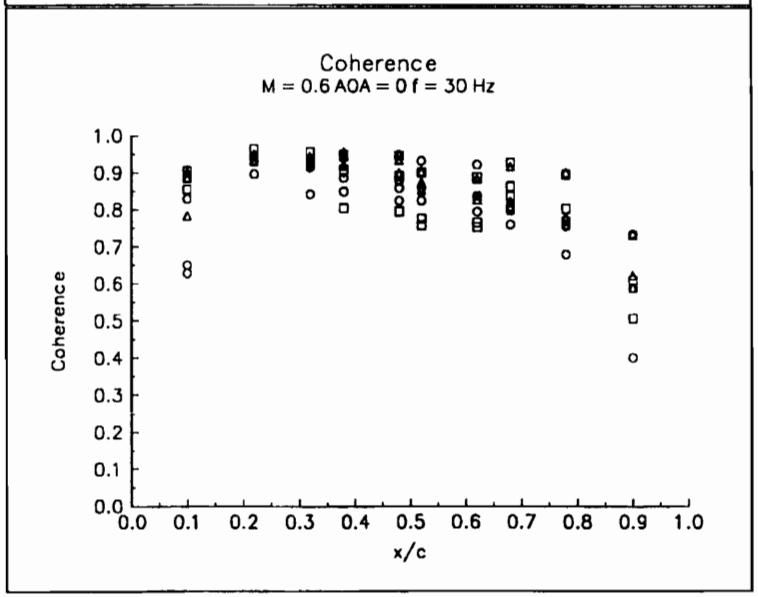
Coherence
M = 0.6 AOA = 0 f = 30 Hz
Coherence
x/c

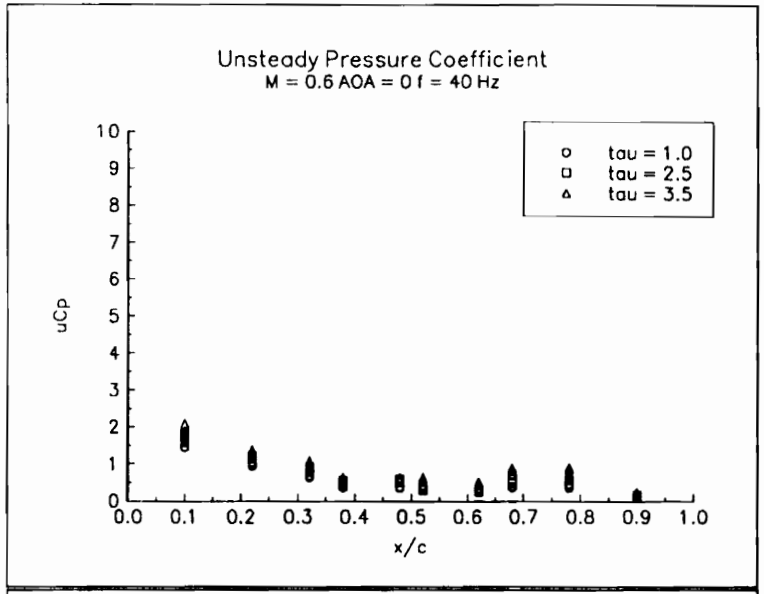
Unsteady Pressure Coefficient
M = 0.6 AOA = 0 f = 40 Hz
tau = 1.0
tau = 2.5
tau = 3.5
uCp
x/c

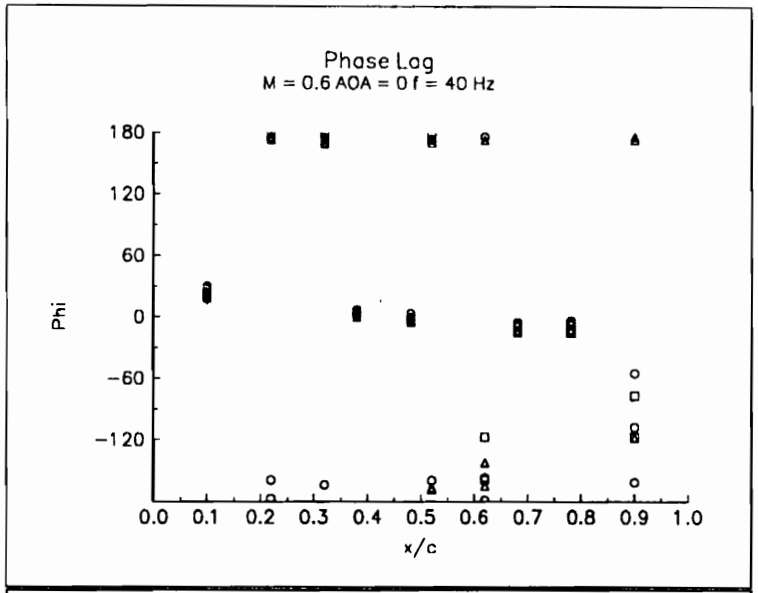
Phase Lag
M = 0.6 AOA = 0 f = 40 Hz
Phi
x/c

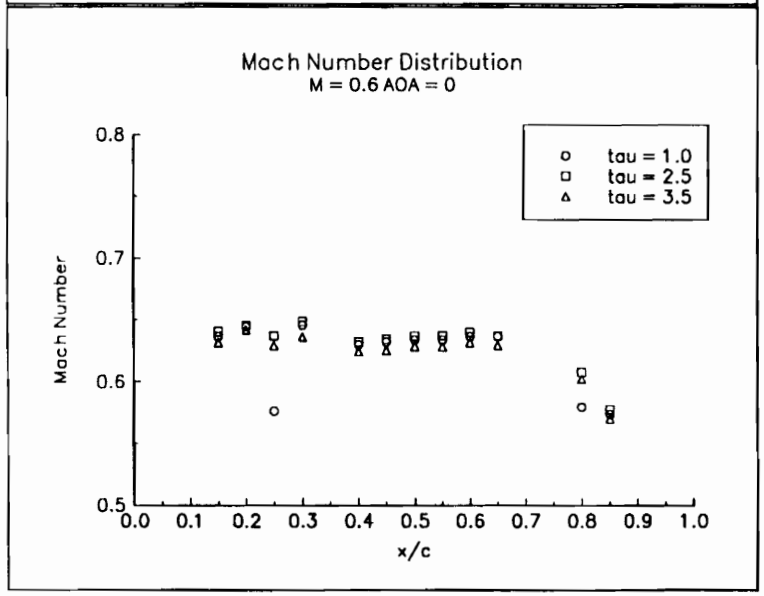
Mach Number Distribution
M = 0.6 AOA = 0
tau = 1.0
tau = 2.5
tau = 3.5
Mach Number
x/c

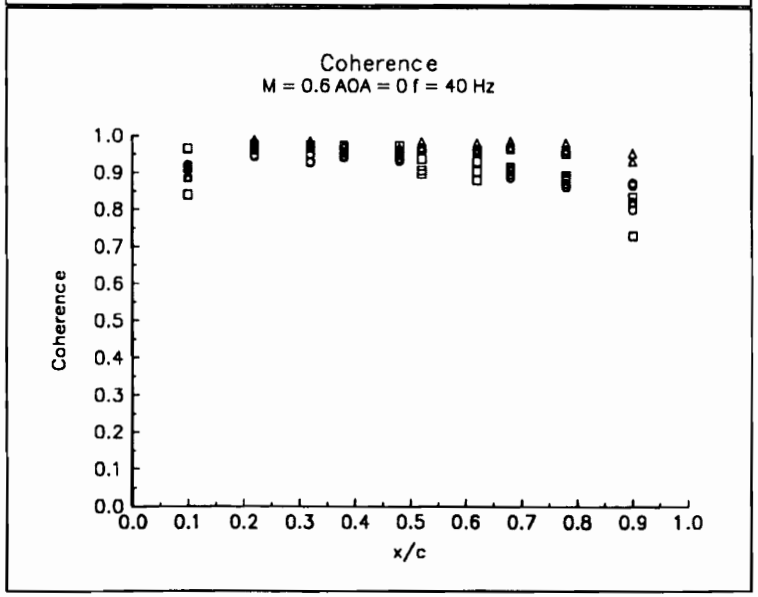
Coherence
M = 0.6 AOA = 0 f = 40 Hz
Coherence
x/c

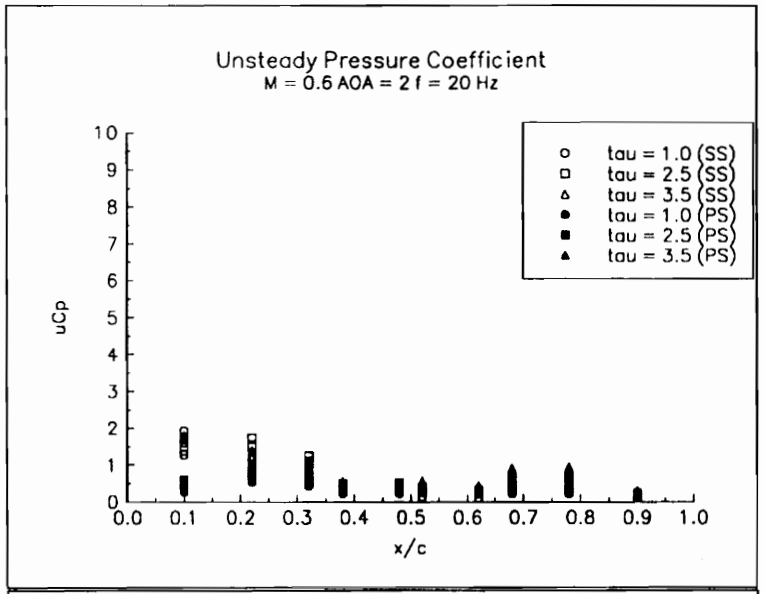
Unsteady Pressure Coefficient
M = 0.6 AOA = 2 f = 20 Hz
tau = 1.0 (SS)
tau = 2.5 (SS)
tau = 3.5 (SS)
tau = 1.0 (PS)
tau = 2.5 (PS)
tau = 3.5 (PS)
uCp
x/c

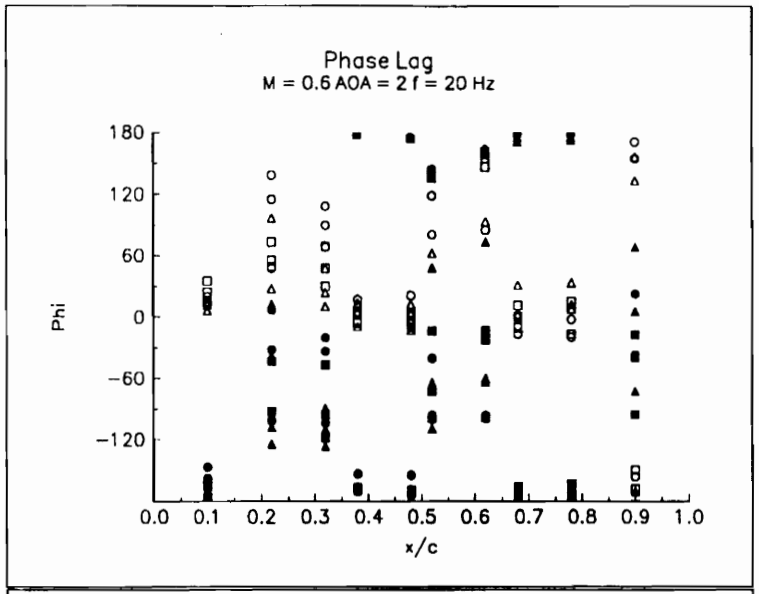
Phase Lag
M = 0.6 AOA = 2 f = 20 Hz
Phi
x/c

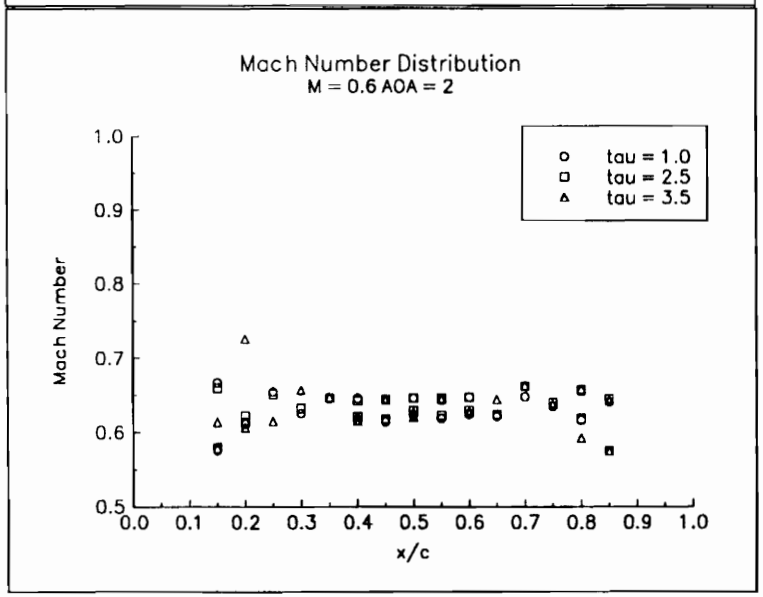
Mach Number Distribution
M = 0.6 AOA = 2
tau = 1.0
tau = 2.5
tau = 3.5
Mach Number
x/c

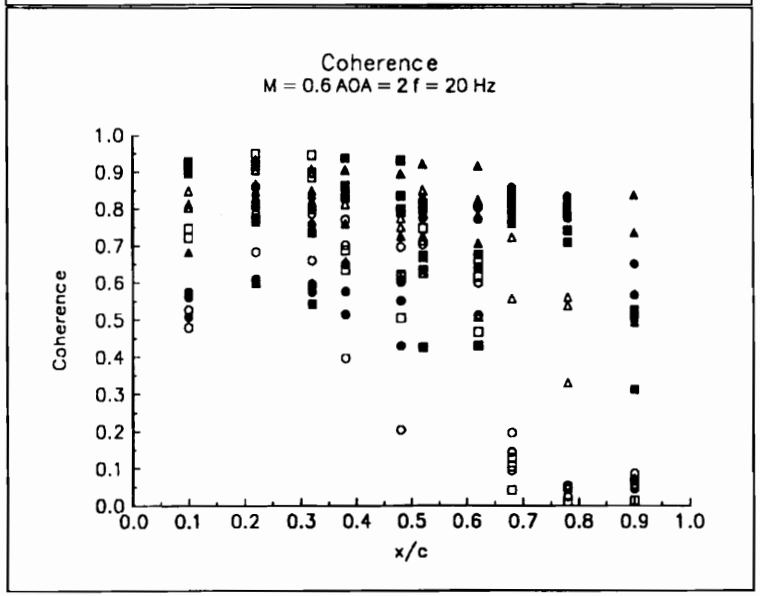
Coherence
M = 0.6 AOA = 2 f = 20 Hz
Coherence
x/c

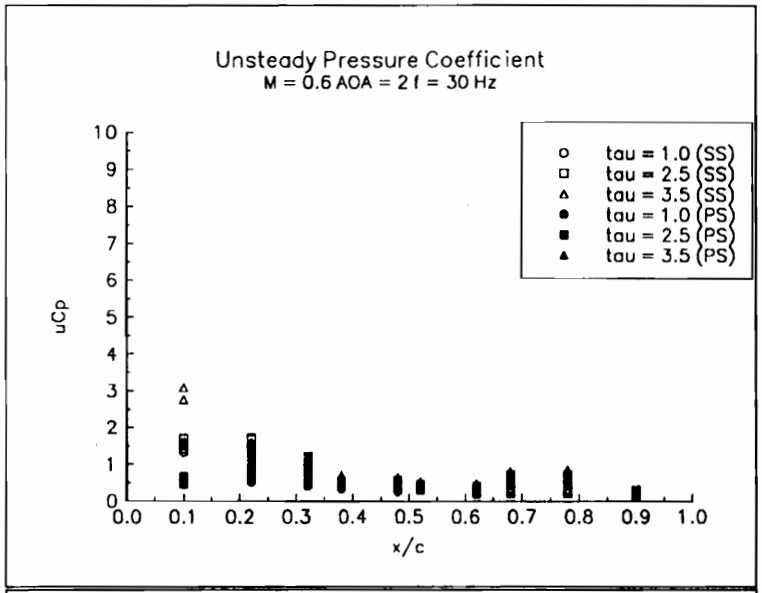
Unsteady Pressure Coefficient
M = 0.6 AOA = 2 f = 30 Hz
tau = 1.0 (SS)
tau = 2.5 (SS)
tau = 3.5 (SS)
tau = 1.0 (PS)
tau = 2.5 (PS)
tau = 3.5 (PS)
uCp
x/c

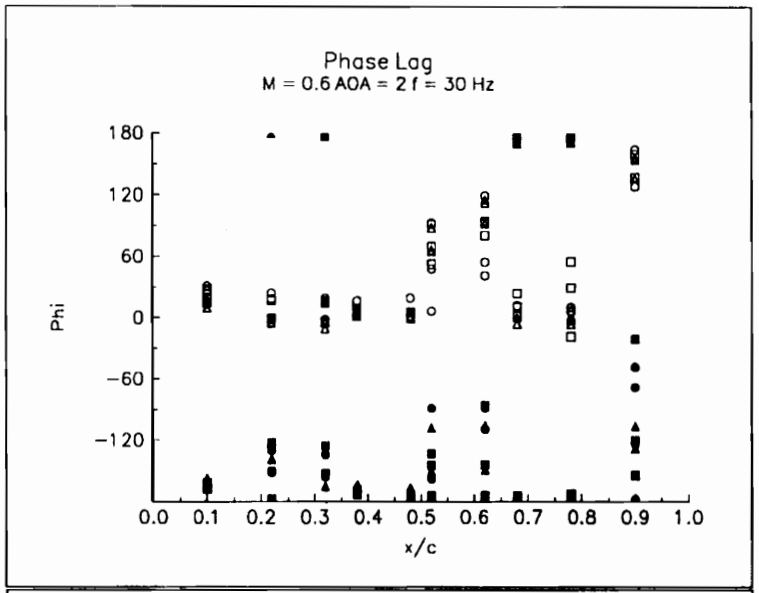
Phase Lag
M = 0.6 AOA = 2 f = 30 Hz
Phi
x/c

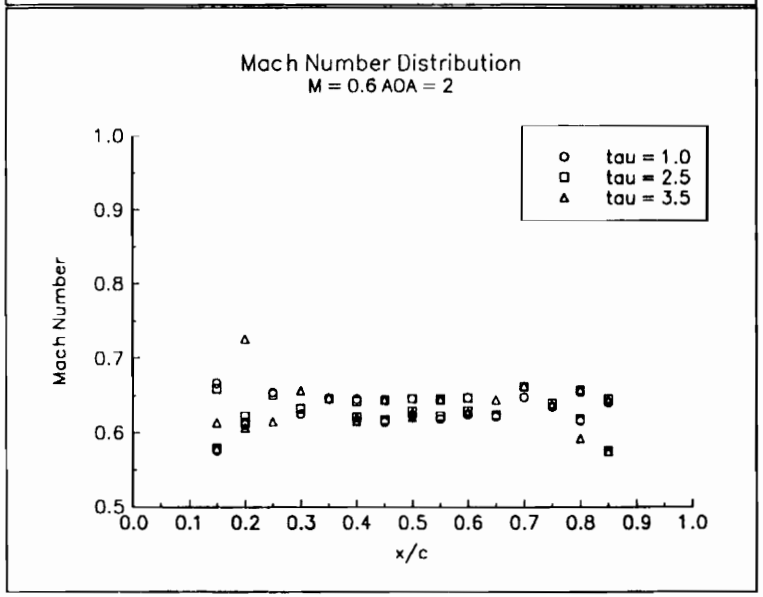
Mach Number Distribution
M = 0.6 AOA = 2
tau = 1.0
tau = 2.5
tau = 3.5
Mach Number
x/c

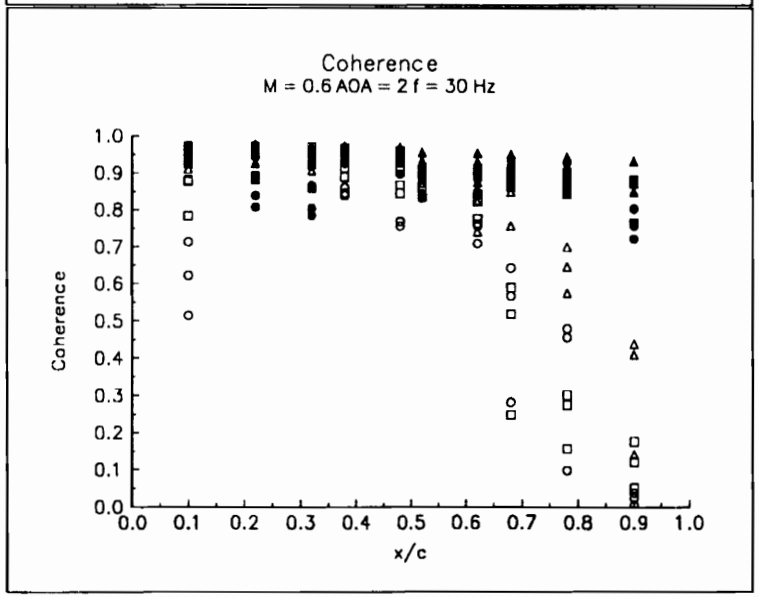
Coherence
M = 0.6 AOA = 2 f = 30 Hz
Coherence
x/c

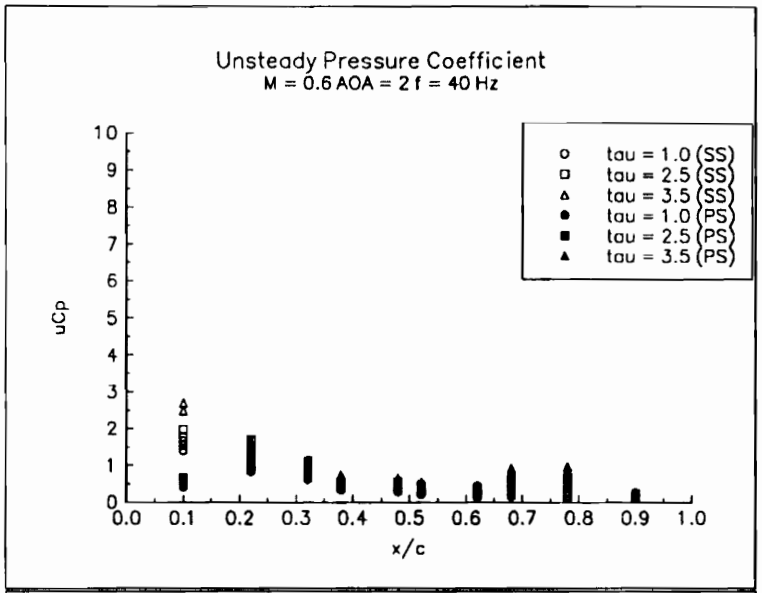
Unsteady Pressure Coefficient
M = 0.6 AOA = 2 f = 40 Hz
uCp
x/c
tau = 1.0 (SS)
tau = 2.5 (SS)
tau = 3.5 (SS)
tau = 1.0 (PS)
tau = 2.5 (PS)
tau = 3.5 (PS)

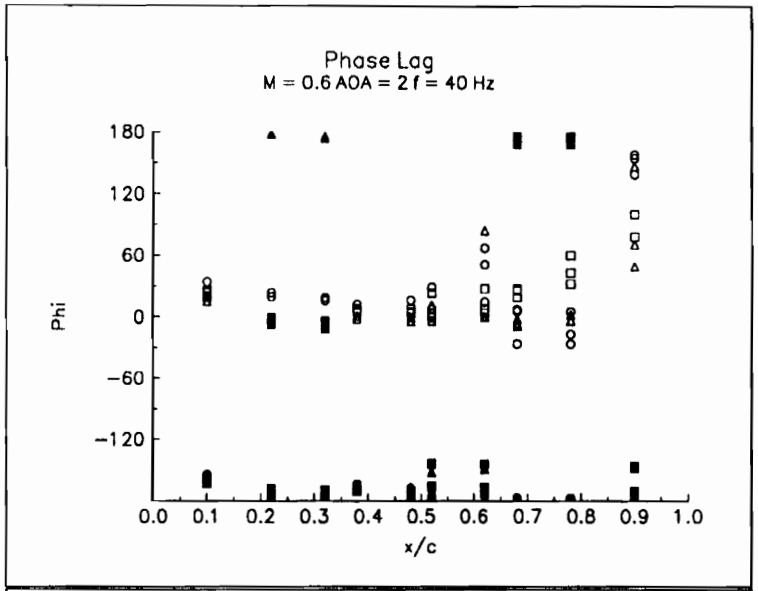
Phase Lag
M = 0.6 AOA = 2 f = 40 Hz
Phi
x/c

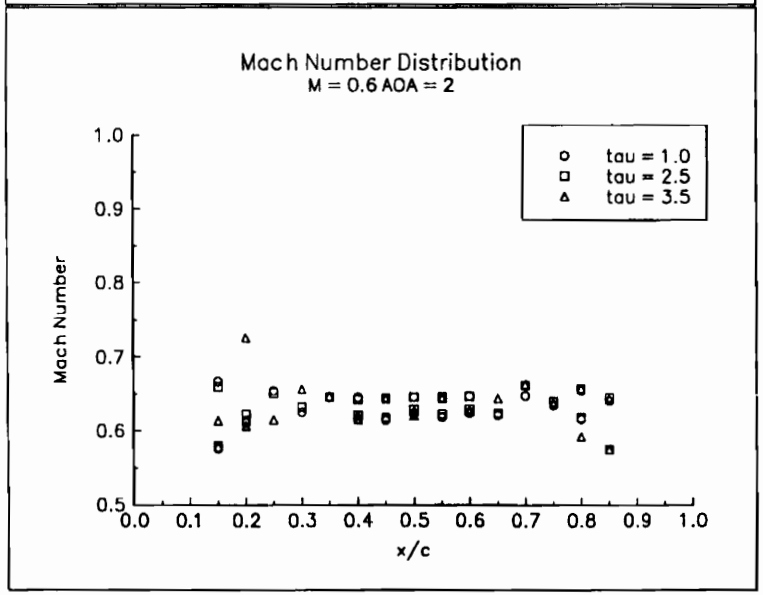
Mach Number Distribution
M = 0.6 AOA = 2
Mach Number
x/c
tau = 1.0
tau = 2.5
tau = 3.5

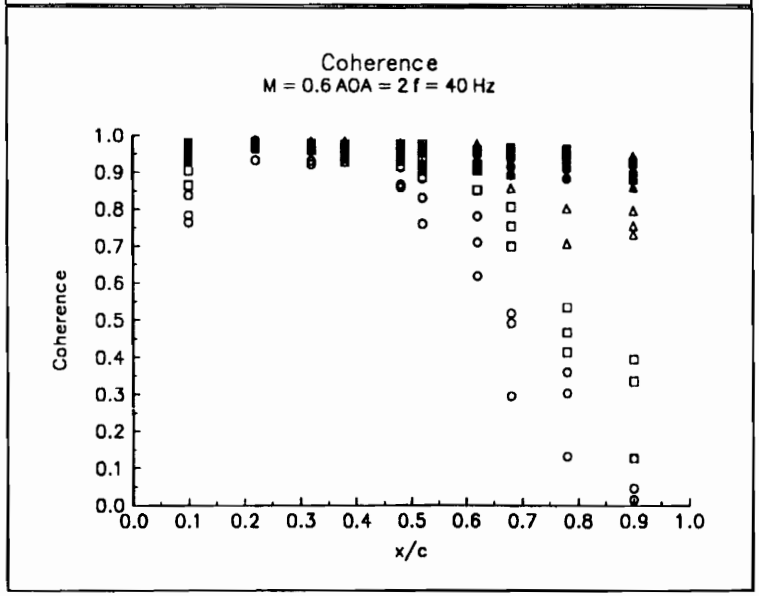
Coherence
M = 0.6 AOA = 2 f = 40 Hz
Coherence
x/c

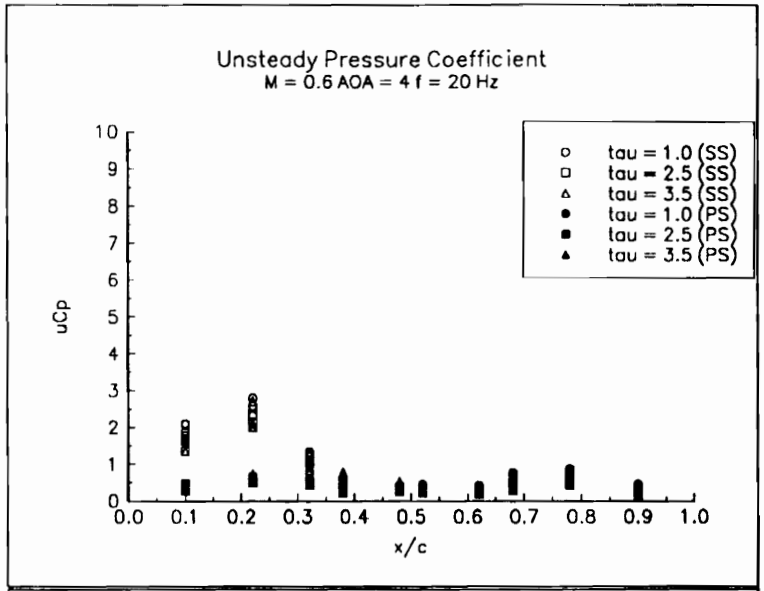
Unsteady Pressure Coefficient
M = 0.6 AOA = 4 f = 20 Hz
uCp
x/c
tau = 1.0 (SS)
tau = 2.5 (SS)
tau = 3.5 (SS)
tau = 1.0 (PS)
tau = 2.5 (PS)
tau = 3.5 (PS)

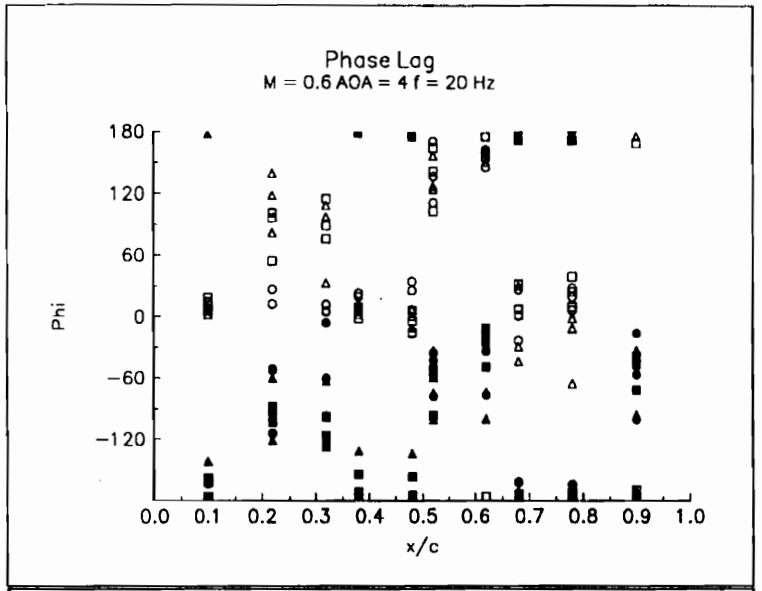
Phase Lag
M = 0.6 AOA = 4 f = 20 Hz
Phi
x/c

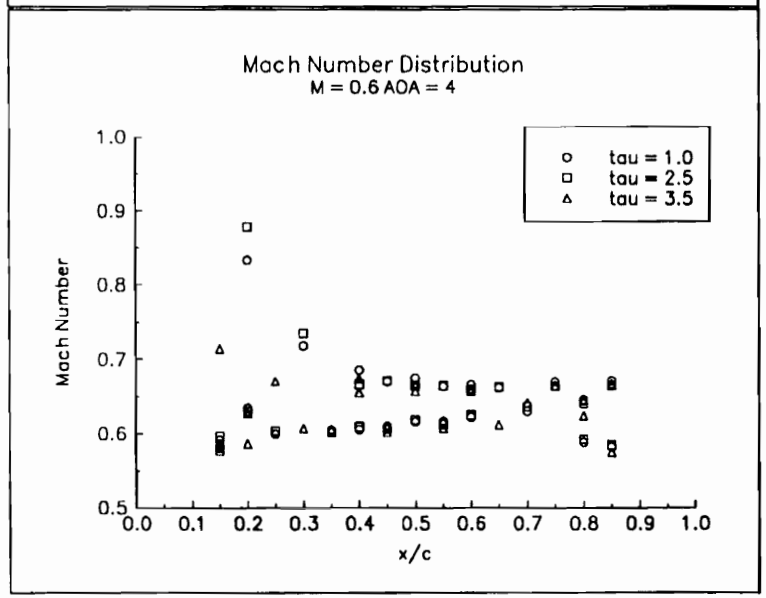
Mach Number Distribution
M = 0.6 AOA = 4
Mach Number
x/c
tau = 1.0
tau = 2.5
tau = 3.5

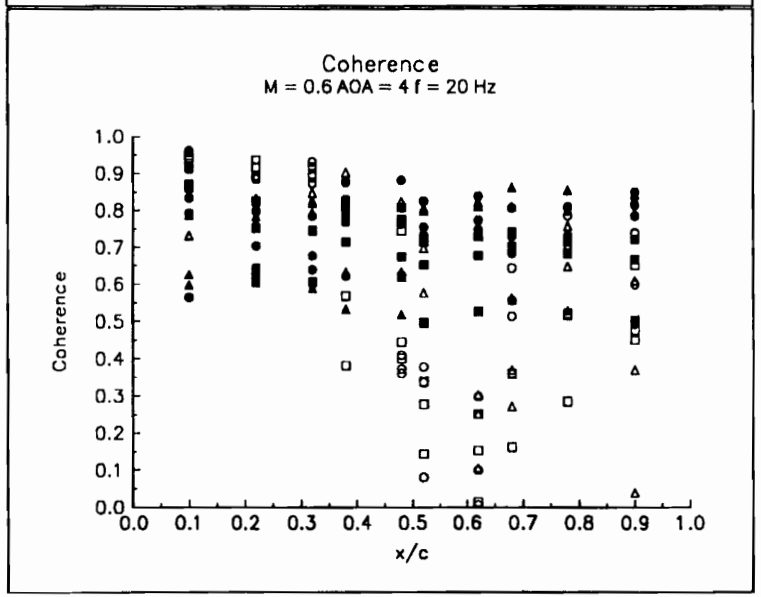
Coherence
M = 0.6 AOA = 4 f = 20 Hz
Coherence
x/c

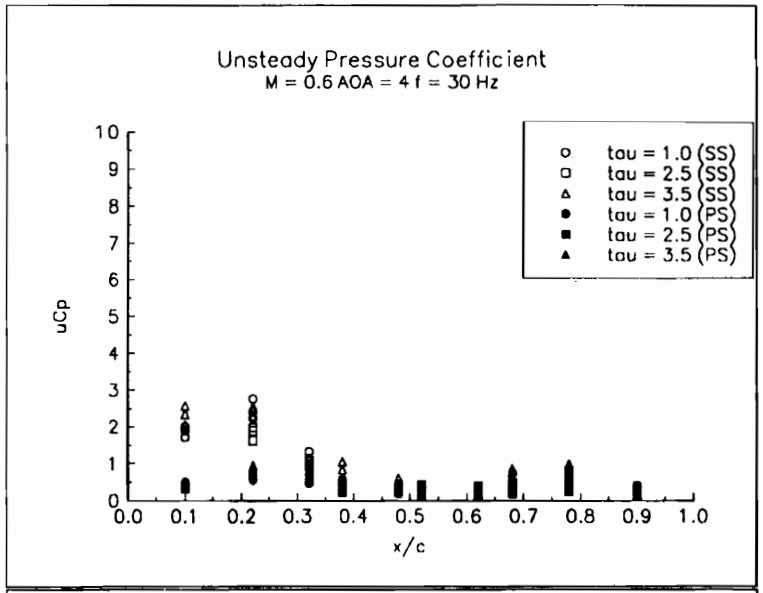
Unsteady Pressure Coefficient
M = 0.6 AOA = 4 f = 30 Hz
tau = 1.0 (SS)
tau = 2.5 (SS)
tau = 3.5 (SS)
tau = 1.0 (PS)
tau = 2.5 (PS)
tau = 3.5 (PS)
uCp
x/c

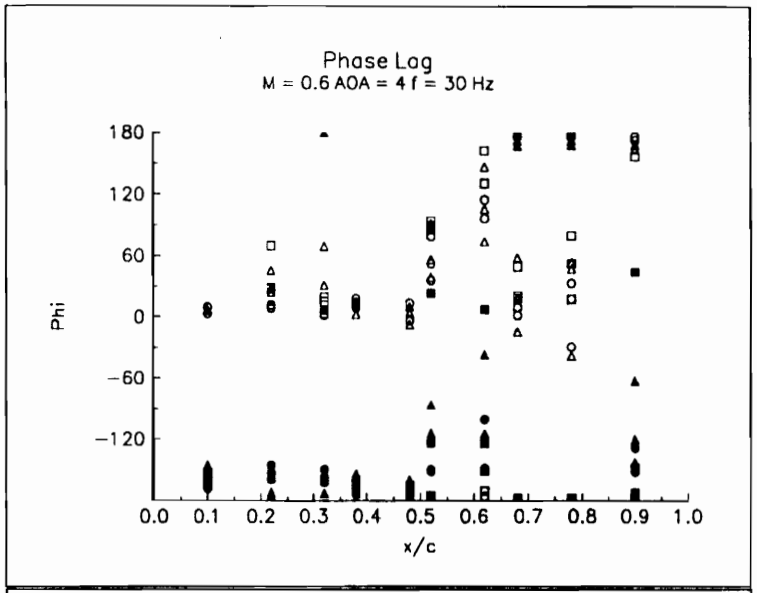
Phase Lag
M = 0.6 AOA = 4 f = 30 Hz
Phi
x/c

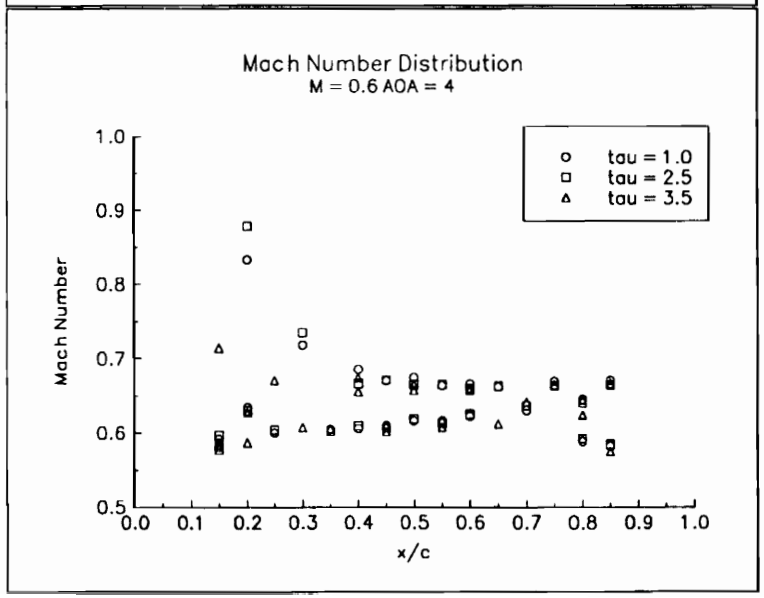
Mach Number Distribution
M = 0.6 AOA = 4
tau = 1.0
tau = 2.5
tau = 3.5
Mach Number
x/c

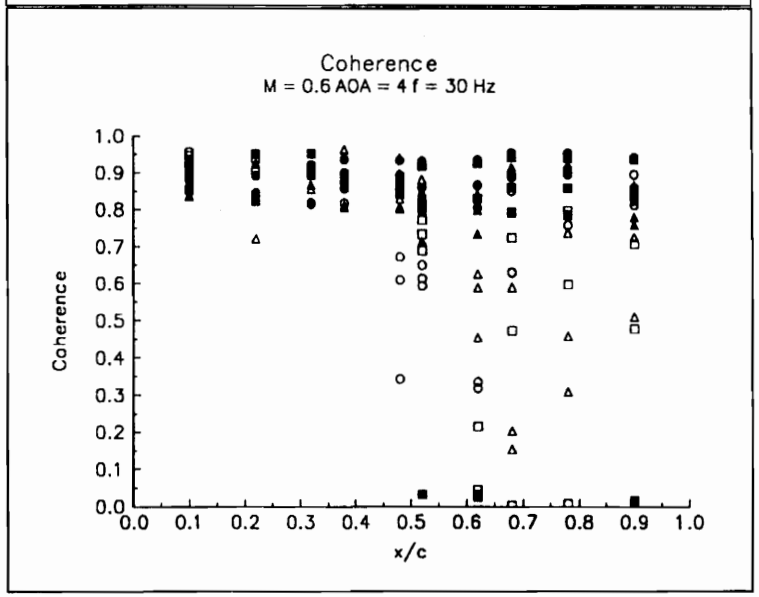
Coherence
M = 0.6 AOA = 4 f = 30 Hz
Coherence
x/c

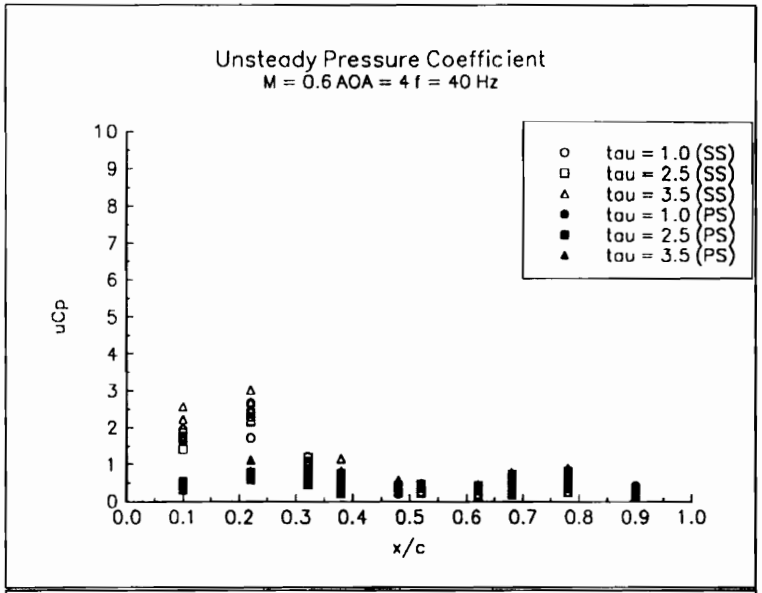
Unsteady Pressure Coefficient
M = 0.6 AOA = 4 f = 40 Hz
tau = 1.0 (SS)
tau = 2.5 (SS)
tau = 3.5 (SS)
tau = 1.0 (PS)
tau = 2.5 (PS)
tau = 3.5 (PS)
uCp
x/c

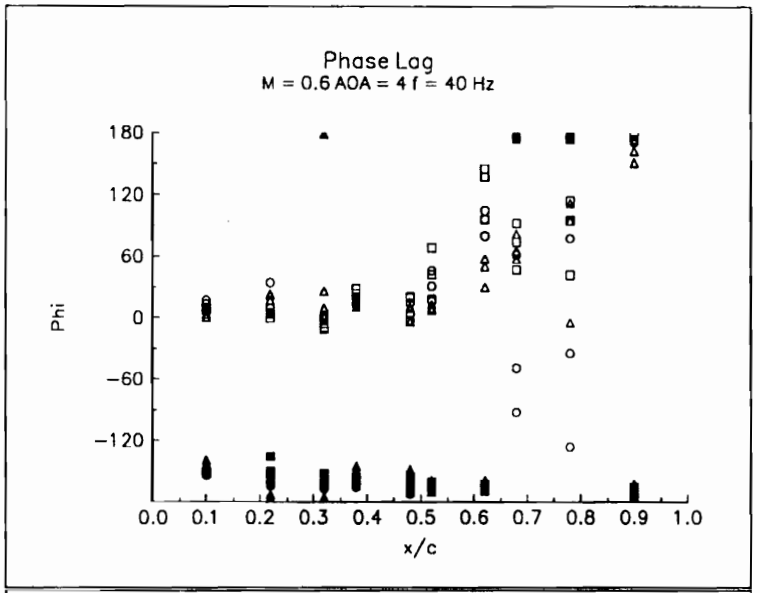
Phase Lag
M = 0.6 AOA = 4 f = 40 Hz
Phi
x/c

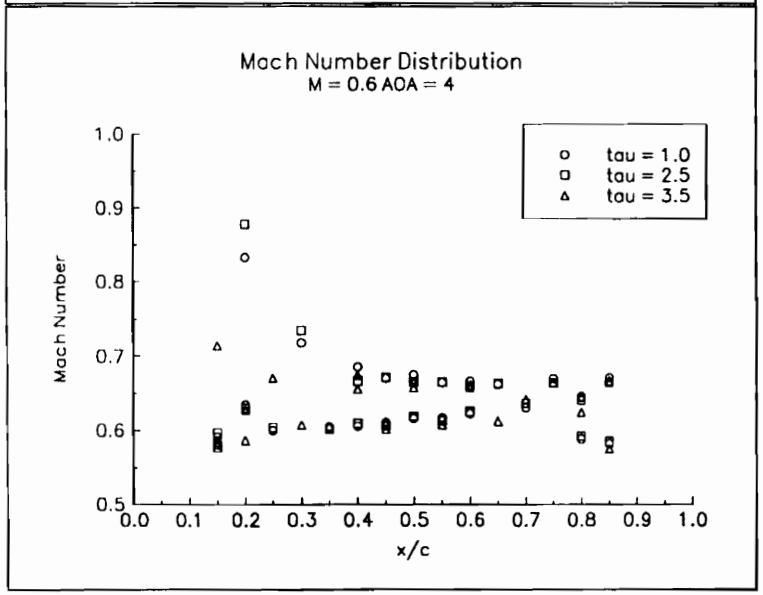
Mach Number Distribution
M = 0.6 AOA = 4
tau = 1.0
tau = 2.5
tau = 3.5
Mach Number
x/c

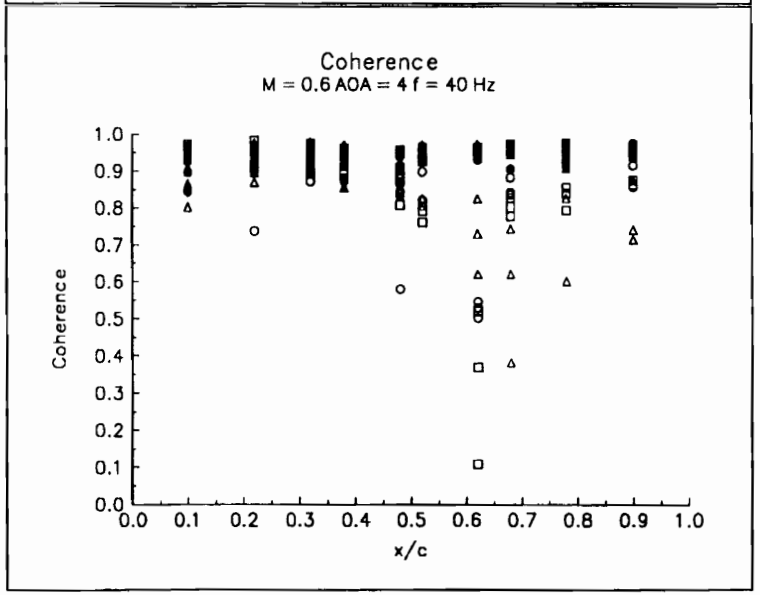
Coherence
M = 0.6 AOA = 4 f = 40 Hz
Coherence
x/c

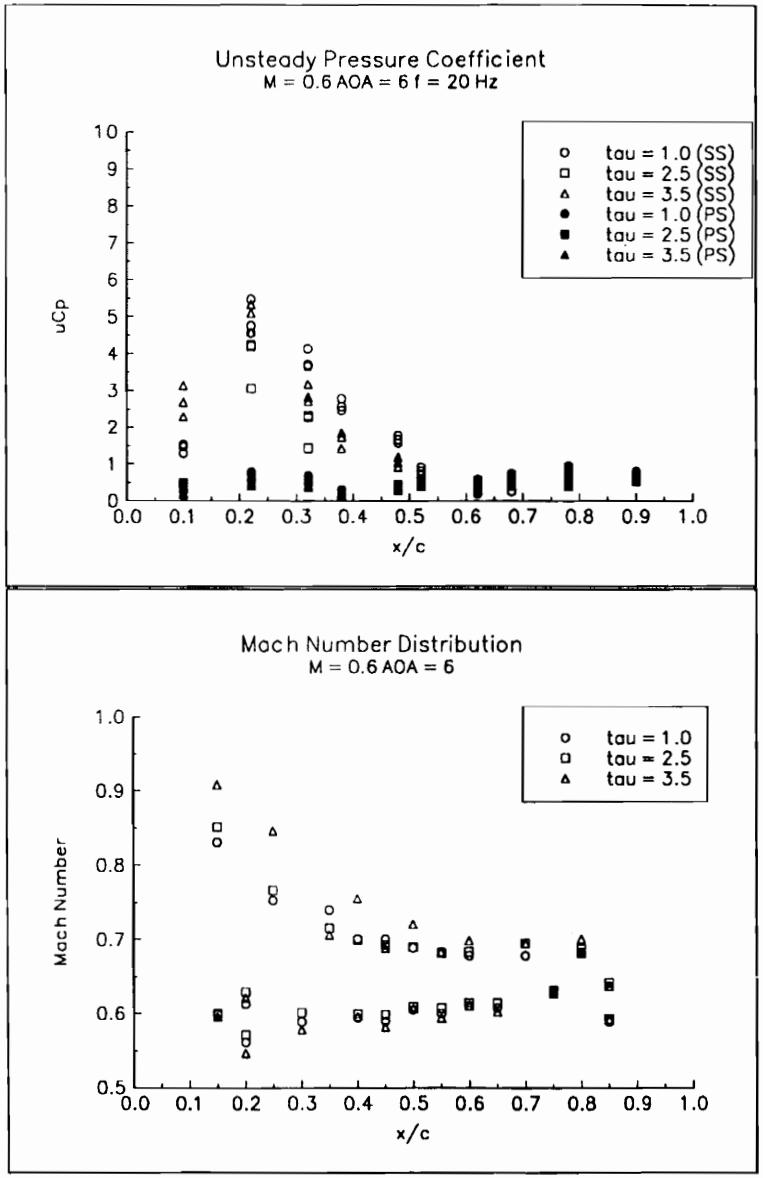
Unsteady Pressure Coefficient
M = 0.6 AOA = 6 f = 20 Hz
tau = 1.0 (SS)
tau = 2.5 (SS)
tau = 3.5 (SS)
tau = 1.0 (PS)
tau = 2.5 (PS)
tau = 3.5 (PS)
uCp
x/c

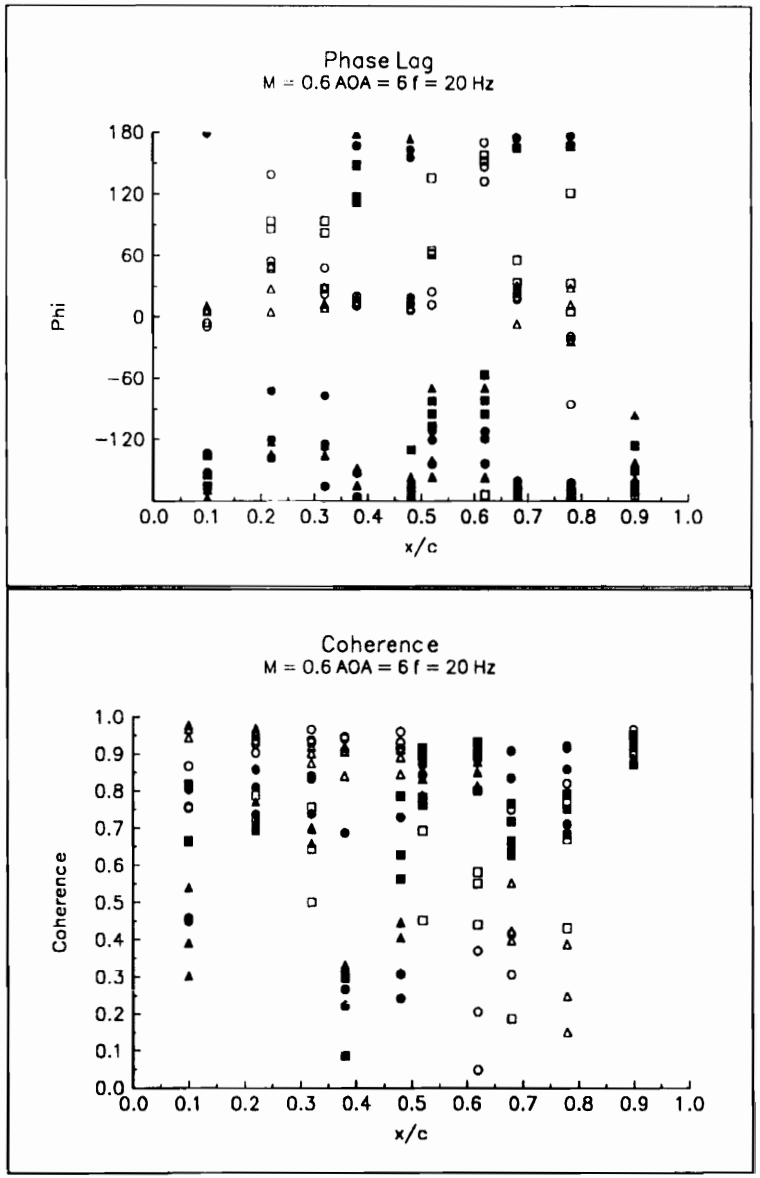
Phase Lag
M = 0.6 AOA = 6 f = 20 Hz
Phi
x/c

Mach Number Distribution
M = 0.6 AOA = 6
tau = 1.0
tau = 2.5
tau = 3.5
Mach Number
x/c

Coherence
M = 0.6 AOA = 6 f = 20 Hz
Coherence
x/c

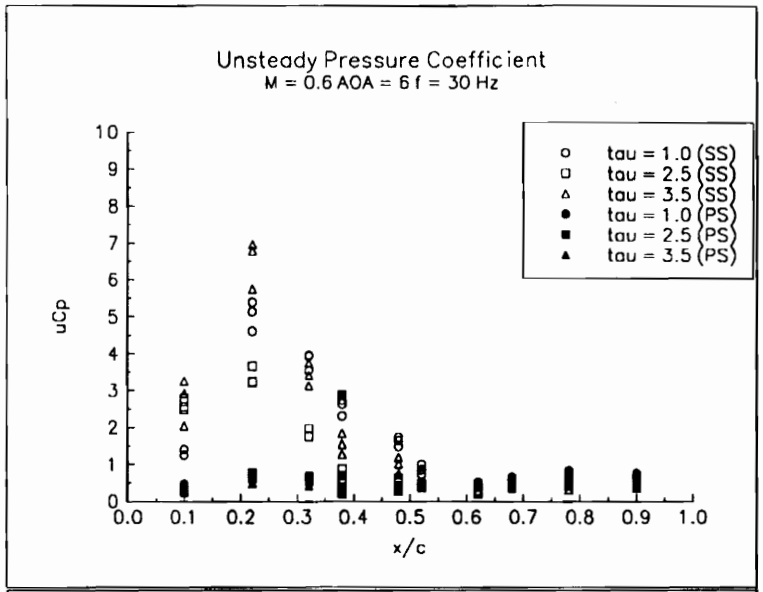
Unsteady Pressure Coefficient
M = 0.6 AOA = 6 f = 30 Hz
uCp
x/c
tau = 1.0 (SS)
tau = 2.5 (SS)
tau = 3.5 (SS)
tau = 1.0 (PS)
tau = 2.5 (PS)
tau = 3.5 (PS)

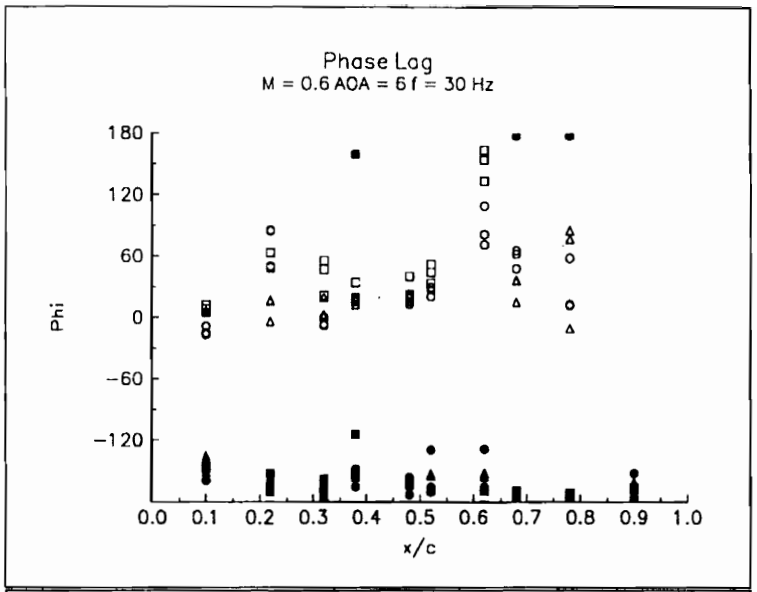
Phase Lag
M = 0.6 AOA = 6 f = 30 Hz
Phi
x/c

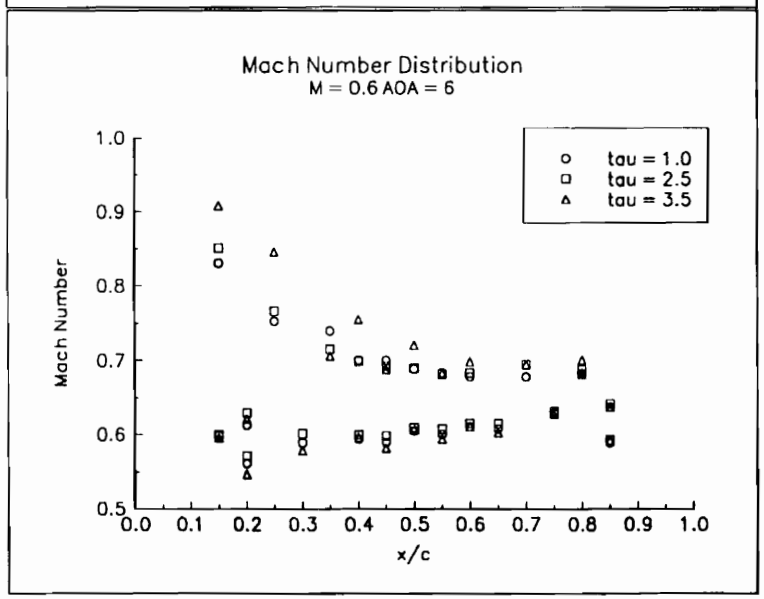
Mach Number Distribution
M = 0.6 AOA = 6
Mach Number
x/c
tau = 1.0
tau = 2.5
tau = 3.5

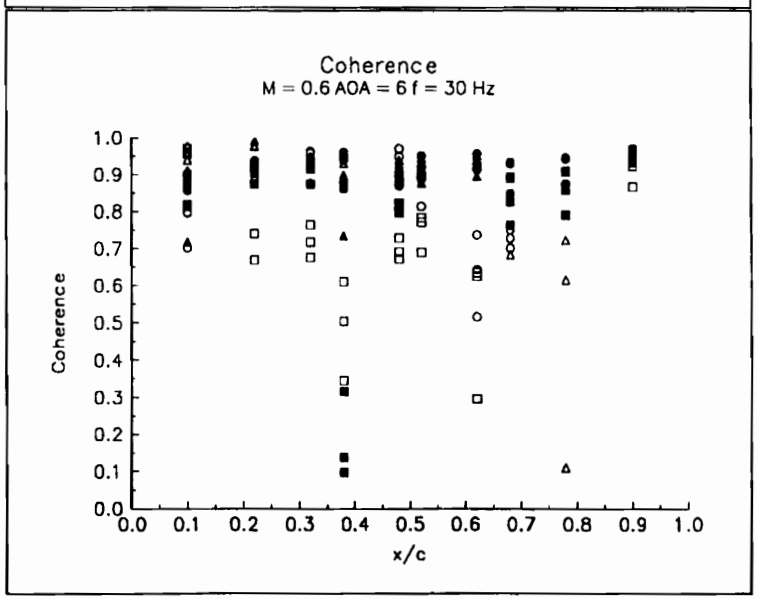
Coherence
M = 0.6 AOA = 6 f = 30 Hz
Coherence
x/c

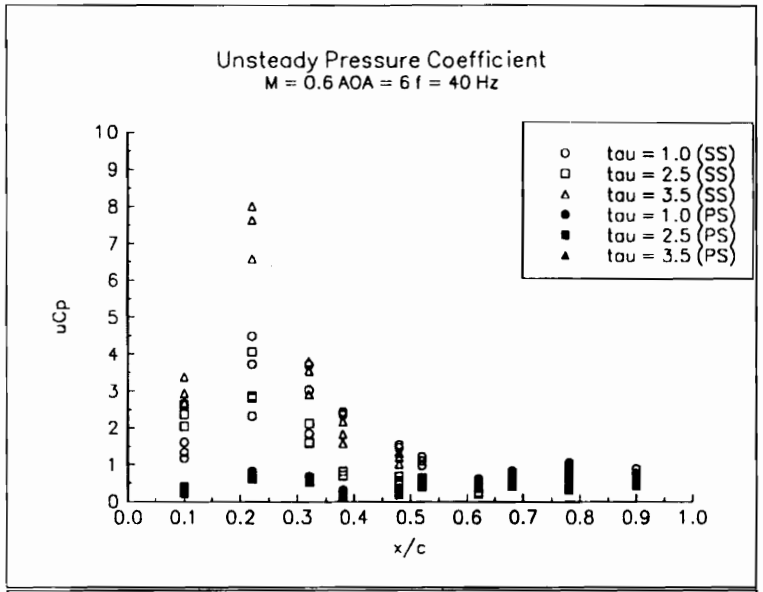
Unsteady Pressure Coefficient
M = 0.6 AOA = 6 f = 40 Hz
tau = 1.0 (SS)
tau = 2.5 (SS)
tau = 3.5 (SS)
tau = 1.0 (PS)
tau = 2.5 (PS)
tau = 3.5 (PS)
uCp
x/c

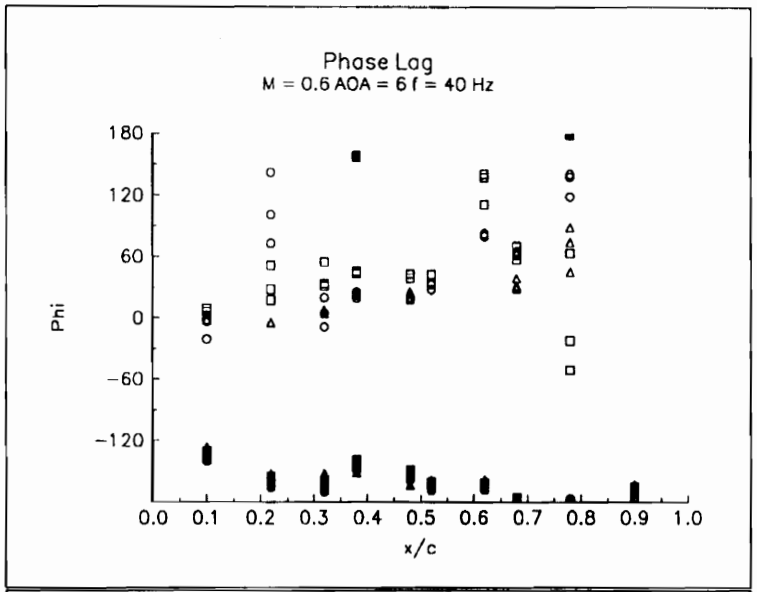
Phase Lag
M = 0.6 AOA = 6 f = 40 Hz
Phi
x/c

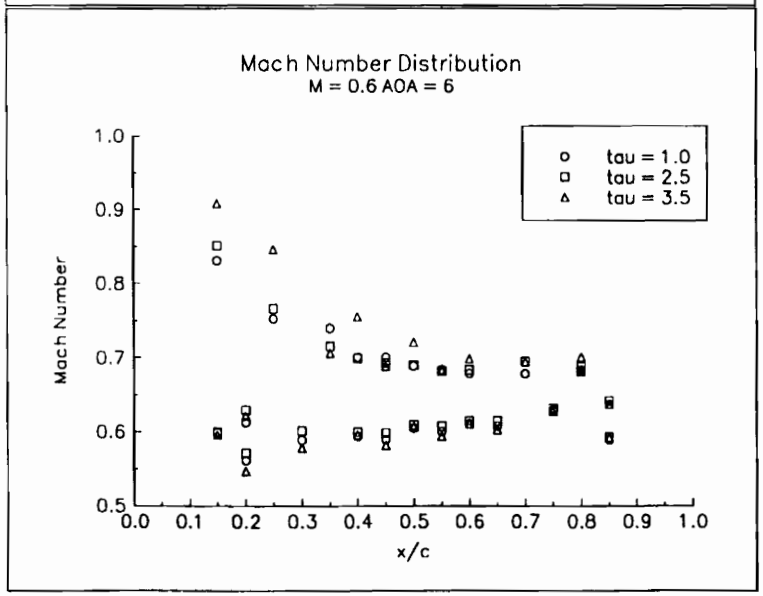
Mach Number Distribution
M = 0.6 AOA = 6
tau = 1.0
tau = 2.5
tau = 3.5
Mach Number
x/c

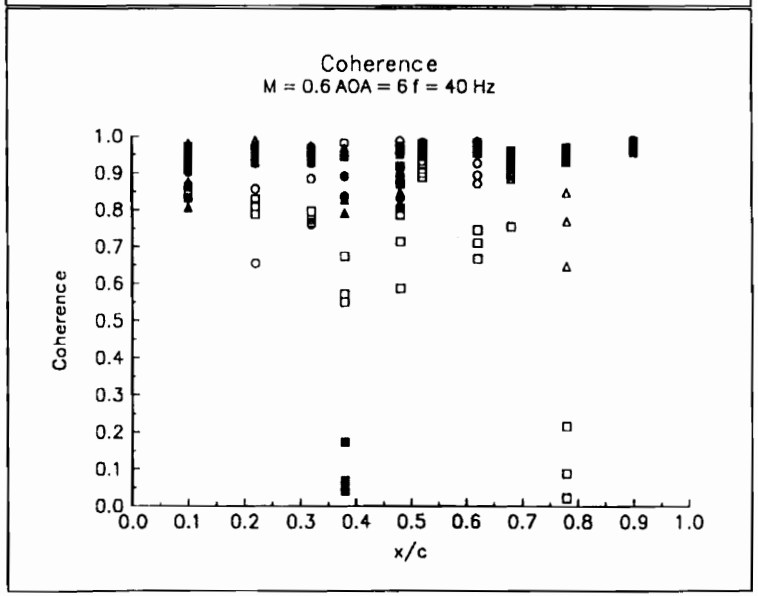
Coherence
M = 0.6 AOA = 6 f = 40 Hz
Coherence
x/c

Appendix II

The angle of incidence of the flow on the blade does not greatly change during the oscillation of the blade. The greatest change in incidence angle would occur for the blade at a 0° angle of attack with a Mach number of 0.2 and a frequency of 40 Hz. The angle change for this case will be calculated below.

The blade velocity can be expressed as follows:

$$v = a\omega \cos \omega t$$

where ω is the angular velocity and a is the amplitude of the oscillations, 0.3 mm. This results in a maximum velocity of 0.075 m/s for the plate.

The velocity of the flow can be determined knowing the Mach number, 0.2, and the total temperature of about 50° C. This results in a flow speed of 71.9 m/s.

A velocity triangle can be drawn to determine the angle of incidence of the flow on the blade as follows:

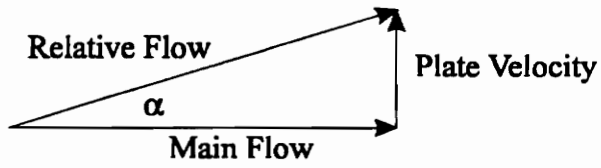

The angle α can be calculated.

$$\alpha = \tan^{-1} \frac{0.075 \frac{m}{s}}{71.9 \frac{m}{s}} = 0.06°$$

Thus, it is seen that the change in the angle of incidence is very small during the oscillation of the blade. At angles of attack the change in incidence angle is approximately the same as at a 0° angle of attack due to the small angles involved.

Appendix III

REDUCE.FOR

```
$STORAGE:2
$DEBUG
C234567

      PROGRAM REDUCE

C     This program computes an averaged signal for each of the chan
nels.
C     All the scans for each channel are averaged together

C     Last modified: 17/9/92 DJL

C     T0 - REAL - TIME PERIOD FOR BLADE VIBRATION
C     FINPUT - INTEGER - NUMBER FOR INPUT FILE
C     FOUTPUT - INTEGER - NUMBER FOR OUTPUT FILE
C     FDATA   - INTEGER - NUMBER FOR DATA FILE
C     DATAFILE - CHAR. - NAME OF DATA FILE
C     INPFILE  - CHAR. - NAME OF INPUT FILE
C     OUTFILE  - CHAR. - NAME OF OUTPUT FILE
C     FREQ - REAL - INPUT FREQUENCY OF BLADE VIBRATION
C     MACH - REAL - INPUT MACH NUMBER OF FREESTREAM FLOW
C     ALPHA - REAL - INPUT ANGLE OF ATTACK
C     TAU - REAL - INPUT TIP CLEARANCE
C     PTOT - REAL - INPUT TOTAL PRESSURE
C     TTOT - REAL - INPUT TOTAL TEMPERATURE
C     AMP - REAL - INPUT AMPLITUDE OF BLADE VIBRATION
C     VIBCHAN - INTEGER - INPUT NUMBER OF CHANNEL FOR BLADE VIBRATI
ON
C     GRCHAN - INTEGER - INPUT NUMBER OF GROUNDED CHANNEL
C     X - INTEGER - INPUT X COORDINATE OF PRESSURE TRANSDUCER
C     Y - INTEGER - INPUT Y COORDINATE OF PRESSURE TRANSDUCER
C     Z - INTEGER - INPUT Z COORDINATE OF PRESSURE TRANSDUCER
C     NSCAN - INTEGER - INPUT NUMBER OF SCANS
C     FILENAME - CHAR. - INPUT NAME OF TEST RUN
C     DATE - CHAR. - DATE
C     IVERS - INTEGER - INPUT VERSION OF DATA ACQUISITION PROGRAM
C     NCHAN - INTEGER - INPUT NUMBER OF CHANNELS
C     NCNT1 - INTEGER - INPUT VALUE FOR ACQUISITION RATE
C     NCNT2 - INTEGER - INPUT VALUE FOR ACQUISITION RATE
C     NSAMP - INTEGER - INPUT NUMBER OF SAMPLES IN ONE SCAN
C     NCHREF - INTEGER - INPUT FLAG FOR REFERENCE CHANNEL (GROUND)
C     ISCAN - INTEGER - NUMBER OF PRESENT SCAN
C     VAL1 - INTEGER - VALUE OF SIGNAL
C     VAL0 - INTEGER - VALUE OF SIGNAL
C     M - INTEGER - CURRENT NUMBER OF SCAN FOR SUBROUTINE CHREAD
C     SMAX - INTEGER - MAXIMUM NUMBER OF SCANS FOR SUBROUTINE CHREA
D
C     I, J - INTEGER - LOOP COUNTERS
C     ESSUNT - INTEGER - INPUT FILE NUMBER FOR INPUT FILE
C     VAL - INTEGER - ARRAY CONTAINING DATA
C     ITIME - CHAR. - INPUT TIME OF DATA ACQUISITION
C     IDATE - CHAR. - INPUT DATE OF DATA ACQUISITION
C     MEAN - REAL - MEAN VALUE OF SIGNAL
C     T0 - REAL - TIME OF FIRST CROSS THROUGH ZERO
C     T1 - REAL - TIME OF LAST CROSS THROUGH ZERO
C     BLFREQ - REAL - BLADE FREQUENCY OF A GIVEN SCAN
C     MBF - REAL - MEAN BLADE FREQUENCY
C     TR - REAL - PERIOD OF VIBRATION
C     PHASE - REAL - OUTPUT PHASE ANGLE DIFFERENCE FOR GIVEN CHANNE
```

```
L
C      SENS - REAL - INPUT SENSITIVITY OF PRESSURE TRANSDUCER I
C      LAG - REAL - INPUT PHASE LAG OF PRESSURE TRANSDUCER I
C      PHI - REAL - CALCULATED PHASE LAG FOR CURRENT TRANSDUCER
C      CF  - REAL - COHERENCE FUNCTION
C      GXX - REAL - AUTOSPECTRUM OF BLADE
C      GYY - REAL - AUTOSPECTRUM OF PRESSURE MEASUREMENT
C      FRF - REAL - FREQUENCY RESPONSE FUNCTION


       INTEGER*4    AVP,IAV
       INTEGER      FINPUT,FOUTPUT,FDATA
       CHARACTER*20 DATAFILE,INPFILE,OUTFILE
       REAL         FREQ,MACH,ALPHA,TAU,PTOT,TTOT,AMP,SENS(10),LAG(1
0)
       INTEGER*2    VIBCHAN,GRCHAN,X(20),Y(20),Z(20),NSCAN
       CHARACTER*12 FILENAME
       CHARACTER*8  DATE
       INTEGER*2    IVERS,NCHAN,NCNT1,NCNT2,NSAMP,NCHREF,ISCAN
       INTEGER*2    VAL1(6,8192),VAL0(8192),M,SMAX,I,J,ESSUNT,VAL(81
92)
       CHARACTER*10 ITIME,IDATE,dec
       INTEGER*4    IMEAN(10)
       REAL*4       MEAN(10),T0(40),T1(40),BLFREQ(40),MBF,TR(40),PAM
P(10)
       REAL*4       PHASE(10),PHI,PI,GXX(256),GYY(512),CF(5,256,15)
       REAL*4       REDF,CP(10),SPEC(6,1024),GXY(512),SPEC0(1024)
       REAL*4       CFMEAN(5,512),FRFR,FRFI,GXYSUM(5,512)
       REAL*4       PHASEMEAN(5,512),AMPMEAN(5,512),GXXSUM(256)
       REAL*4       AMPDEV(10),PHASEDEV(10),FFTPHASE(5,256,15)
       REAL*4       FFTAMP(5,256,15),CFDEV(10),GYYSUM(5,512)
       COMMON /FILDAT/ ESSUNT,NCHAN,NSAMP,SMAX,VAL1

C      INITIALIZE VALUES AND OPEN FILES

       WRITE(*,*)'INPUT FILENAME (without extension)'
       READ(*,'(A)') FILENAME
       INPFILE        = FILENAME
       INPFILE(9:12)  = '.UPI'
       FINPUT         = 21
       OUTFILE        = FILENAME
       OUTFILE(9:12)  = '.UPO'
       FOUTPUT        = 22
       DATAFILE       = FILENAME
       DATAFILE(9:12) = '.DAT'
       ESSUNT         = 20
       WRITE(*,*)'OPENING DATA FILE'
       OPEN (20,FILE=DATAFILE,STATUS='OLD',FORM='BINARY',
     $   BLOCKSIZE=16000,ERR=310)
       WRITE(*,*)'OPENING INPUT FILE'
       OPEN (21,FILE=INPFILE,STATUS='OLD',ERR=310)
       WRITE(*,*)'OPENING OUTPUT FILE'
       WRITE(*,*)OUTFILE
       OPEN (22,FILE=OUTFILE,ERR=310)

C      CALL FR SUBROUTINE TO READ IN FROM INPUT FILE
       WRITE(*,*)'READING INPUT FILE'
       CALL FR(DATE,FREQ,MACH,AMP,ALPHA,TAU,PTOT,TTOT,NCHAN,
     $              VIBCHAN,GRCHAN,X,Y,Z,NSCAN,FINPUT,SENS,LAG)
```

```
      DO I=1,NCHAN-2
         WRITE(*,*)'INPUT SENSITIVITY FOR PRESSURE TRANSDUCER',I
         READ(*,*) SENS(I)
         WRITE(*,*)'SENSITIVITY IS',SENS(I)
         WRITE(*,*)
      END DO
      WRITE(*,*)'INPUT STATIC PRESSURE'
      READ(*,*)PSTAT

C     INITIALIZE VALUES
      PI = 4*ATAN(1.0)
      AVP = 128
      MBF =   0.0
      NCHECK =0
      MAXSPEC=0
      SPECMAX=0.
      DO I=1,512
        IF (I.LT.257) GXX(I)=0.
        DO L=1,5
           GYY(I)=0.
           GXY(I)=0.
        END DO
      END DO

C     ENTER MAIN LOOP OF PROGRAM
      WRITE(*,*)'THERE ARE ',NSCAN,' SCANS'
      WRITE(*,*)'THERE ARE ',NCHAN,' CHANNELS'
      WRITE(*,*)'VIBCHAN IS',VIBCHAN
      NSCAN=1
      DO I=1,NSCAN

         WRITE(*,*)
         WRITE(*,*)'THIS IS SCAN NUMBER ',I
C        FIND FREQUENCY AND START POINT OF SIGNAL OF BLADE
C        READ IN COUNTER VALUES
         REWIND (ESSUNT)
         READ (ESSUNT) IVERS
         IF (IVERS.GT.1000) THEN
            IF (IVERS.EQ.1001) THEN
               READ (ESSUNT) IDATE
               READ (ESSUNT) ITIME
            END IF
            READ (ESSUNT) NCHAN,NCNT1,NCNT2,NSAMP,NCHREF
         ELSE
            REWIND (ESSUNT)
            READ (ESSUNT) NCHAN,NCNT1,NCNT2,NSAMP,NCHREF
         END IF

C     CALCULATE ACQUISTION FREQUENCY
         FCLOCK = 8.0E6/FLOAT(NCNT1)/FLOAT(NCNT2)
         FTRIG  = FCLOCK
         FSAMP  = FTRIG/FLOAT(NCHAN)
         IF (NCHREF.GT.0) FSAMP = FTRIG/FLOAT(NCHAN+1)
C        TSAMP IS TIME BETWEEN SAMPLES ON A GIVEN CHANNEL
C        TTRIG IS TIME BETWEEN ANY TWO CONSECUTIVE DATA POINTS

         TTRIG  = 1.0/FTRIG
         TSAMP  = 1.0/FSAMP
         WRITE(*,*)'SAMPLING DONE AT ',FSAMP,' Hz'
```

```
         W0 = 1./(TSAMP*1024.)
C         WRITE(*,*)'W0 IS ',W0
         NBOX = 2*INT(FREQ/W0)-1

C     CALL CHREAD TO READ IN DATA
         WRITE(*,*)'READING IN SIGNAL'
         CALL CHREAD(I,NSCAN)

C     SUBTRACT LOCAL MEAN FROM BLADE SIGNAL
         DO K=1,128
         IMEAN(1)=0
            DO J=1,64
               IMEAN(1)=IMEAN(1)+VAL1(1,(K-1)*64+J)
            END DO
            DO J=1,64
               VAL((K-1)*64+J)=VAL1(1,(K-1)*64+J)-INT(IMEAN(1)/64)
               VAL1(1,(K-1)*64+J)=VAL1(1,(K-1)*64+J)-INT(IMEAN(1)/6
4)
            END DO
C            WRITE(*,*)'IMEAN(1) IS',IMEAN(1)/64
         END DO

C     SUBTRACT MEAN VALUE FROM ARRAY
         DO K=2,NCHAN
           IMEAN(K)=0
            DO J=1,NSAMP,1
               IMEAN(K)=IMEAN(K)+VAL1(K,J)
  100       END DO

            MEAN(K)=FLOAT(IMEAN(K))/FLOAT(NSAMP)
C           WRITE(*,*)'MEAN VALUE OF',K,' IS ',MEAN(K)
            DO J=1,NSAMP,1

               IF(K.EQ.1) VAL(J)=VAL1(1,J)-INT(MEAN(1))
               VAL1(K,J)=VAL1(K,J)-INT(MEAN(K))
  200       END DO
         END DO

C     PERFORM FOURIER TRANSFORM OF 1024 WITH 50% OVERLAP ON CHANNEL
S

         DO J=1,15

            DO L=1,6
               DO K=1,1024
                  SPEC0(K)=FLOAT(VAL1(L,(J-1)*512+K))
               END DO
               CALL REALFT(SPEC0,512,1)
               DO K=1,1024
                  SPEC(L,K)=1./512.*SPEC0(K)
               END DO
            END DO

C     CALCULATE GXX,GXY,GYY AND FFT
            DO L=1,6
               DO K=1,511,2
                  IF (L.EQ.1) THEN
                     GXX((K+1)/2)=SPEC(1,K)*  SPEC(1,K)+
     $                        SPEC(1,K)*   SPEC(1,K+1))
```

```
                        GXXSUM((K+1)/2)=GXX((K+1)/2)+GXXSUM((K+1)/2)
                        GXY(K+1)=SPEC(L,K+1)*SPEC(1,K)-SPEC(L,K)*SPEC(
1,K+1)
                        GXY(K)=SPEC(L,K)*SPEC(1,K)+SPEC(L,K+1)*SPEC(1,
K+1)
                        GXYSUM(L-1,K)=GXY(K)+GXYSUM(L-1,K)
                        GXYSUM(L-1,K+1)=GXY(K+1)+GXYSUM(L-1,K+1)
                        GYY(K)=SPEC(L,K)*  SPEC(L,K)+
     $                          SPEC(L,K+1)*SPEC(L,K+1)
                        GYY(K+1)=GYY(K)
                        GYYSUM(L-1,(K+1)/2)=GYYSUM(L-1,(K+1)/2)+GYY(K)
C     CALCULATE AMPLITUDE AND PHASE
                        FFTAMP(L-1,(K+1)/2,J)=SQRT(GYY(K))
                        AMPMEAN(L-1,(K+1)/2)=FFTAMP(L-1,(K+1)/2,J)+
     $                                       AMPMEAN(L-1,(K+1)/2)

C     CALCULATE FREQUENCY RESPONSE FUNCTION
                        FRFR=GXY(K)/GXX((K+1)/2)
                        FRFI=GXY(K+1)/GXX((K+1)/2)
                        FFTPHASE(L-1,(K+1)/2,J)=ATAN2(FRFI,FRFR)*180./
PI
                        PHASEMEAN(L-1,(K+1)/2)=FFTPHASE(L-1,(K+1)/2,J)
+
     $                                  PHASEMEAN(L-1,(K+1)/2)

C     CALCULATE COHERENCE FUNCTION 0 = NONE     1 = TOTAL
                    END IF
                  END DO
               END DO

C     END OF 1024 SCAN
         END DO

C     END OF SCAN LOOP
  400 END DO

C     CALCULATE MEANS AND FIND PRIMARY FREQUENCY
      MAXSPEC=0
      SPECMAX=0.
      DO K=1,511,2
         IF (GXXSUM((K+1)/2).GT.SPECMAX) THEN
            MAXSPEC=K
            SPECMAX=GXXSUM((K+1)/2)
         END IF
         DO L=1,5
            CF(L,(K+1)/2,J)=(GXYSUM(L,K)*GXYSUM(L,K)+GXYSUM(L,K+1)*
     $                    GXYSUM(L,K+1))/ (GXXSUM((K+1)/2)*GYYSUM(L,K
))
            WRITE(*,*)'CF IS ',CF(L,(K+1)/2,J)
            PHASEMEAN(L,K)=PHASEMEAN(L,K)/15.
            AMPMEAN(L,K)=AMPMEAN(L,K)/15.
         END DO
      END DO
      WRITE(*,*)'MAXSPEC IS ',MAXSPEC
C     CALCULATE STANDARD DEVIATIONS
      DO L=1,5
        PHASE(L)=PHASEMEAN(L,MAXSPEC)
        PAMP(L)=AMPMEAN(L,MAXSPEC)
        DO J=1,15
```

```
            CFDEV(L)=CFDEV(L)+(CF(L,MAXSPEC,J)-CFMEAN(L,MAXSPEC))**2
            PHASEDEV(L)=PHASEDEV(L)+(FFTPHASE(L,MAXSPEC,J)-PHASE(L))
**2
            AMPDEV(L)=AMPDEV(L)+(FFTAMP(L,MAXSPEC,J)-PAMP(L))**2
          END DO
        END DO

C       WRITE TO OUTPUT FILE
        DO L=1,512
C          WRITE(22,'(I5,6(F10.5))'))
        END DO

        DO L=1,5
           PAMP(L)  = PAMP(L)*10./4096*SENS(L)
           WRITE(*,*)'CF FOR CHANNEL',L,' IS ',CFMEAN(L,MAXSPEC)
        END DO

C*********INSERT PHASE LAG
        MBF = (MAXSPEC+1)/2*W0

        PHASE(1) = 15.066 -1.2561*MBF+6.32E-3*  MBF*MBF+PHASE(1)
        PHASE(2) = 14.028-1.0572* MBF+4.8144E-3*MBF*MBF+PHASE(2)
        PHASE(3) = 8.2589-.93814* MBF+3.0264E-3*MBF*MBF+PHASE(3)
        PHASE(4) = 7.5861-0.87442*MBF+2.6425E-3*MBF*MBF+PHASE(4)
        PHASE(5) = 7.3069-1.1122* MBF+2.3537E-3*MBF*MBF+PHASE(5)

C        WRITE(22,'(6(F10.5))'))

C       CORRECT PHASE TO +/- 180 DEGREES
        DO I=1,5
           IF ((ALPHA .LT. 0.) .AND. (I.GT.1)) PHASE(I)=PHASE(I)+180.
           IF (PHASE(I).GT. 180.) PHASE(I)=PHASE(I)-360.
           IF (PHASE(I).LT.-180.) PHASE(I)=PHASE(I)+360.
        END DO

C       CALCULATE Cp
        DO I=1,5
           CP(I)=(PAMP(I)*100.)/(((PTOT*100.)-(PSTAT*100.))*AMP)
        END DO

C       CALCULATE BLADE FREQUENCY
        WRITE(*,*)
        WRITE(*,1200)
        DO I=1,5
           WRITE(*,1210)I,PAMP(I),CP(I),PHASE(I)
        END DO

C       CALCULATE REDUCED FREQUENCY
        RMACH = SQRT(5.*((PTOT/PSTAT)**(2./7.)-1))
C        WRITE(*,'(A,F10.3)')'MACH NUMBER IS',RMACH
C        WRITE(*,*)'TEMPERATURE IS',TTOT/(1.+0.2*RMACH*RMACH)
C        WRITE(*,*)'SOUND SPEED IS',SQRT(1.4*287.*(TTOT+273.15)/(1.+0
.2*
C       $ RMACH**2))
        W=RMACH*SQRT(1.4*287.*(TTOT+273.15)/(1.+0.2*RMACH*RMACH))
C        WRITE(*,*)'W IS:',W
        REDF = PI*MBF*100.E-3/W
        WRITE(*,*)
        WRITE(*,*)'AVERAGE BLADE FREQUENCY: ',MBF
```

```
      WRITE(*,*)'REDUCED FREQUENCY      : ',REDF

C     OUTPUT TO DATA FILE

      WRITE(*,*)'WRITING TO OUTPUT FILE'
      WRITE(22,1000)DATE
      WRITE(22,1010)FREQ,MACH
      WRITE(22,1020)AMP,ALPHA
      WRITE(22,1030)TAU
      WRITE(22,1040)PTOT,TTOT
      WRITE(22,1050)NCHAN,NSCAN
      WRITE(22,1060)VIBCHAN,GRCHAN
      WRITE(22,1070)

      DO I=2,NCHAN
         WRITE(22,1080)X(I),Y(I),Z(I)
      END DO

      WRITE(22,1090)MBF
      WRITE(22,1095)REDF
      WRITE(22,1096)RMACH
      WRITE(22,1200)

      DO I=1,5
         WRITE(22,1210)I,PAMP(I),CP(I),PHASE(I)
      END DO
      WRITE(22,*)

C     CLOSE FILES
      CLOSE (20)
      CLOSE (21)
      CLOSE (22)

      STOP

 310  WRITE(*,*)'ERROR reading file'

 1000 FORMAT(1X,'DATE:          ',A15)
 1010 FORMAT(1X,'FREQUENCY (Hz)',F15.3,'   MACH NUMBER       ',F15.
3)
 1020 FORMAT(1X,'AMPLITUDE (mm)',F15.3,'   ATTACK ANGLE (deg)',F15.
3)
 1030 FORMAT(1X,'TIP GAP    (mm)',F15.3)
 1040 FORMAT(1X,'TOTAL PRES(mb)',F15.3,'   TOTAL TEMP (K)     ',F15.
3,/)
 1050 FORMAT(1X,'NUMBER OF CHANNELS',I10,'    NUMBER OF SCANS  ',I1
0)
 1060 FORMAT(1X,'VIBRAX CHANNEL     ',I10,'    REFERENCE CHANNEL',I1
0)
 1070 FORMAT(/,10X,'X-POSITION',T27,'Y-POSITION',T42,'Z-POSITION')
 1080 FORMAT(1X,3I15)
 1090 FORMAT(/,/,/,1X,'ACTUAL BLADE FREQUENCY          ',F15.3,'   H
z')
 1095 FORMAT(      1X,'REDUCED FREQUENCY               ',F15.3)
 1096 FORMAT(      1X,'ACTUAL MACH NUMBER              ',F15.3)
 1100 FORMAT(1X,  'PHASE ANGLE FOR CHANNEL',I5,'  =',F15.3,'   DEGR
EES',
     $   F10.3,' Pa')
```

```
 1200 FORMAT(1X,'PRESSURE TRANSDUCER',T23,'AMPLITUDE',T40,'COEFFICI
ENT',
     $ T64,'PHASE')
 1210 FORMAT(1X,T5,I10,T20,F10.3,T40,F10.3,T60,F10.3)
      END

C234567
      SUBROUTINE CHREAD (ISCAN,NSCAN)

C     This subroutine is taken from RAWDAT.FOR It reads the binary
data into an
C     array called VAL1(chan,samp) for a given scan number (ISCAN)
from a given
C     file number (ESSUNT).
C     This can then be used by other programs.

      INTEGER*2 IVERS,NCHAN,NCNT1,NCNT2,NSAMP,NCHREF,ISCAN,VAL1(6,8
192)
      INTEGER*2 VAL0(8192),M,SMAX,I,J,ESSUNT,NSCAN
      CHARACTER*10 ITIME,IDATE

      COMMON /FILDAT/ ESSUNT,NCHAN,NSAMP,SMAX,VAL1

C     READ CHANNELS FOR SPECIFIED SCAN
C     READ DATA FILE INFORMATION HEADER IF EXISTANT


C      REWIND (ESSUNT)
      REWIND (20)
      READ (20) IVERS
      IF (IVERS.GT.1000) THEN
         IF (IVERS.EQ.1001) THEN
            READ (20) IDATE
            READ (20) ITIME
         END IF
         READ (20) NCHAN,NCNT1,NCNT2,NSAMP,NCHREF
      ELSE
         REWIND (20)
         READ (20) NCHAN,NCNT1,NCNT2,NSAMP,NCHREF
      END IF

      M=0
C     READ CHANNELS

      DO K=1,ISCAN
         M=M+1
         IF (M.GT.1) THEN
            READ(20,ERR=310,END=210) NCHAN,NCNT1,NCNT2,NSAMP,NCHREF
         END IF
         DO I=1,NCHAN
            READ(20,ERR=310) (VAL0(J),J=1,NSAMP)
            IF (K.EQ.ISCAN) THEN
C              WRITE(*,*)'FOUND RIGHT SCAN NUMBER STARTING TRANSFER
',M,I
               DO J=1,NSAMP
                  VAL1(I,J)=VAL0(J)
               END DO

            END IF
```

```
         END DO
      END DO
      SMAX=M
      write(*,*)'Returning to main program'
  210 RETURN
  310 WRITE(*,*)'ERROR during file read!'
      STOP
      END

      SUBROUTINE FR(DATE,FREQ,MACH,AMP,ALPHA,TAU,PTOT,TTOT,NCHAN,
     $              VIBCHAN,GRCHAN,X,Y,Z,NSCAN,FINPUT,SENS,LAG)

C     This subroutine reads the input file.

      REAL          FREQ,MACH,ALPHA,TAU,PTOT,TTOT,AMP,SENS(10),LAG(1
0)
      INTEGER*2     NCHAN,VIBCHAN,GRCHAN,X(20),Y(20),Z(20),FINPUT
      CHARACTER*12 FILENAME
      CHARACTER*8  DATE

      READ(FINPUT,1000)DATE
      READ(FINPUT,1010)FREQ,MACH
      READ(FINPUT,1020)AMP,ALPHA
      READ(FINPUT,1030)TAU
      READ(FINPUT,1040)PTOT,TTOT
      READ(FINPUT,1050)NCHAN,NSCAN
      READ(FINPUT,1060)VIBCHAN,GRCHAN
      READ(FINPUT,1070)
      DO I=1,NCHAN-2
         READ(FINPUT,1080)X(I),Y(I),Z(I)
      END DO
      READ(FINPUT,1085)
      DO I=1,NCHAN-2
         READ(FINPUT,1090)KL,SENS(I),LAG(I)
      END DO

      RETURN

 1000 FORMAT(15X,A15)
 1010 FORMAT(1X,14X,F15.3,21X,F15.3)
 1020 FORMAT(1X,14X,F15.3,21X,F15.3)
 1030 FORMAT(1X,14X,F15.3)
 1040 FORMAT(1X,14X,F15.3,21X,F15.3,/)
 1050 FORMAT(1X,18X,I10,21X,I10)
 1060 FORMAT(1X,18X,I10,21X,I10)
 1070 FORMAT(/,10X)
 1080 FORMAT(1X,3I15)
 1085 FORMAT(10X)
 1090 FORMAT(1X,I15,T20,F15.3,T35,F15.3)

      END
C***  This FFT-subroutines can be found in:
C***     NUMERICAL RECIPES p.394
C***     LTT-bibl. 3.44
C***  single precision

      SUBROUTINE FOUR1(data,nn,isign)

      real*4 wr,wi,wpr,wpi,wtemp,theta
```

```
      dimension data(2*nn)

      n=2*nn
      j=1
      pi2=6.2831853
      do i=1,n,2
        if (j.gt.i) then
          tempr=data(j)
          tempi=data(j+1)
          data(j)=data(i)
          data(j+1)=data(i+1)
          data(i)=tempr
          data(i+1)=tempi
        endif
        m=n/2
1       continue
        if ((m.ge.2).and.(j.gt.m)) then
          j=j-m
          m=m/2
          goto1
        endif
        j=j+m
      end do

      mmax=2
2     continue
      if (n.gt.mmax) then
        istep=2*mmax
        theta=pi2/(isign*mmax)
        wpr=-2.*sin(0.5*theta)**2
        wpi=sin(theta)
        wr=1.
        wi=0.
        do m=1,mmax,2
          do i=m,n,istep
            j=i+mmax
            tempr=wr*data(j)-wi*data(j+1)
            tempi=wr*data(j+1)+wi*data(j)
            data(j)=data(i)-tempr
            data(j+1)=data(i+1)-tempi
            data(i)=data(i)+tempr
            data(i+1)=data(i+1)+tempi
          end do
          wtemp=wr
          wr=wr*wpr-wi*wpi+wr
          wi=wi*wpr+wtemp*wpi+wi
        end do
        mmax=istep
        goto 2
      endif

      RETURN
      END


      SUBROUTINE REALFT(data,n,isign)

      real*4 wr,wi,wpr,wpi,wtemp,theta
      dimension data(2*n)
```

```
theta=3.1415927/float(n)
C1=0.5

if (isign.eq.1) then
  c2=-0.5
  CALL FOUR1(data,n,+1)
else
  c2=0.5
  theta=-theta
endif
wpr=-2.*sin(0.5*theta)**2
wpi=sin(theta)
wr=1.+wpr
wi=wpi
n2p3=2*n+3

do i=2,n/2
  i1=2*i-1
  i2=i1+1
  i3=n2p3-i2
  i4=i3+1
  wrs=wr
  wis=wi
  h1r=c1*(data(i1)+data(i3))
  h1i=c1*(data(i2)-data(i4))
  h2r=-c2*(data(i2)+data(i4))
  h2i=c2*(data(i1)-data(i3))
  data(i1)=h1r+wrs*h2r-wis*h2i
  data(i2)=h1i+wrs*h2i+wis*h2r
  data(i3)=h1r-wrs*h2r+wis*h2i
  data(i4)=-h1i+wrs*h2i+wis*h2r
  wtemp=wr
  wr=wr*wpr-wi*wpi+wr
  wi=wi*wpr+wtemp*wpi+wi
end do
if (isign.eq.1) then
  h1r=data(1)
  data(1)=h1r+data(2)
  data(2)=h1r-data(2)
else
  h1r=data(1)
  data(1)=c1*(h1r+data(2))
  data(2)=c1*(h1r-data(2))
  CALL FOUR1(data,n,-1)
endif

RETURN
END
```

Vita

Daniel Joseph Lewis was born on February 12, 1968 in Syracuse, New York. He grew up in McLean, Virginia and graduated from McLean High School in June 1986. He then enrolled at Virginia Polytechnic Institute and State University graduating with a B.S. in Mechanical Engineering magna cum laude and a B.A. in History magna cum laude and tied for first in his class in May 1991. After graduation Daniel continued his studies by enrolling in the Masters program at Virginia Polytechnic Institute and State University. He conducted his research with a Fulbright grant at the Ecole Polytechnique Fédérale de Lausanne, Switzerland. Upon completion of his degree he plans on moving to France to live and work.